Spreading depolarizations, migraine and ischemia: A detrimental triangle in subarachnoid hemorrhage and ischemic stroke?

Hamming, A.M.

Spreading depolarizations, migraine and ischemia

A detrimental triangle in subarachnoid hemorrhage and ischemic stroke?

Arend Hamming

ISBN 978-90-823440-7-3

Spreading depolarizations, migraine and ischemia

Arend Hamming

Spreading depolarizations, migraine and ischemia

A detrimental triangle in subarachnoid hemorrhage and ischemic stroke?

Arend Hamming

Spreading depolarizations, migraine and ischemia

A detrimental triangle in subarachnoid hemorrhage and ischemic stroke?

Cover image: © A.M. Hamming; *Waves and sun while sailing on Jottum* - 2019

Layout: A.M. Hamming, thanks to Anouk de Jong
Printing: UFB Grafische Producties
Printing of this thesis was financially supported by the Dutch Headache Society

Publisher: Tim Gard
ISBN: 978-90-823440-7-3

Proefschrift

ter verkrijging van
de graad van Doctor aan de Universiteit Leiden,
op gezag van Rector Magnificus prof.mr. C.J.J.M. Stolker,
volgens besluit van het College voor Promoties
te verdedigen op donderdag 12 november 2020
klokke 15.00 uur

door

Arend Maarten Hamming

geboren te Amsterdam

in 1979

Promotores

Prof. dr. M.J.H. Wermer

Prof. dr. R.M. Dijkhuizen, UMCU

Prof. dr. M.D. Ferrari

Promotiecommissie

Prof. dr. W.C. Peul

Prof. dr. J. Hofmeijer, Rijnstate

Prof. dr. G.J.E. Rinkel, UMCU

Dr. L. van der Weerd

To Mirjam, Fenna and Maarten
the waves and sunshine in my life

Abbreviations

ACA	anterior cerebral artery
ACM	middle cerebral artery
ADC	apparent diffusion coefficient (MR imaging)
aHR	adjusted hazard ratio
aOR	adjusted odds ratios, adjusted for age and sex in this study
aRR	adjusted relative risk (ratio)
aSAH	aneurysmal subarachnoid hemorrhage
BOLD	blood oxygenation level-dependent (MR imaging)
b-SSFP	balanced-steady-state-free-precession (MR imaging)
CBF	cerebral blood flow
CI	confidence interval
CoW	circle of Willis
CT	X-ray computerized axial tomography
CSD	cortical spreading depression (of electrical activity)
CTA	CT angiography (imaging)
CTP	CT perfusion (imaging)
DC	direct current
DCI	delayed cerebral ischemia (after SAH)
DUST	Dutch acute Stroke Trial
DT2	multi-spin-echo (MR imaging)
EEG	electro encephalography
fMRI	functional MRI
FWHM	Full width at half maximum/minimum
GE3d-EPI	a gradient-echo 3D echo-planar (MR) imaging
HR	hazard ratios
ICHD	International Classification of Headache Disorders
KCl	potassium chloride
LDF	Laser-Doppler Flowmetry
MA	migraine with aura
MACC	median artery corpus callosi
MISS	Migraine Screener for Stroke (questionnaire)
MO	migraine without aura
MR(I)	magnetic resonance (imaging)
mRS	modified Rankin Scale
NaCl	sodium chloride
NCCT	non-contrast CT
NIHSS	National Institutes of Health Stroke Scale
NIRS	near infrared spectroscopy
OR	odds ratios
PCA	posterior cerebral artery
Pcom	posterior communicating artery
RR	relative risk (ratio)
SAH	subarachnoid hemorrhage
SD	spreading depolarization
TIA	transient ischemic attack
WFNS	World Federation of Neurosurgical Societies (WFNS) SAH grading scale

Table of contents

Chapter 1

Introduction

Stroke is the second leading cause of death worldwide, causing 6 million deaths per year.[1] It is also the third leading cause of disease burden, resulting in the loss of 100 million disability-adjusted life years.[2] Stroke is a disease of the arteries and small blood vessels supplying the brain of blood. There can be an obstruction, causing an ischemic stroke, or a rupture of a blood vessel, causing a hemorrhage. When one of the blood vessels ruptures in the subarachnoid space surrounding the brain, the hemorrhage is called a subarachnoid hemorrhage (SAH).

After the initial impact of stroke, secondary brain damage can occur which can further affect clinical outcome. Several mechanisms play a role in this secondary damage. One of those mechanisms is spreading depolarization. The aim of this thesis is to investigate the relation between spreading depolarizations and secondary damage after ischemic stroke and subarachnoid hemorrhage. In this introduction the knowledge on stroke and spreading depolarization (first described as spreading depression of electrocorticographic activity) is reviewed, gaps in this knowledge are delineated and an outline of the thesis is presented.

Ischemic stroke

Signs and symptoms of ischemic stroke are related to the affected brain region and may include affected speech and vision, muscle weakness of the face and limbs, impaired motor coordination and numbness.[3, 4] When obstruction of a blood vessel causes the blood flow (perfusion) to the brain tissue to drop below a critical minimum, around 20 mL/100 g/min, the brain tissue will stop functioning.[5, 6] If the perfusion of the tissue is restored within hours, the tissue can function again and the signs and symptoms will disappear within minutes to hours. Hence, this is termed a transient ischemic attack (TIA).[7] If, however, the blood flow is not restored in time or drops below around 10 mL/100 g/min, the brain tissue will be permanently damaged, termed an ischemic stroke or brain infarct[5, 6], after which recovery of functions is only possible through functional compensation, rehabilitation and neuroplasticity, in which other parts of the brain take over lost functions.[8, 9] Common causes of blood vessel obstruction are large artery atherosclerosis, embolisms from the heart, small vessel disease and dissection of artery walls.[10] Important risk factors for stroke include hypertension, smoking, atrial fibrillation, diabetes mellitus, and hyperlipidemia.[11-13]

Subarachnoid hemorrhage and delayed cerebral ischemia

Only 5-10% of strokes are subarachnoid hemorrhages, but these are fatal in up to half the patients[14] and occur at a younger age than ischemic stroke; half the patients are younger than 55 years at the time of subarachnoid hemorrhage.[15] Therefore, the impact on society, measured by loss of productive life years, is similar to that of ischemic stroke.[16] The cause of 85% of the spontaneous subarachnoid hemorrhages is an aneurysm in one of the arteries that make up the circle of Willis or its direct branches.[17] The circle of Willis is a roundabout which interconnects the major arteries to the brain. This provides redundancy, although the circle

is incomplete in the majority of people.[18] In the course of life, a weakness in the wall of these arteries can develop, causing it to bulge out. This is called an aneurysm and is found in 3% of the healthy population.[19] When an aneurysm ruptures, blood spreads into the subarachnoid space, leading to a subarachnoid hemorrhage.[20] This can cause sudden headache, vomiting, seizures, focal neurological signs and symptoms, such as vision disturbances, and a lower level of consciousness that can progress to death.[20]

For patients that initially survive an aneurysmal subarachnoid hemorrhage, secondary complications can be detrimental to the outcome. One feared complication is cerebral ischemia in the subacute phase after subarachnoid hemorrhage called delayed cerebral ischemia (DCI), which occurs in approximately one-third of subarachnoid hemorrhage patients.[21] Delayed cerebral ischemia is characterized by clinical deterioration, such as decreased consciousness, aphasia and limb weakness, usually accompanied by radiologically detectable lesions.[22] The clinical features can be reversible or become permanent when the brain tissue becomes permanently infarcted.[23] Delayed cerebral ischemia has a peak occurrence on day 4-10 after subarachnoid hemorrhage and often occurs in a different brain region than that of the aneurysm or its perfusion territory.[24] Vasospasm of the large arteries has been implicated, because it occurs in the same timeframe and would account for the diffuse localization of delayed cerebral ischemia.[22] Several publications even refer to the clinical syndrome of delayed cerebral ischemia as “vasospasm”, suggesting a conclusive etiology.[22] Vasospasm is indeed correlated with delayed cerebral ischemia, poor outcome and mortality.[25] However, not all patients with vasospasm develop delayed cerebral ischemia and vasospasm is not detected in all patients who develop delayed cerebral ischemia.[26] Furthermore, a study with a potent vasospasm inhibitor, clazosentan, did not result in improved outcome compared with placebo.[27] Hence, other mechanisms than vasospasm also have been implicated in the development of delayed cerebral ischemia. While brain tissue damage in the first days after a subarachnoid hemorrhage is by definition not delayed cerebral ischemia-induced tissue damage, early processes may contribute to the later development of delayed cerebral ischemia. Transient cerebral ischemia and the presence of blood in the subarachnoid space may be accompanied by direct tissue damage from the force of the blood spraying out of an artery, increased intracranial pressure, and mechanical damage caused by brain shift and herniation. These processes can make the brain tissue more susceptible to damage in following days.[28] Besides these early processes and vasospasm of the large arteries, other implicated mechanisms include arteriolar constriction, microthrombosis[29], inflammation[30, 31], vasoconstrictor receptor upregulation[32] and spreading depolarizations.[33]

Spreading depolarizations

Spreading depolarization is defined as transient depolarization and inactivity of neurons and glial cells, spreading across brain tissue like waves in water.[34] Spreading depolarizations were first reported by Leão in 1944 as cortical spreading depression of electrocorticographic

activity.[35] In experimental animal models, spreading depolarization can be initiated by a multitude of stimuli, such as cortical application of potassium, a pinprick and direct electrical stimulation of the brain.[34] Additionally, many factors can sensitize brain tissue to spreading depolarizations, such as drugs[36], high extracellular potassium and low nitrous oxide concentrations.[37] Under such circumstances, or in sufficient strength in normal tissue, the stimulus causes neurons to completely depolarize from the normal resting potential and become functionally inactive. This depolarization spreads to surrounding tissue across the cortex at a speed of 2-6 mm/min.[35] That speed is markedly slower than the propagation of physiological action potentials across neural axons, which are propagated as a controlled partial axonal depolarization. This supports the theory that spreading depolarizations may propagate through gap junctions between neurons.[38] Another hypothesis is that glial cells play a leading role in the propagation of spreading depolarization waves.[39, 40]

Spreading depolarizations and migraine

The first clinical manifestation associated with spreading depolarizations is visual aura, a symptom of migraine.[41] Migraine is a debilitating brain disorder that manifests as severe headache attacks, often accompanied by nausea, vomiting and sensitivity to light and sound.[42] In one-third of patients, headaches are accompanied by an aura.[43, 44] The most common symptom of aura is a scintillating scotoma, or flickering, that spreads throughout the peripheral visual field. Scintillating scotomas are likely caused by a spreading depolarization wave front that spreads across the primary visual brain cortex.[41] Migraine is considered a neurovascular disorder but it is a matter of debate whether neuronal or vascular mechanisms play a greater role. Likely they both play a role as migraine headache is thought to originate from the action of nerves innervating cerebral and meningeal blood vessels.[45] In a transgenic mouse model of migraine with an increased susceptibility to spreading depolarization[46-48] and ischemic depolarizations resulting in increased ischemic stroke vulnerability[49], the underlying genetic defect causes neuronal hyperexcitability.[46, 48, 50] Other factors suggest a more prominent role of vascular mechanisms in migraine. Patients who have migraine with aura, have a doubled risk of ischemic stroke and the risk seems to be greater for patients with more frequent migraine attacks.[51, 52] Furthermore, several diseases and genetic disorders cause both migraine and ischemic stroke.[53-55] A third argument for the importance of vascular mechanisms in migraine is that some studies suggested that a different anatomy of the arterial circle of Willis compared with controls.[18] People with migraine more often had a missing segment and thus an incomplete circle. However this was not found in all studies and it’s unknown whether in migraine patients with stroke the circle of Willis is different compared with stroke patients without migraine.[56]

Spreading depolarizations in relation to delayed cerebral ischemia

Spreading depolarization is accompanied by a strong disruption of the concentration gradient of electrolytes such as sodium and potassium between the intra- and extracellular

space, causing neurons to swell.[57] During a refractory period, as the electrolyte balance is restored, electrolyte pumps require an increased supply of oxygen and nutrients.[58] Under normal conditions, an spreading depolarization is accompanied by an increase in perfusion to meet this demand.[34] However, in pathological states, such as after brain trauma, ischemic stroke or subarachnoid hemorrhage, a paradoxical decrease in perfusion can occur after spreading depolarization.[59] It is hypothesized that the imbalance between increased metabolic demand and decreased supply in oxygen and nutrients may cause the depolarizations to last longer, called intermediate or ischemic depolarizations, or become permanent (terminal or anoxic) depolarizations.[59] Spreading depolarizations are therefore a mechanism implicated in the development of delayed cerebral ischemia after a subarachnoid hemorrhage.[33, 59]

After a subarachnoid hemorrhage, the threshold for spreading depolarization initiation and the subsequent vascular response may be altered by hemolysis products such as potassium[60], decreased nitrous oxide, upregulation of vasoconstrictor receptor expression in the neurovascular unit[32] and inflammation.[31] Under such circumstances, spreading depolarization may become permanent (terminal or anoxic) depolarization.[61] Induced hypertension is an often implied treatment for subarachnoid hemorrhage patients with delayed cerebral ischemia.[62] Although the effectiveness of induced hypertension has not been established yet, it can be hypothesized that hypertension in theory might counteract cerebral hypoperfusion caused by vasospasm and spreading depolarizations. Spontaneous spreading depolarizations were described in rats after subarachnoid hemorrhage and magnesium was found to inhibit spreading depolarizations and decrease brain lesion volume.[63] Spontaneous SDs were also demonstrated after subarachnoid hemorrhage in humans who had cortical electrode strips placed during surgery for aneurysm clipping.[33] A total of 298 spreading depolarizations was recorded in 13 of the 18 patients. Moreover, in the seven patients that developed delayed cerebral ischemia, it was always time-locked to a sequence of recurrent spreading depolarizations in every single case with high positive and negative predictive values (85% and 100%).[33] Until now, however, a direct relationship between spreading depolarizations and the occurrence of delayed cerebral ischemia has not been shown.

Recording of spreading depolarizations

Spreading depolarization leads to a local disruption of neural activity that can be recorded in animals by electrodes on or in the cortex. In humans, in case part of the skull is surgically removed, electrocorticography can be performed directly on the cortex without the interference of the skull which is present in regular electro encephalography (EEG).[64] This allows for measuring a direct current shift and a depression of neural activity during a refractory period. Recently, however, possibilities were found that seem to allow detection of spreading depolarizations with non-invasive EEG in humans.[65] Alternatively, spreading depolarization events can be detected in humans and experimental animals based on the cerebral perfusion response. The perfusion response can be recorded with continuous superficial techniques such

as laser speckle imaging, near infrared spectroscopy (NIRS) and Laser-Doppler Flowmetry (LDF).[66-68] With LDF, a laser beam penetrates the brain tissue, is then scattered by red blood cells, and reflected back.[69] Recording the Doppler shift allows for measurement of the blood flow of the microcirculation. In some experimental models, changes caused by spreading depolarizations are visible even to the naked eye.[37, 70, 71]

The previously discussed techniques are all limited to recording of spreading depolarization events and their effects at the cortical surface. For three-dimensional imaging, and non-invasive recording of spreading depolarization, magnetic resonance (MR) imaging can be used.[72, 73] It is also used in regular health care, for diagnostic purposes, to support radiotherapy or surgery, and for identification of prognostic markers.[74] MR imaging relies on a strong magnetic field in which the spins of hydrogen ^{1}H and other atoms align.[75] By manipulating the phase and orientation of ^{1}H spins (which are abundantly present in soft tissues) using magnetic field gradients and radio frequency pulses, and by recording the radio frequency the atoms emit, it is possible to create a three-dimensional image based on MR signals with different properties for different tissues. Relaxation of the atoms' magnetization occurs in the direction of the primary magnetic field (T1 relaxation) and in the plane perpendicular to the primary magnetic field (T2 relaxation). In reality, the spins' magnetization dephases quicker than the T2 relaxation because of inhomogeneities in the primary magnetic field, this is called T2* relaxation. ^{1}H MR images can be sensitized to these relaxation times, providing different anatomical contrasts.[74] MR imaging produces images with a greater detail of soft tissue anatomy than computerized tomography (CT) imaging, which is based on ionizing X-rays.[74] Functional imaging is possible by imaging at a high temporal resolution to record dynamic physiological or functional processes.

MR imaging of spreading depolarizations is based on either hemodynamic changes or cellular changes. Hemodynamic changes, such as increased oxygenation and perfusion, have been measured with T_2- or T_2*-weighted imaging[73] and perfusion imaging[72], respectively. Blood oxygenation level-dependent (BOLD) MR imaging is an indirect measure of neuronal activity. Under normal circumstances, an increase in neuronal activity gives rise to an increase in oxygen supply and uptake. However, the oxygen supply exceeds the oxygen consumption, leading to a change in the balance of the principal blood oxygen transporter, oxyhemoglobin and its deoxygenated state, deoxyhemoglobin. The consequent decrease in deoxyhemoglobin, which has a different magnetic susceptibility, can be detected in MR imaging.[76] The first scans of spreading depolarization in a patient with a migraine aura were made with BOLD MR imaging.[41] Cellular changes, such as transient cell swelling, in relation to spreading depolarization have been measured with diffusion-weighted ^{1}H MR imaging.[77] In biological tissue, diffusion of water is limited by structures such as cells, fibers and macromolecules. This diffusion restriction changes when cells depolarize and swell, which can be measured statically or dynamically with diffusion-weighted MRI imaging.[77] The physiological mechanisms underlying a spreading depolarization wave and the interaction between cellular and hemodynamic mechanisms are not yet fully understood, especially pathological mechanisms such as the inverse hemodynamic

hypoperfusion response that occurs in pathological brain tissue.[59] Improved imaging techniques could contribute to unraveling these mechanisms.

Spreading depolarization-modulating drugs

In experimental animal studies, many drugs were found to either inhibit or facilitate spreading depolarizations.[36] This spreading depolarization modulation could apply to several parameters, such as initiation threshold, propagation speed, duration or frequency of spreading depolarizations.[36] In some animal models, the spreading depolarization inhibiting effect of some drugs increased with a longer pretreatment duration, which should be taken into consideration when interpreting negative results from studies with a short or no pretreatment.[36] Conversely, eventual translational therapeutic efforts based on pharmacological spreading depolarization inhibition might be more successful when employing drugs that do not require extensive pre-treatment. A final caveat when interpreting animal studies on spreading depolarizations is that drug doses may also be higher in animal studies, but this is needed due to a higher metabolism in smaller animals.[78] While many influences, such as extracellular potassium and nitrous oxide concentrations, may facilitate spreading depolarizations, only few drugs such as barbiturates are known to do so in animal studies.[79-82] In contrast, multiple drugs were found to inhibit spreading depolarization in animal models.[36, 81, 83, 84] Categories of spreading depolarization-inhibiting drugs include antiepileptic drugs (e.g. valproate, phenytoin and topiramate), migraine prophylactics (e.g. propranolol, valproate), drugs affecting the NMDA receptor and calcium antagonists (e.g. nimodipine).[36, 85, 86] Some of these drugs, such as valproate, have been well established as spreading depolarization inhibitors in multiple animal studies by several groups.[87-89] Nimodipine is used clinically to prevent delayed cerebral ischemia in people after subarachnoid hemorrhage and may decrease the calcium influx in neurons or glial cells.[85, 90] However, it is not known on what mechanism the effect of nimodipine is based. It is unknown if spreading depolarization inhibition is a potential therapeutic target for reducing delayed cerebral ischemia after subarachnoid hemorrhage or reducing delayed brain injury after ischemic stroke.

Outline of this thesis

In **chapter 2** we studied the hypothesized link between spreading depolarizations and delayed brain injury in a randomized controlled experiment in rats in which a subarachnoid hemorrhage was induced by endovascular puncture and spreading depolarizations were induced by KCl application in one of the two groups.

To test whether the effects of spreading depolarizations on lesion expansion could be diminished by drugs, we used the same model in **chapter 3** to assess if spreading depolarization inhibitor valproate prevents spreading depolarization-induced delayed brain injury after subarachnoid hemorrhage.

To be able to investigate spreading depolarizations more easily in animals and patients, we evaluated non-invasive MRI techniques for recording of spreading depolarizations. In **chapter 4**, we tested the effectiveness of two novel MR techniques for imaging spreading depolarizations. One technique, diffusion-weighted multi-spin-echo (DT2) MRI, aims to measure both the hemodynamic and cellular response, which can provide unique information on the interaction between these two physiological processes. The other technique, balanced-steady-state-free-precession (b-SSFP) MRI, aims to improve the sensitivity and a spatial specificity compared to conventional gradient-echo MRI techniques.

In a first step to translate this research to the clinical setting, we investigated the clinical association between spreading depolarization and secondary ischemia through observational studies. In **chapter 5** we investigated in a large cohort of subarachnoid hemorrhage patients whether spreading depolarization-inhibiting home medication would reduce the development of delayed cerebral ischemia and improves clinical outcome after three months.

In **chapter 6**, we tested in an ischemic stroke cohort the hypothesis that variations in the arterial circle of Willis are more common in stroke patients with migraine compared with stroke patients without migraine.

In **chapter 7**, I reviewed the conclusions of the chapters and discuss implications and suggestions for future research on spreading depolarization and stroke.

Chapter 2

Spreading depolarizations increase delayed brain injury in a rat model of subarachnoid hemorrhage

Hamming AM, Wermer MJ Umesh Rudrapatna S, Lanier C, van Os HJ,
van den Bergh WM, Ferrari MD, van der Toorn A, van den Maagdenberg AM,
Stowe AM, Dijkhuizen RM

J Cereb Blood Flow Metab 2016 Jul; 36(7):1224-31

Abstract

Our study demonstrates that artificially induced SDs after experimental SAH in rats augment delayed brain injury. Our findings are in line with the hypothesis that SDs contribute to the development of DCI in SAH patients,[66] which may be triggered by early brain injury leading to further progression of post-SAH tissue damage.

SAH was induced by endovascular puncture of the right internal carotid bifurcation. After one day, brain tissue damage was measured with T_2-weighted MRI, followed by application of 1M KCl (SD group, N=16) or saline (no-SD group, N=16) to the right cortex. Cortical laser-Doppler flowmetry (LDF) was performed to record SDs. MRI was repeated on day 3, after which brains were extracted for assessment of SAH severity and histological damage.

5.0±2.7 SDs were recorded in the SD group. SAH severity and mortality were similar between the SD and no-SD groups. SAH-induced brain lesions expanded between days 1 and 3. This lesion growth was larger in the SD group (241±233 mm^3) than in the no-SD group (29±54 mm^3) (p=0.001).

We conclude that induction of SDs significantly advances lesion growth after experimental SAH. Our study underscores the pathophysiological consequence of SDs in the development of delayed cerebral tissue injury after SAH.

Introduction

Aneurysmal subarachnoid hemorrhage (SAH) has a poor prognosis.[20] A feared complication is the development of delayed cerebral ischemia (DCI), which occurs in approximately one third of patients. The cause of DCI has been an ongoing matter of debate and suggested mechanisms include vasospasm, (micro-)thrombosis and cortical spreading depolarization.[28, 91] It has been shown in rats that accumulation of the hemolysis products hemoglobin and K^+ in the subarachnoid space can induce spreading ischemia – an inverse hemodynamic response (i.e. transient hypoperfusion) to spreading depolarization in tissue at risk – contributing to expanding cortical infarction.[33] Furthermore, electrocorticography measurements in cortical tissue of SAH patients have revealed spreading depolarizations (SDs) in association with development of delayed ischemic damage.[33]

SDs are slow waves of neural cell depolarization, self-propagating through the cortex at a speed of 2-6 mm/min.[35] Under normal conditions, a SD is a reversible phenomenon accompanied by an increase in perfusion to support restoration of the electrolyte balance.[34] However, SDs may lead to irreversible damage in metabolically compromised brain tissue, such as after SAH or ischemic stroke.[59] In rats, occasional SD-like phenomena have been detected acutely after experimental SAH.[63, 92] In a small series of 13 patients, electrocorticographic activity and perfusion were measured from a strip of opto-electrodes on the cortex after surgery for aneurysm clipping.[66] Clusters of prolonged SDs, accompanied by transient hypoperfusion, were measured in close proximity to ischemic brain damage in five patients.[66]

Despite these observations, a direct link between the occurrence of SDs and (delayed) progression of cerebral tissue injury after SAH has not yet been demonstrated. Therefore, we tested the hypothesis that SDs, artificially induced in rats after SAH, increase delayed brain injury, measured with MRI and histology.

Materials and Methods

Study design

This study was performed in accordance with guidelines of the European Communities Council Directive and approved by the Animal Experiments Committee of the University Medical Center Utrecht and Utrecht University. Data reporting is in compliance with the ARRIVE guidelines (www.nc3rs.org.uk/arrive-guidelines).

A sample size of 16 animals (male Wistar rats (200-250 g); Charles River, Sulzfeld, Germany) per group was *a priori* calculated based on a Chi-square test with a hypothesized SD-induced lesion growth from 200 ± 75 mm^3 to 300 ± 75 mm^3, and 35% mortality before day 3, based on a previous study from our group.[93] Rats were housed under standard conditions and received daily intraperitoneal saline injections. Rats were excluded if no SAH was identified on post-mortem investigation.

An additional six healthy control rats were used in a pilot study to measure the consequences of SD induction in healthy brain.

Subarachnoid hemorrhage model

Rats were anesthetized, endotracheally intubated and mechanically ventilated with 2% isoflurane in air/O_2 (80%/20%). Intracranial endovascular perforation at the bifurcation of the right anterior cerebral artery and middle cerebral artery was induced by transiently advancing a sharpened prolene 3-0 suture through the right internal carotid artery, as described previously.[63] After this, anesthesia was ended and rats were extubated.

Induction and recording of SDs

One day after SAH, rats were endotracheally intubated and mechanically ventilated with 2% isoflurane in air/O_2 (80%/20%) for MRI (see below). Directly after MRI, rats remained anesthetized, and a 2-mm burr hole was drilled in the skull at 2 mm anterior of lambda and 2 mm right of the sagittal suture, and the underlying dura was opened. Laser-Doppler flowmetry (LDF) probes (Moor Instruments, Devon, UK) were positioned at 1 and 2 mm anterior of the burr hole (2 mm right of the sagittal suture) after skull thinning at these positions. A saline-soaked cotton ball was placed in the burr hole. After ten minutes of baseline recording, the cotton ball was replaced by a cotton ball soaked in 1.0 M KCl (pilot study (N=6) and SD group (N=16)) or saline (no-SD group (N=16)). LDF recording was continued for 50 minutes. Distinct transient increases in LDF were scored as SDs by an observer blinded to group assignment.

Sensorimotor function test

Functional status was assessed daily before any procedures with an inclination test (SD group: N=11; no-SD group: N=12).[94] To this end, rats were placed on a triplex plane, of which the horizontal angle was increased in steps until the rat slid down.

MRI of brain lesions

On days 1 and 3 post-SAH, rats were endotracheally intubated and mechanically ventilated with 2% isoflurane in air/O_2 (80%/20%) for MRI on a 4.7T/40cm MR system (Varian Inc., Palo Alto, CA, USA). A 90-mm Helmholtz volume coil and an inductively coupled surface coil (2.5-cm diameter) were used for excitation and detection of radio frequency signals, respectively. The MRI protocol included T_2-weighted multi-echo MRI (repetition time (TR) 3000 ms; echo times (TE) 12-144 ms in twelve 12-ms steps; field-of-view (FOV) 32x32 mm^2; data matrix 256x128; 19 slices of 1 mm; number of acquisitions (NA) 2).

T_2 maps were calculated from a non-linear least squares fitting routine. Images were registered to a reference T_2-weighted image using FLIRT.[95] Lesion regions, characterized by clear T_2 hyperintensity, were drawn using FSL software (3.1.8, University of Oxford, Oxford, UK) by two independent, observers who were blinded to group assignment, from which the intersection was taken. A cortical tissue volume of 2x2x1 mm^3 below the burr hole was excluded from lesion volume calculation to prevent inclusion of tissue that was directly affected by KCl. Lesion growth was calculated as the difference between lesion volumes on day 3 and day 1.

SAH severity scoring

After spontaneous death or after sacrificing of the rat on day 3, brains were perfusion-fixed with 4% paraformaldehyde and removed from the skull. Pictures of the ventral side of the brain were scored according to Sugawara's SAH severity score[96], ranging from 0 (no subarachnoid blood) to 18 (large SAH).

Histology of tissue damage

Extracted brains were stored in phosphate-buffered saline with 0.5 g/L sodium azide (Sigma-Aldrich, St. Louis, MO, USA). We selected brain samples from rats (SD group: N=4, no-SD group: N=5) with different patterns of lesion development after SAH: MRI-detectable lesions on days 1 and 3; MRI-detectable lesions only on day 3; and no MRI-detectable lesions on days 1 and 3. The brains were cryoprotected by subsequent immersion in 15% sucrose (for 48 h) and 30% sucrose solutions (for 48 h). Coronal sections (30 µm) were cut on a freezing microtome, followed by Nissl staining according to standard protocols.[97]

Images of complete coronal sections corresponding with MRI slices were acquired using digital microscopy (Nanozoomer 2.0HT; Hamamatsu, Hamamatsu-shi, Shizuoka-ken, Japan). Further analysis was done on 20X images of four selected regions, characterized by: (i) T_2 hyperintensity on post-SAH days 1 and 3 ('early lesion'); (ii) T_2 hyperintensity only on post-

SAH day 3 ('delayed injury'); and (iii) two contralesional counterparts (regions 1, 2, 3 and 4, respectively, in Figure 4A). Presence of neuronal injury/death, identified by pyknotic cell staining patterns, was scored for each quadrant of the respective regions by an observer blinded to group assignment, resulting in neuronal injury scores ranging from negative to ++++ for each region.

Statistics

A repeated measures ANOVA with post-hoc paired *t*-testing was used to analyze scores on the inclination test. An independent samples *t*-test was used for comparing T_2 values between (sub)groups, and a paired samples *t*-test for comparing T_2 values within individuals. Lesion volumes on MRI and SAH severity scores were compared with a Mann-Whitney U test. Lesion incidence and mortality were analyzed with a Chi-square test. Spearman's Rho was calculated to measure correlation between SAH severity and mortality, and between number of SDs and lesion volume. Values are shown as mean ± SD. A p-value <0.05 was considered statistically significant.

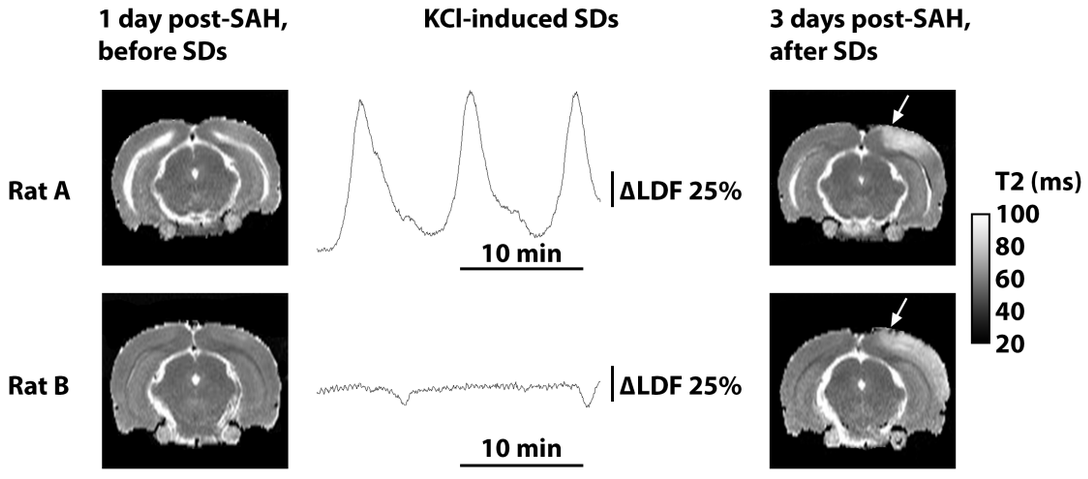

Figure 1. T_2 maps of lesions, and LDF recordings of SDs. T_2 maps of a posterior brain slice at day 1 post-SAH, before SD induction (left panel), and at day 3 post-SAH, after SD induction (right panel), in two rats from the SD group. Arrows indicate the KCl application site (right panel). Middle panel: LDF recordings from the same two rats, showing KCl-induced SDs with associated transient flow increases (top row) or reductions (bottom row (recordings from both LDF probes)). Lesion growth between days 1 and 3 was larger in the animal with SD-associated transient hypoperfusions.

Results

One rat was excluded based on the absence of a SAH on post-mortem investigation, resulting in final sample sizes of 16 (for the SD group) and 15 (for the no-SD group).

In the six healthy control rats, KCl application led to 6.7 ± 1.8 SDs, depicted by transient increases in blood flow as measured during the 50-min LDF recording. MRI of the underlying cortical tissue one day after KCl application showed no signs of tissue damage (T_2 values: 58 ± 1 ms ipsilateral versus 59 ± 1 ms contralateral. In the SD group, 5.0 ± 2.7 SDs were measured in 9 out of 12 surviving rats. Most of these SDs were characterized by transient hyperperfusion (Figure 1, top), similar to the observation in healthy control rats. However, in two rats, we recorded spreading hypoperfusion (Figure 1, bottom). In these two animals, cortical T_2 values below the KCl application site were slightly elevated before SD induction (60 ± 3 ms) as compared to the animals with hyperemic responses (58 ± 1 ms), but this difference was not statistically significant (p=0.32). LDF recordings were unsuccessful in three rats. No SDs were recorded in the no-SD group.

Sensorimotor function, as scored from the horizontal angle on the inclination test, was lower at day 1 (SD group: 35 ± 7; p=0.002; no-SD group: 39 ± 6; p=0.02) and day 3 post-SAH (SD group: 38 ± 7; p=0.01; no-SD group: 40 ± 6; p=0.03) as compared with pre-SAH (SD group: 49 ± 3; no-SD group: 46 ± 3). However, there were no statistically significant differences between the groups.

Mortality, lesion characteristics and SAH severity are shown in Table 1. There were no statistically significant differences in mortality and SAH severity between the SD and no-SD groups.

Lesions, identified as hyperintense tissue on T_2-weighted MR images in ipsi- and contralateral cortical and subcortical areas, had significantly prolonged T_2 values as compared with T_2 values in unaffected tissue (SD group: 52 ± 1 ms; no-SD group: 52 ± 1 ms), at post-SAH day 1 (SD group: 75 ± 7 ms; p<0.001; no-SD group: 68 ± 4 ms; p<0.001) and day 3 (SD group: 62 ± 5 ms; p<0.001; no-SD group: 61 ± 3 ms; p<0.001). Figure 2 shows the lesion incidence maps of the groups at both time points, as well as the lesion growth. Figure 3 shows the lesion volumes of the individual animals at days 1 and 3 post-SAH in the SD and no-SD groups. Lesion occurrence and size were not statistically significantly different between groups at day 1 (before SD induction (Table 1); admittedly this may also be due to the large variations in lesion size. At day 3, the lesion area had expanded, particularly in the SD group, which mostly (but not exclusively) involved ipsilateral cortical regions in both groups (Figures 2 and 3). Lesion occurrence at day 3 was higher in the SD group (100%) as compared to the no-SD group (31%) (p=0.001). Moreover, lesion growth at day 3 was considerably larger in the SD group (241 ± 233 mm^3) as compared to the no-SD group (29 ± 54 mm^3) (p=0.008).

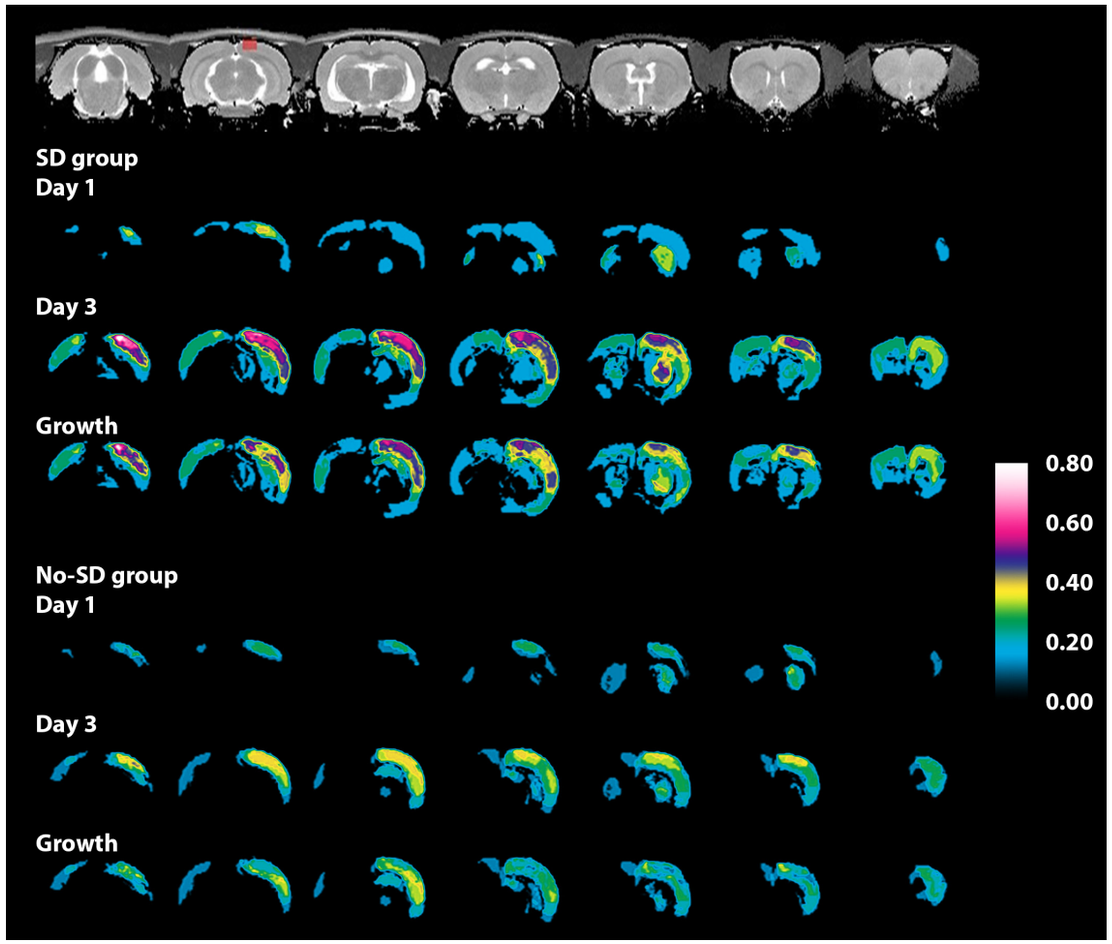

Figure 2. Maps of lesion incidence and growth.
Multislice T_2 maps of rat brain (top row), with the excluded region below the KCl application site in red, and voxel-based representations of fraction of rats with lesioned tissue identified on T_2 maps at days 1 and 3, and the difference between these time-points ('lesion growth'), in SD and no-SD groups. SD = spreading depolarization.

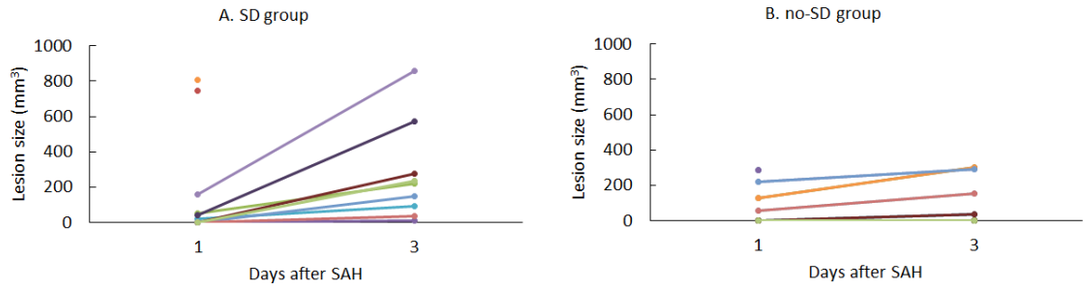

Figure 3. Lesion size. Lesion volumes of individual animals at days 1 and 3 post-SAH in the SD (A) and no-SD groups (B). Each animal is represented by a different color.

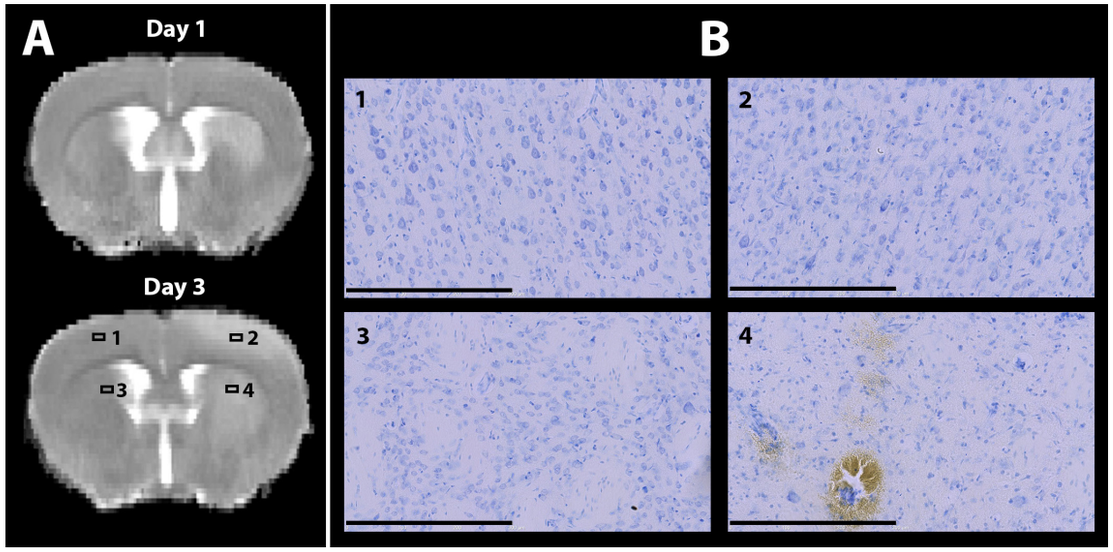

Figure 4. Histology.
A. T_2 maps of a brain slice of a rat from the SD group at post-SAH days 1 (top) and 3 (bottom). A subcortical lesion was present at post-SAH day 1, before SD induction, and a cortical lesion became apparent at post-SAH day 3, i.e. 2 days after SD induction. Regions-of-interest in early injured tissue (region 2), delayed injured tissue (region 4), and unaffected contralesional counterparts (regions 1 and 3, respectively) are displayed in the post-SAH day 3 image. **B.** Nissl-staining of four regions-of-interest (20X magnification) as displayed in fig. 3A. Contralesional regions (1 and 3) show unaffected healthy tissue. Tissue with early injury after SAH (i.e. before SD induction) shows clear signs of blood extravasation into the parenchyma (reddish brown areas), neuronal damage and/or death, as shown by the majority of shrunken, pyknotic nuclei (region 4). The extent of tissue injury is milder in the region with delayed lesion manifestation (i.e. after SD induction) (region 2), with only a few dark, shrunken nuclei interspersed in the parenchyma. Scale bars: 300 μm.

We found no statistically significant correlation between SAH severity and 3-day lesion volume (Rho=0.36; p=0.10) or lesion growth (Rho=0.33; p=0.14). There was a high correlation between number of recorded SDs and lesion growth in the SD group (Rho=0.69, p<0.001).

Because of the large variation in lesion size, we performed a subgroup analysis based on the presence of a small lesion (size of ≤ 20 mm^3) or a large lesion (size of > 20 mm^3) on day 1. The lesion growth in animals with a small lesion at day 1 was significantly larger in the SD group (142 ± 119 mm^3 (N=6)) than in the no-SD group (4 ± 12 mm^3 (N=10)) (p=0.001). In rats with a large lesion at day 1, lesion growth was not significantly different between the SD group (367 ± 298 mm^3 (N=6)) and the no-SD group (114 ± 55 mm^3 (N=4)) (p=0.29); again this may be due to large variation in growth in the SD group.

Lesioned tissue, as identified with MRI on day 1, revealed pyknotic staining patterns with shrunken or absent nuclei on histological sections at day 3 (median injury score: +++) and presence of hemorrhages (Figure 4B, region 4). In lesion growth regions, where tissue lesions were identified with MRI only at day 3, the extent of injury was smaller (median injury score: ++) (Figure 4B, region 2). Neuronal injury was absent in regions identified as non-lesioned with MRI at day 3 (Figure 4B, regions 1 and 3).

Table 1. Mortality, lesion characteristics and SAH severity.

	Day 1 (pre-SD)			Day 3 (post-SD)		
Group	**SD**	**No-SD**	**p**	**SD**	**No-SD**	**p**
Mortality	25% (N=16)	7% (N=15)	0.17	25% (N=12)	7% (N=14)	0.21
Lesion occurrence	50% (N=12)	29% (N=14)	0.26	100% (N=9)	31% (N=13)	0.001*
Lesion size (mm^3)	152 ± 295 (N=12)	49 ± 95 (N=14)	0.35	273 ± 275 (N=9)	60 ± 112 (N=13)	0.008*
Lesion growth (mm^3)	N/A	N/A	N/A	241 ± 233 (N=9)	29 ± 54 (N=13)	0.001*
SAH severity score	N/A	N/A	N/A	11.9 ± 3.4 (N=9)	11.9 ± 2.7 (N=13)	0.84

Day 1 mortality was measured between pre-SAH and post-SAH day 1, i.e. before KCl or NaCl application. Day 3 mortality was measured in the interval between post-SAH days 1 (after KCl or NaCl application) and 3. Lesions were identified as clearly hyperintense brain tissue areas on T_2 maps. Lesion occurrence and size were recorded on days 1 and 3. Lesion growth was defined as brain tissue area with a lesion on day 3 where no lesion was identified on day 1 (which could only be measured in animals that survived until day 3). SAH severity was measured from Sugawara's scoring test.[96]

Discussion

Our study demonstrates that artificially induced SDs after experimental SAH in rats augment delayed brain injury. Our findings are in line with the hypothesis that SDs contribute to the development of DCI in SAH patients,[66] which may be triggered by early brain injury leading to further progression of post-SAH tissue damage.

Cortical SDs have been previously recorded in humans up to two weeks post-SAH,[66] and in laboratory animals within the first hours after SAH.[92, 98] The mechanism leading to SDs after SAH is unknown, but several pathologic conditions such as hypoxia, transient ischemia, high extracellular potassium levels and free hemoglobin may trigger SDs.[28, 59, 99] Under normal, physiological conditions experimentally induced SDs are followed by hyperemia to compensate for the increased energy metabolism. In accordance, we detected clear hyperemic responses with LDF after cortical application of 1 M KCl for less than an hour in healthy control rats, and no signs of tissue injury were detected with MRI one day thereafter. However, since cortical KCl application at higher dosage and for longer duration has been shown to cause direct local tissue damage,[100] we excluded the underlying cortical volume from SAH lesion volume calculations. Nevertheless, possible further effects of KCl on tissue injury development in SAH-affected brain could not be ruled out.

SD-induced hyperemic responses, similar to those observed in healthy control rats, were found after KCl application to the perilesional cortex of rats at 1 day after SAH. However, in two out of nine animals, we detected waves of transient hypoperfusion, which suggests that the underlying tissue was already compromised. This confirms the hypothesis that under pathological conditions, such as after stroke or SAH, paradoxical hypoperfusion can occur after SDs, ultimately leading to ischemic tissue damage.[59, 101, 102] Importantly, SD-induced hypoperfusion may also have occurred outside of our LDF recording region, i.e. in compromised areas with impaired neurovascular coupling, thereby contributing to post-SAH lesion expansion.

Despite large variation in lesion size after SAH, which is a feature of the endovascular puncture model in rats[31], the degree of SAH severity was similar between groups, and we measured statistically significant differences in lesion growth between the SD and no-SD groups. Our study is the first to relate lesion expansion to SDs beyond the first day after SAH in an experimental model. Lesion volume as measured by MRI expanded eight times more after induction of SDs, as compared to conditions without experimentally induced SDs. In a subgroup analysis of rats with small or large lesions on day 1 post-SAH, before cortical KCl or NaCl application, we found that the contribution of SDs to lesion growth was most significant in animals with small initial lesions. This suggests that under pathological conditions SD occurrence in relatively unaffected tissue can have critical impact on remote areas with neuronal or neurovascular impairment.

We did not detect any spontaneous SDs during the relatively short recording time-frame of 1 h. Nevertheless, this does not exclude the occurrence of SAH-induced spontaneous SDs outside of the recording time or outside the observed region. Theoretically, the possible occurrence of spontaneous SDs – conceivably triggered by early brain injury – may have contributed to the 122% delayed lesion growth that was found in the no-SD group, but this could also be explained by other pathological factors that have been previously measured in this rat SAH model, such as vasospasm[96, 103, 104] and luxury perfusion.[93]

Histological analysis revealed clear neuronal pyknosis in all areas identified as lesion areas on T_2 maps at post-SAH day 3, which reflects ischemia-induced apoptosis and/or necrosis. No pyknosis was observed in non-lesioned areas, confirming that absence of MRI-detectable lesions corresponded with intact tissue. The extent of neuronal damage was related to the time of lesion occurrence on MRI, reflecting the different progression of early and delayed injury. However, more detailed histological assessments are required to accurately characterize the status of tissue damage in relation to the different aspects of SAH pathophysiology. Despite the increased lesion expansion, we did not detect statistically significant effects on sensorimotor function between the SD and no-SD groups. This may be related to the relatively crude outcome measure of the inclined plane test, which suggests that more extensive and subtle behavioral tests should be included in future studies.

In conclusion, our study in rats demonstrates that KCl-induced SDs in perilesional cortical tissue aggravate (early) brain tissue damage after SAH leading to augmentation of delayed brain injury. Our animal model of modulation of brain injury by SD induction after SAH may be useful for future studies on the pathogenesis and treatment of evolving brain injury, which may include preclinical testing of therapeutic effects of SD inhibitors.

Acknowledgements

The authors would like to thank Wouter Mol for his biotechnical support, and Lisha Ma, MD, for her contribution to the histological analyses.

Sources of Funding

Dr. Wermer was supported by personal grants from the Netherlands Organization for Scientific Research (ZonMW Veni grant), the Netherlands Heart Foundation (2011T055) and the Dutch Brain Foundation (project 2011(1)-102). This work was partly supported by the Utrecht University High Potential Program (R.M.D.) and the EU Marie Curie IAPP Program “BRAINPATH” (nr 612360) (A.M.J.M.v.d.M.) and the American Heart Association (A.M.S.).

Chapter 3

Valproate reduces brain injury by spreading depolarizations in a rat model of subarachnoid hemorrhage

Hamming AM, van der Toorn A, Rudrapatna US, Ma L, van Os HJ, Ferrari MD, van den Maagdenberg AM, van Zwet E, Poinsatte K, Stowe AM, Dijkhuizen RM, Wermer MJH

Stroke 2017 Feb; 48(2):452-458

Abstract

Background and Purpose

Spreading depolarizations (SDs) may contribute to delayed cerebral ischemia after subarachnoid hemorrhage (SAH). We tested whether SD-inhibitor valproate reduces brain injury in a SAH rat model with and without experimental SD induction.

Methods

Rats were randomized in a 2×2 design and pretreated with valproate (200 mg/kg) or vehicle for 4 weeks. SAH was induced by endovascular puncture of the right internal carotid bifurcation. One day post-SAH, brain tissue damage was measured with T_2-weighted magnetic resonance imaging, followed by cortical application of 1 mol/L KCl (to induce SDs) or NaCl (no SDs). Magnetic resonance imaging was repeated on day 3, followed by histology to confirm neuronal death. Neurological function was measured with an inclined slope test.

Results

In the groups with KCl application, lesion growth between days 1 and 3 was 57±73mm^3 in the valproate-treated versus 237±232mm^3 in the vehicle-treated group. In the groups without SD-induction, lesion growth in the valproate- and vehicle-treated groups was 8±20mm^3 versus 27±52mm^3. On fitting a 2-way analysis of variance model, we found a significant interaction effect between treatment and KCl/NaCl application of 161mm^3 (P=0.04). Number and duration of SDs, mortality and neurological function were not statistically significantly different between groups. Lesion growth on magnetic resonance imaging correlated to histological infarct volume (Spearman's rho=0.83;P=0.0004), with areas of lesion growth exhibiting reduced neuronal death compared with primary lesions.

Conclusions

In our rat SAH model, valproate treatment significantly reduced brain lesion growth after KCl application. Future studies are needed to confirm that this protective effect is based on SD-inhibition.

Introduction

Delayed cerebral ischemia (DCI) is a common and feared complication after subarachnoid hemorrhage (SAH) which occurs in approximately one third of patients.[20] The mechanisms that are involved in DCI development are largely unknown. Spreading depolarizations (SDs) have been suggested to be associated with DCI in experimental and clinical SAH studies.[59]

SDs are waves of depolarizations of neurons and glial cells that spread across brain tissue at a speed of 2 to 6 mm/min.[105] SD is the underlying mechanism of a migraine aura, but may also be associated with other brain diseases. In migraine aura, the tissue recovers from the electrolyte imbalance caused by SDs, presumably through temporary hyperperfusion.[41] However, after an acute ischemic brain insult, such as SAH, SDs may cause permanent tissue injury arising from spreading ischemia because of an inverse hemodynamic response to SD combined with an increased metabolic demand.[33, 59] In a small study of SAH patients who needed surgery for their ruptured aneurysm, SDs were recorded by electrocorticography and seemed associated with the development of DCI.[33] Inhibition of SD is therefore a potential therapeutic approach to prevent brain injury after SAH.

Multiple drugs, including antiepileptic drugs and migraine prophylactics, have SD-inhibiting properties.[36] For SAH patients, nimodipine is the only established drug for the clinical prevention of DCI.[20] Although the mechanism of action of nimodipine has not been elucidated, it has shown to be effective in inhibiting SDs in animal studies.[85, 106] Valproate is another effective SD-inhibiting drug.[87-89] Intraperitoneal injection of valproate was found to decrease lesion size after ischemic stroke in a rat model,[107] where SDs have been shown to contribute to lesion growth.[108, 109] Valproate treatment has also been shown to improve the outcome in a mouse model with SAH induced by subarachnoid blood injection.[110] However, the mechanisms through which valproate may reduce brain injury after SAH remains unknown.

We recently developed a rat model for SD-induced delayed brain injury after SAH.[111] The aim of our study was to investigate whether valproate inhibits post-SAH lesion growth after SAH with and without experimental induction of SDs.

Methods

Study Design

This study was performed in accordance with guidelines of the European Communities Council Directive and approved by the Animal Experiments Committee of the University Medical Center Utrecht. Data reporting is in compliance with the Animal Research: Reporting of In Vivo Experiments guidelines (ARRIVE; www.nc3rs.org.uk/arrive-guidelines). Adult male Wistar rats of 200 to 250 g (Charles River, Sulzfeld, Germany) were housed in a 12-hour light, 12-hour dark cycle and had access to standard laboratory chow and water ad libitum. A sample size of 16 to 17 animals per group was a priori calculated based on the Chi-square test with a hypothesized valproate-induced lesion reduction from 300 (±75) mm^3 to 200 (±75) mm^3 and 35% mortality before day 3, based on previous research from our group.[93] Rats were randomized in a 2×2 design with randomization through an electronically generated list by an independent person with allocation concealment. Animals were treated daily, starting 4 weeks before SAH induction, with 0.2 mL/100 g of 100 mg/mL intraperitoneally administered sodium valproate (200 mg/kg; valproate groups) or saline (with a similar osmolarity and pH as valproate; vehicle groups). Four weeks after treatment onset, SAH was induced in all animals, followed by cortical application of KCl – to induce SDs – (KCl groups) or application of saline – which does not induce SDs – (NaCl groups). The treatment was continued until 2 days after SAH. This resulted in the following groups: valproate-KCl group (N=17); vehicle-KCl group (N=16); valproate-NaCl group (N=17), and vehicle-NaCl group (N=16). Rats were excluded if their body weight dropped below 280 g after pretreatment, and in case no SAH was present on postmortem investigation. Data from the vehicle groups have also been used for an earlier study.[111]

Subarachnoid Hemorrhage Model

Rats were anesthetized, endotracheally intubated, and mechanically ventilated with 2% isoflurane in air/O_2 (4/1). Core temperature was maintained at 37.5ºC using a temperature-controlled heating pad. SAH was induced by intracranial endovascular perforation as described previously.[63] In brief, a stump was created from the right external carotid artery, through which a sharpened 3-0 prolene suture was advanced into the right internal carotid artery to perforate the intracranial bifurcation at the base of the middle and anterior cerebral arteries. After SAH induction, the suture was withdrawn, and temporary clips on the common carotid artery were removed to enable reperfusion, after which anesthesia was ended.

Induction and Recording of Spreading Depolarizations

One day after SAH (and after the first magnetic resonance imaging [MRI] session, see below), a 2-mm burr hole was drilled in the skull at 2 mm anterior to lambda and 2 mm right of the sagittal suture, and the underlying dura was opened. In addition, the skull was indented

with a drill at 1 and 2 mm anterior of the burr hole. A small amount of mineral oil was placed in the indents and a glass fiber probe was placed at each indent, connected to a laser-Doppler flowmetry (LDF) device, which continuously measured cerebral blood flow (CBF) for 1 hour. A cotton ball soaked with saline was placed in the burr hole. After 10 minutes, the ball was replaced by a cotton ball soaked in 1.0 mol/L KCl to induce SDs (KCl groups) or in saline (NaCl groups). LDF recording was continued for 50 minutes. Number of SDs, estimated from distinct, propagating, transient increases or decreases in LDF were scored by an observer who was not present during LDF recording and blinded to group assignments. We also measured the total duration of the LDF response to SD by visually scoring the duration of all flow transients We have previously shown that the KCL-application did not induce MRI-identifiable lesions in rats without SAH.[111]

Sensorimotor Function Test

In subgroups of rats (N=10 [group valproate-KCl], 12 [group valproate-NaCl], 10 [group vehicle-KCl] and 12 [group vehicle-NaC])) we daily assessed functional status with an inclination test.[94] This test assesses a rat's ability to keep from sliding down a triplex plane with increasing horizontal angle, scored by the maximum angle before a rat slid down. The inclination test is a relatively simple and easily applicable test, which we have used in a previous study in rats after SAH.[20]

MRI of Brain Lesions and Perfusion

On days 1 and 3 post-SAH, rats were endotracheally intubated and mechanically ventilated with 2% isoflurane in air/O_2 (4/1) for MRI on a 4.7T/40 cm magnetic resonance system. The MRI protocol included T_2-weighted multi-echo MRI and a flow-sensitive alternating inversion recovery (ITS-FAIR)[112] protocol with a 2-shot gradient-echo echo planar imaging acquisition for perfusion measurement (see Data Supplement).

T_2-maps were calculated from a non-linear least squares fitting routine. Images were registered to a reference T_2-weighted image using Oxford Centre for Functional MRI of the Brain (FMRIB's) Linear Image Registration Tool (FLIRT).[95] In this reference image, regions of interest encompassing the ipsilateral and contralateral sensorimotor cortex and striatum were drawn (by a blinded observer) for cortical and subcortical perfusion measurements. Lesion regions, characterized by clear T_2-hyperintensity, were drawn using FMRIB Software Library (FSL) software by 2 independent observers who were blinded to group assignment. The intersection of both sets of lesion regions was taken for further lesion size analyses. We subdivided lesion regions in ipsilateral and contralateral cortical and subcortical regions for additional analysis. A cortical tissue volume of 3×3×2 mm^3 below the burr hole was excluded from lesion volume calculation to prevent inclusion of tissue that was directly affected by KCL-application. Lesion growth was calculated as the difference between lesion volumes on days 3 and 1 post-SAH. Cerebral blood flow (CBF) was measured in the ipsilateral and contralateral cortical and

subcortical regions after registering the CBF images to the T_2-weighted reference image.[112] Cortical CBF was expressed as percentage of the CBF value in the unaffected subcortical area contralateral to the side of SAH induction.

SAH Severity Scoring

Surviving rats were euthanized on day 3 post-SAH, after MRI, by an intraperitoneal overdose of pentobarbital. Brains were perfusion-fixed with 4% paraformaldehyde and removed from the skull. Pictures were taken from the base of the brain. To score SAH severity, ventral brain images were segmented into 6 segments, followed by SAH severity scoring between 0 (no subarachnoid blood) and 18 (large SAH) according to Sugawara et al.[96]

Histology of Tissue Damage

Extracted brains were stored in phosphate-buffered saline with 0.5 g/L sodium azide. A randomly chosen cohort of brains were used for a separate microthrombi study and was unavailable for histological analysis. From the remaining brains, we selected brain samples from rats (group valproate-KCl, N=6; group valproate-NaCl, N=0; group vehicle-KCl, N=4; group vehicle-NaCl, N=5) with the following patterns of lesion development after SAH: MRI-detectable lesions on days 1 and 3; MRI-detectable lesions only on day 3; and no MRI-detectable lesions on days 1 and 3 post-SAH. Brains were cryoprotected by immersion in 15% sucrose for 48 hours followed by immersion in 30% sucrose solutions for another 48 hours. Coronal sections (30 µm) were serially cut on a freezing microtome, followed by a combined Nissl or Luxol fast blue (LFB) stain.[97] Images of complete serial coronal sections were acquired using digital microscopy. Severity analysis was done on 20× images of 4 or 5 selected regions of interest (ROIs), characterized by: (1) T_2 hyperintensity on post-SAH days 1 and 3 (‘early lesion’); (2) T_2 hyperintensity only on post-SAH day 3 (‘delayed injury’); or (3) no T_2 hyperintensities. Presence of neuronal injury/death, identified by pyknotic cell staining patterns, was scored for each quadrant of each ROI on a scale ranging from 0 to 4 (ie, least to greatest severity) by an observer blinded to group assignment.[111] Total infarct volume was determined using area annotations (μm^2) in NDP view (Nanozoomer Digital Pathology software by Hamamatsu [Hamamatsu City, Japan]) by a second blinded observer.

Outcome Measures

The primary outcome measure (lesion growth) was defined as tissue with a lesion on day 3 where no lesion was seen on day 1 post-SAH. Other outcome measures were sensorimotor function score and mortality. Mortality was determined between pre-SAH and 1 day post-SAH, before SD-induction, and between days 1 and 3 post-SAH, after SD-induction.

Statistics

To assess the effect of SD (KCl versus NaCl) and pretreatment (valproate versus vehicle) on lesion growth, we used a 2-way analysis of variance. The interaction between medical treatment and NaCl/KCl was of particular interest to us because it captures the difference in pretreatment effect between the NaCl and KCl groups. We observed considerable skewedness of the distribution of the lesion growth and possibly also heteroskedasticity between the 4 groups. To account for this, we used the robust Huber-White sandwich estimator for the standard errors. We computed this estimator by fitting a generalized estimating equations (GEE) model in SPSS with the robust option and independent correlation structure.[113, 114] Inclination test scores were analyzed with the same statistical model. Difference in mortality between days 1 and 3 between valproate-KCl versus vehicle-KCl and valproate-NaCl versus vehicle-NaCl groups was analyzed with a Fisher exact test. Spearman’s Rho was calculated to measure correlation between lesion sizes as scored by the 2 observers; between MRI-based and histological lesion volumes; and between T_2-hyperintensity and neuronal injury severity scores. Number of SDs and total duration of the SD-induced LDF change were statistically compared between the KCl groups with an unpaired Student’s *t* test. Cortical CBF values from MRI measurement on day 1 were compared between treatment groups and between ipsi- and contralateral sides with a 2-way analysis of variance. Values are shown as mean±standard deviation. A *P* value <0.05 was considered statistically significant.

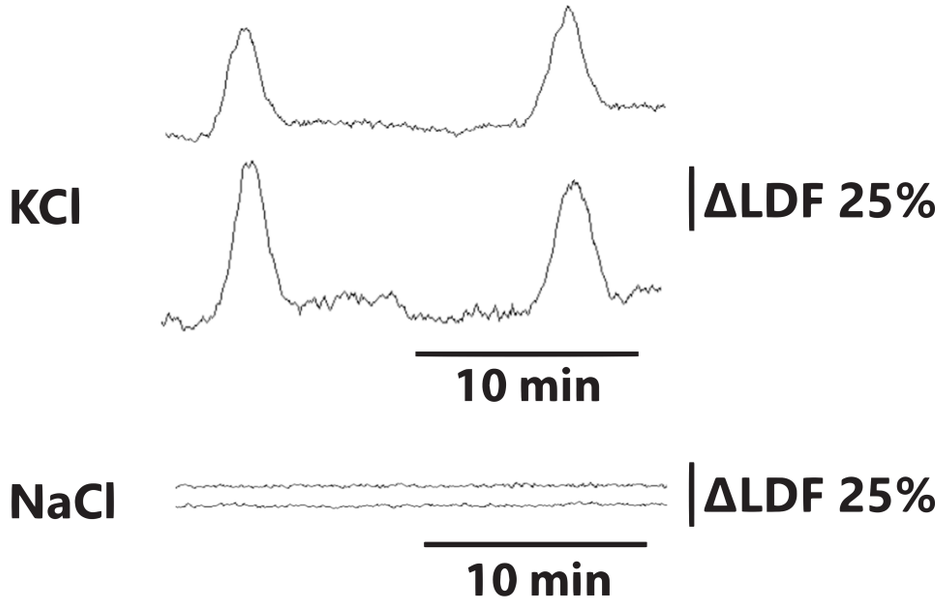

Figure 1. Laser-Doppler flormetry (LDF) recordings. One rat from the valproate-KCl group showing transient flow increases on both probes typical of spreading depolarization (SD) In the NaCl groups, no pattern of transient increases or decreases were seen.

Results

Four rats were excluded because of significant loss of body weight (N=1) or absence of subarachnoid blood (N=3), resulting in the following final group sizes: valproate-KCl group (N=15); vehicle-KCl group (N=16); valproate-NaCl group (N=16) and vehicle-NaCl group (N=15). SAH severity of surviving rats at day 3 was moderate, with group scores of 11±2 (valproate-KCl), 12±3 (vehicle-KCl), 10±3 (valproate-NaCl) and 12±3 (vehicle-NaCl), and no statistically significant differences between groups.

Spreading Depolarizations

In the rats with experimental SD-induction, we measured 4.1±2.9 (valproate-KCl group) and 5.0±2.7 SDs (vehicle-KCl group) (*P*=0.54) during 50 minute recording after KCL-application (figure 1). The average total duration of LDF change was 642±571s in the valproate-KCl group and 1158±508s in the vehicle-KCl group (*P*=0.09). No spontaneous SDs were recorded after cortical saline application in the NaCl groups. Figure 1 shows typical LDF recordings after cortical KCl or NaCl application.

Brain Lesion Development

MRI revealed lesions with prolonged tissue T_2 in ipsilateral and contralateral cortical and subcortical areas, which expanded between days 1 and 3 after SAH (figure 2). Delineated lesions volumes, identified as hyperintense tissue in ipsilateral and contralateral cortical and subcortical areas on T_2-weighted magnetic resonance images, correlated between raters with Rho=0.96 ($P<10^{-5}$). In the groups with SD-induction, lesion growth from day 1 to day 3 post-SAH was 57±73mm^3 in the valproate group as compared to 237±232mm^3 in the vehicle-treated group (figure 3A). In the groups without experimental SD-induction, lesion growth was 8±20mm^3 in the valproate group and 27±52mm^3 in the vehicle treated group. On fitting a 2-way analysis of variance model, we found a significant interaction effect between treatment and KCL/NaCL application of 161mm^3 (*P*=0.04). Analysis of subregions within the lesion territory revealed that statistically significant effects for treatment (*P*=0.004), NaCl/KCl (*P*<0.001) and their interaction (*P*=0.021) were only detectable in the ipsilateral cortical lesion subregion, and not in the other lesion subregions (Table 1.).

Cerebral Blood Flow

On day 1 after SAH, before KCl/NaCl application, cortical CBF values were 134±91% (of reference) in the ipsilateral and 131±86% in the contralateral hemisphere in the vehicle-treated animals. In valproate-treated animals, ipsi- and contralateral CBF values were 111±39% and 96±30%, respectively. There was a significant main effect of treatment on cortical CBF; CBF was lower in valproate-treated rats (*P*=0.04). There was no significant main effect of hemispheric

side (*P*=0.51), and no significant interaction effect between treatment and hemispheric side (*P*=0.69).

Sensorimotor function

Sensorimotor function, expressed by the inclination test score was significantly reduced at 1 (valproate-KCl group:33±7; vehicle-KCl:38±7; valproate-NaCl:38±10; vehicle-NaCl:40±6) and 3 days after SAH (valproate-KCl group:34±6; vehicle-KCl:35±7; valproate-NaCl:36±6; vehicle-NaCl:39±6) as compared with before SAH (valproate-KCl group 46±4; vehicle-KCl:49±3; valproate-NaCl:45±6; vehicle-NaCl:46±3; $P<10^{-4}$ in all groups). There were no significant group differences in the inclination test score change between days 1 and 3 (figure 3B).

Mortality

Figure 3C shows survival in the experimental groups. Between day 1 and 3 post-SAH, none of the 11 rats in the valproate-treated group died after KCL-application, whereas 3 of 11 rats had died in the vehicle-treated group (*P*=0.21). In the NaCl groups, 4 out of 11 rats that had died in the valproate-treated group, and 1 out of 14 rats in the vehicle-treated group (*P*=0.13).

Histology

Histological assessment of neuronal death with Nissl staining showed that lesioned tissue, as identified with T_2-weighted MRI on day 1 post-SAH (early lesion), had pyknotic staining patterns with shrunken or absent nuclei and reduced Luxol fast blue staining, indicative of demyelination, when the rats were euthanized at day 3 post-SAH (Figure 4; neuronal injury severity score 3±1). In regions where tissue lesions were identified with T_2-weighted MRI only at day 3 (lesion growth), the histological degree of injury was generally less severe (neuronal injury severity score 2±1). Neuronal injury was absent in all regions identified as non-lesioned with T_2-weighted MRI at day 3 (neuronal injury severity score 0±0). The neuronal injury severity score was significantly correlated with absent, late or early presence of T_2-lesions (Spearman's rho=0.91; $P=2*10^{-24}$). Histologically measured infarct volumes were significantly correlated with T_2-based lesion volumes (Spearman's rho=0.83; *P*=0.0004), confirming infarction in MRI-identified lesion areas.

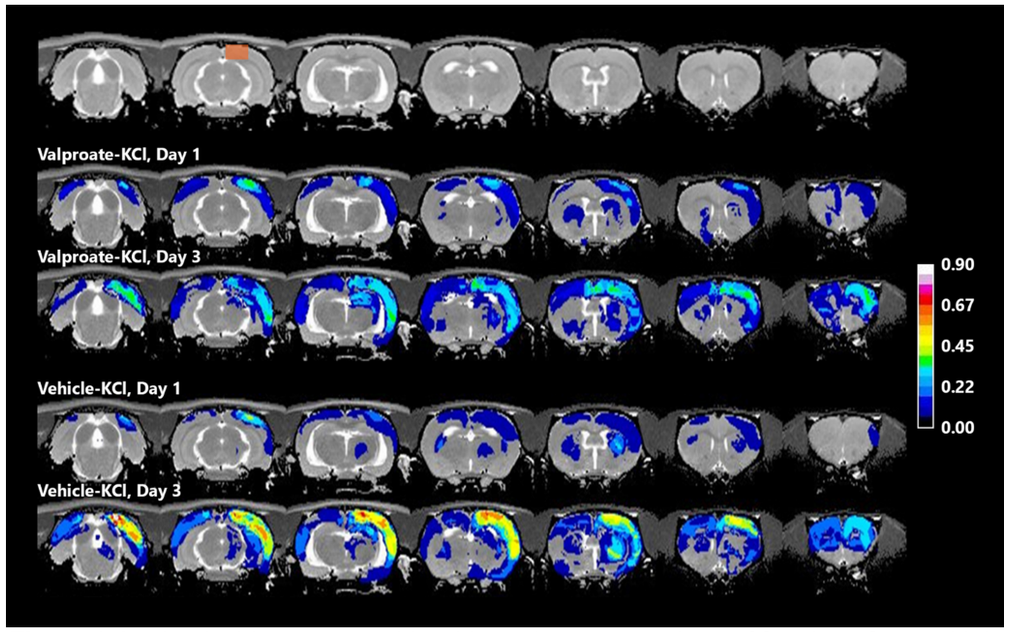

Figure 2. Lesion incidence maps. Voxel-based representations of fraction of rats with lesioned tissue identified on multislice T_2-maps at days 1 and 3 after subarachnoid hemorrhage (SAH), in the KCl-groups with valproate or vehicle treatment, projected over a rat brain T_2 template. The red rectangle overlaid on the rat brain T_2 template (top row) is the area below NaCl/KCL application, which was excluded from analysis. There was significantly less lesion growth in the valproate-treated group than in the vehicle-treated group.

Table 1. Mortality, lesion characteristics and SAH severity.

	Day 1 (pre-SD)			Day 3 (post-SD)		
Group	**SD**	**No-SD**	**p**	**SD**	**No-SD**	**p**
Mortality	25% (N=16)	7% (N=15)	0.17	25% (N=12)	7% (N=14)	0.21
Lesion occurrence	50% (N=12)	29% (N=14)	0.26	100% (N=9)	31% (N=13)	0.001*
Lesion size (mm^3)	152 ± 295 (N=12)	49 ± 95 (N=14)	0.35	273 ± 275 (N=9)	60 ± 112 (N=13)	0.008*
Lesion growth (mm^3)	N/A	N/A	N/A	241 ± 233 (N=9)	29 ± 54 (N=13)	0.001*
SAH severity score	N/A	N/A	N/A	11.9 ± 3.4 (N=9)	11.9 ± 2.7 (N=13)	0.84

Day 1 mortality was measured between pre-SAH and post-SAH day 1, i.e. before KCl or NaCl application. Day 3 mortality was measured in the interval between post-SAH days 1 (after KCl or NaCl application) and 3. Lesions were identified as clearly hyperintense brain tissue areas on T_2 maps. Lesion occurrence and size were recorded on days 1 and 3. Lesion growth was defined as brain tissue area with a lesion on day 3 where no lesion was identified on day 1 (which could only be measured in animals that survived until day 3). SAH severity was measured from Sugawara's scoring test.[96]

For figure 3, please turn over.

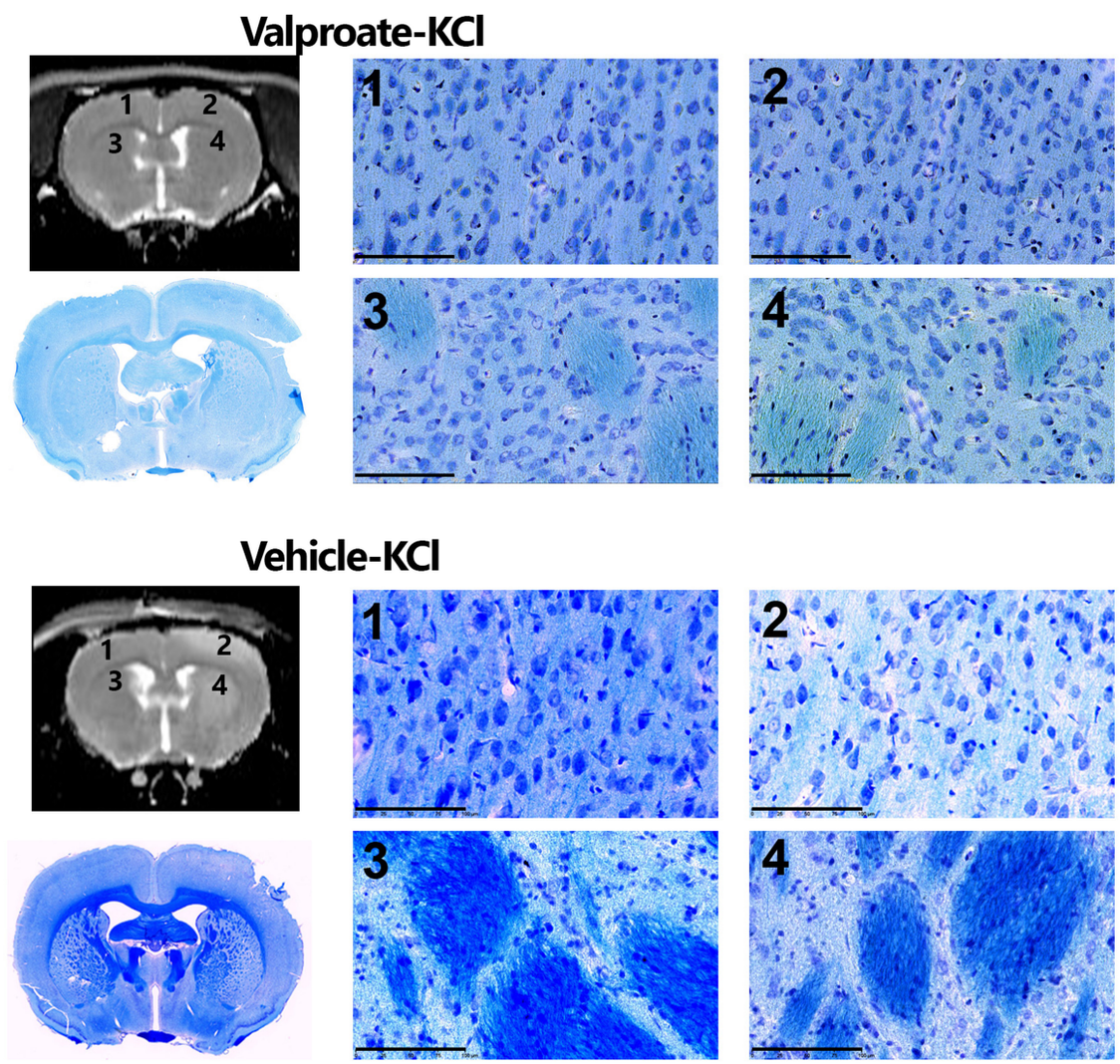

Figure 4. Histology. Data from a rat from the valproate-KCl group and a rat from the vehicle-KCl group. For each rat, the upper left image shows a T_2 map of a coronal slice with four regions of interest. The lower left image shows the corresponding histological section with Nissl and Luxol fast blue staining, from which 40x magnifications of the 4 regions of interest are shown. Shrunken, pyknotic nuclei, indicating neuronal damage and/or death, were clearly observed in tissue with magnetic resonance imaging (MRI)-detectable injury at day 1 (region 4), and to lesser extent in tissue with later lesion manifestation (ie, after spreading depolarization [SD]-induction; region 2). No lesions were detected on the MRI and histology sections of the displayed rat from the valproate-KCl group. Scale bars: 100 µm.

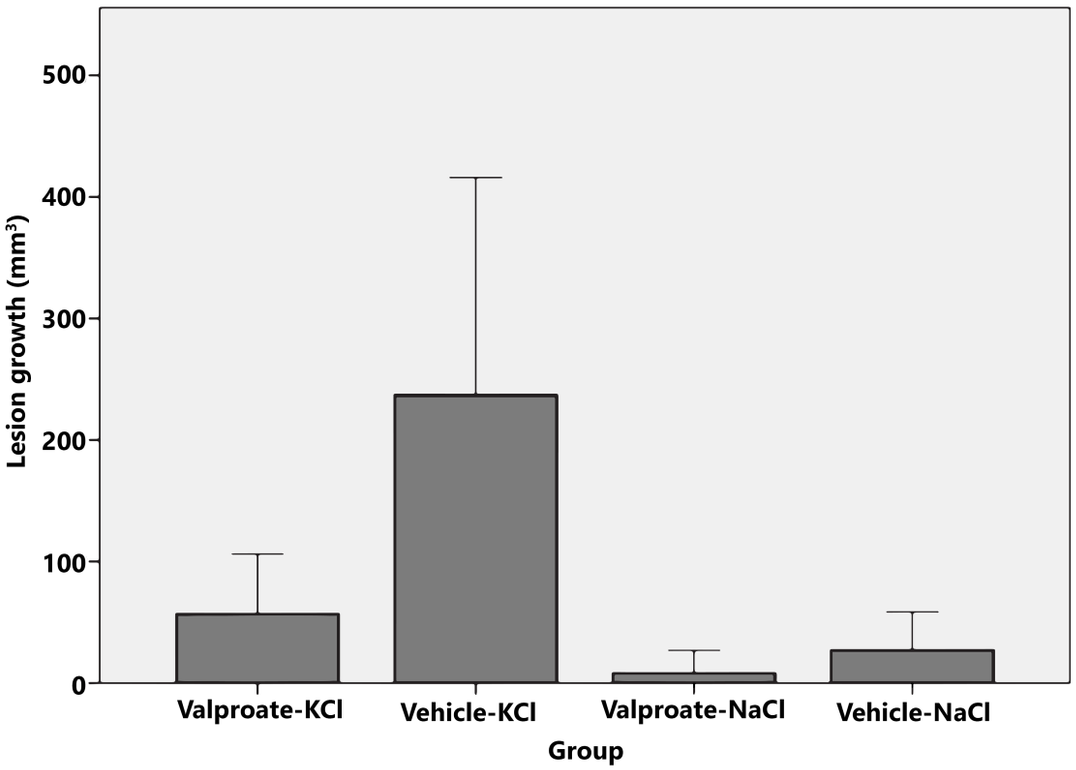

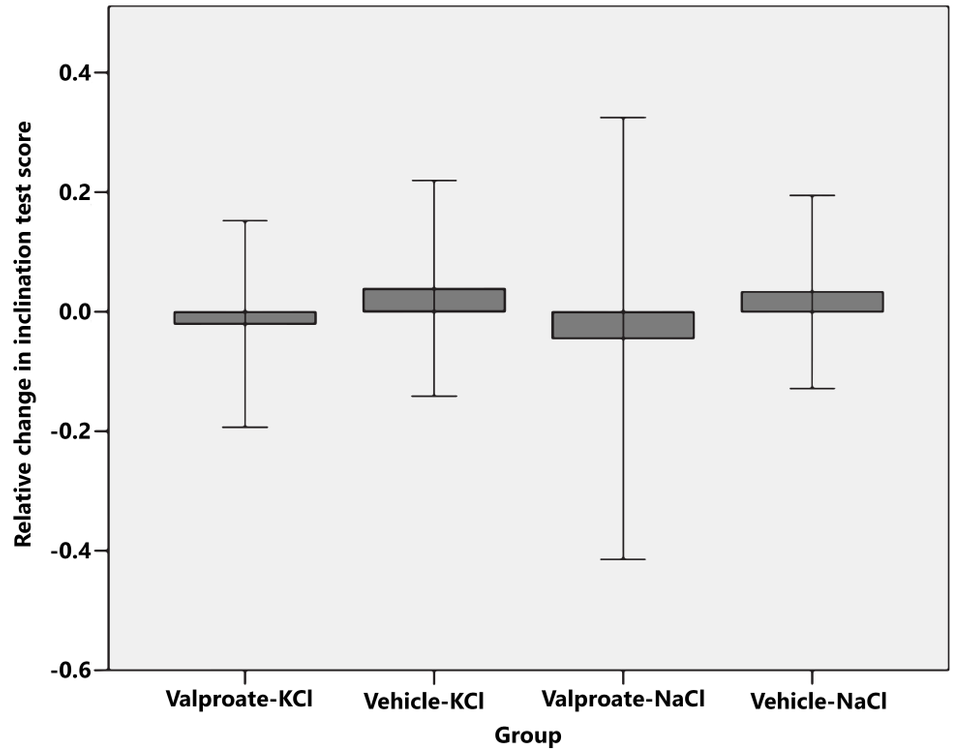

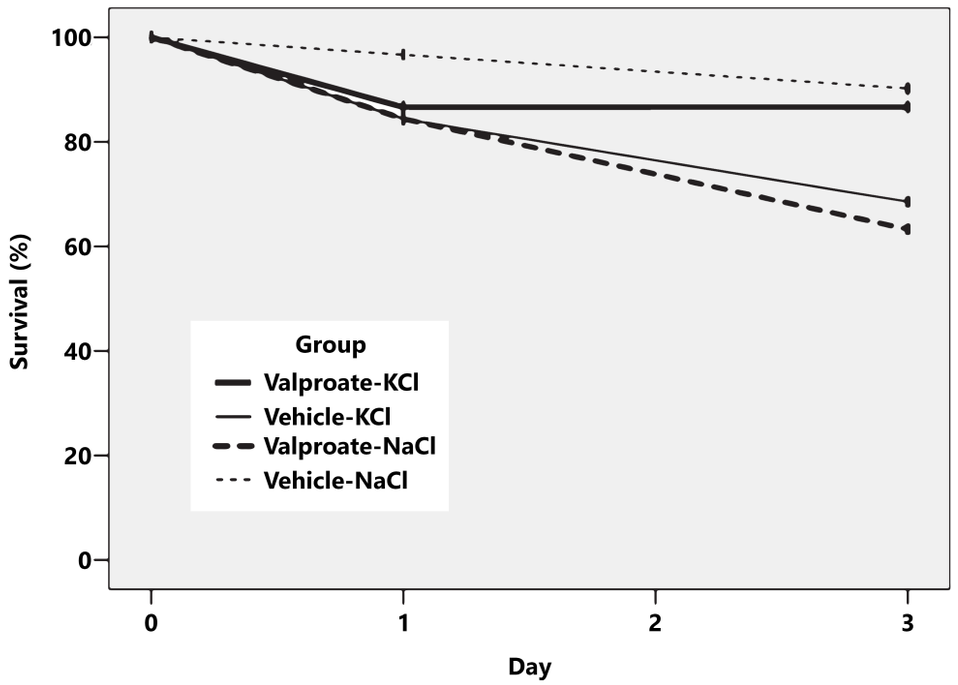

Figure 3. Outcome measures.

***A (above)*,** Lesion growth. Change in lesion volume between days 1 and 3 after subarachnoid hemorrhage (SAH) in the different experimental groups. **P*<0.05 vs. Vehicle-KCl.

***B (right top)*,** Sensorimotor function change. Relative change in inclination test score (mean slope angle at which rats slid down) between days 1 and 3 after SAH in the different experimental groups.

***C (right bottom)*,** Mortality. Percentage of surviving animals between pre-SAH and day 1 post-SAH (before cortical KCl/NaCl application), and between days 1 and 3 post-SAH (after cortical KCl/NaCl application) in the valproate-KCl (N=15) vehicle-KCl (N=16), valproate-NaCl (N=16) and vehicle-NaCl (N=15) groups.

Discussion

In our randomized, vehicle-controlled rat SAH study, treatment with valproate reduced lesion growth after KCL application to induce of SDs. This protective effect was not found in absence of experimental SD induction. We previously reported that experimental SD induction with cortically applied KCl advances lesion growth after SAH in rats.[111]

The mechanism leading to SDs after clinical SAH is unknown, but it may be related to hemolysis products such as potassium.[60] In animal studies, many drugs have been shown to influence occurrence, frequency or duration of SDs through modification of the induction threshold, refractory period, or even SD amplitude or length.[36] We chose valproate as an SD-inhibiting treatment because, after sufficient pretreatment, this drug has proven to be an effective inhibitor of SD.[87-89] One earlier study also reported beneficial effects of valproate treatment after SAH.[110] In that randomized, vehicle-controlled study, valproate administration decreased the number of degenerating neurons and improved neurobehavioral outcome after SAH in mice. However, that study involved a prechiasmatic blood injection model of SAH, without development of delayed injury.[115] Furthermore, a potential SD-inhibiting mechanism was not investigated.

An advantage of valproate for the translation of our results to clinical practice is the long experience with the drug as a therapy in different patient populations. Valproate is prescribed for prevention of epilepsy, migraine, manic episodes, and neurogenic pain in humans.[116] Although the exact pharmacological action of valproate is unknown, it probably acts through multiple mechanisms.[116] Our hypothesis was that valproate directly inhibits the effect of SDs on lesion growth.[36] However, the difference in number and duration of SDs was not statistically significant between the groups. Therefore, valproate may also have indirectly mitigated the effect of SDs through its anti-excitotoxic properties[116] or by influencing (acute) hemodynamics –we did measure a significant treatment effect on cortical CBF before SD induction. We accounted for the effects of valproate early after SAH by selecting lesion growth after day 1 as our outcome measure. Although the effect of valproate on lesion growth was only significantly present in the KCl group, and most pronounced in the cortex ipsilateral to KCL application, an effect through CBF modulation cannot be excluded. Furthermore, one could rationalize that measurement of systemic parameters, such as blood pressure, would have been beneficial to ascertain the efficacy of valproate treatment, but because we performed survival experiments we opted to leave out such invasive procedures.

Our study has several limitations. First, valproate was administered as pretreatment, starting 4 weeks before SAH induction. Future studies should test the potential of valproate, or other SD inhibiting drugs, to reduce delayed brain injury when administered acutely after SAH. Second, we did not detect spontaneous SDs, which may be explained by the relatively short recording time limited to 2 cortical regions. SDs were induced by cortical application of 1 mol/L

KCl close to the lesion site, which may have directly affected lesion development in addition to the SD-induced pathophysiological effects. We accounted for this by excluding underlying cortical tissue from lesion volume calculations. With the current design we cannot exclude effects of perforation-induced focal ischemia on lesion volume, the magnitude of this effect could be established in future experiments by application of KCl to the hemisphere contralateral to the perforation. Third, despite the observed difference in delayed brain injury between the valproate- and vehicle-treated groups, we did not measure significant differences in (changes in) sensorimotor function scores. This may be explained by lack of sensitivity of the inclination test to measure potential subtle effects on neurological function on top of the effect of the SAH and the limited sample size (only a subset of rats was tested). Fourth, the final time point of our study was at 3 days after SAH. This may be too early to represent DCI in SAH patients. Nevertheless, our model in rats – which have higher metabolism than humans – clearly demonstrates development of delayed brain injury in relation to SDs, which was the target for our therapeutic intervention. Finally, the induced brain lesions are likely to be in part because of direct effects on CBF after endovascular puncture, leading to early ischemic injury. This may explain why a relatively large part of the lesion is present in the ipsilateral hemisphere. To assess the effects of valproate treatment on delayed brain injury, and minimize the influence of direct ischemic injury, we used lesion growth after day 1 post-SAH as our outcome measure.

Conclusions

In conclusion, we found that pretreatment with valproate, a clinically prescribed drug, decreases delayed brain injury in a rat model of SAH with experimental SD induction after KCL-application., Future studies are needed to confirm that this protective effect is based on SD induction and to investigate the therapeutic potential of SD-inhibiting drugs in the prevention of DCI in humans.

Acknowledgements

We thank Wouter Mol for his biotechnical support and Christian Lanier for his contribution to the histological analyses.

Sources of Funding:

Netherlands Organization for Scientific Research (Nederlandse organisatie voor gezondheidsonderzoek en zorginnovatie [ZonMW] Veni grant), the Netherlands Heart Foundation (2011T055) and the Netherlands Brain Foundation (project 2011(1)-102; Dr Wermer).

This work was partly supported by the Utrecht University High Potential Program (R.M.D.) and the EU Marie Curie IAPP Program “BRAINPATH” (nr 612360; Dr Van den Maagdenberg) and the American Heart Association 14SDG18410020 (A.M.S).

Supplemental material

MRI protocol

4.7T/40 cm MR system (Varian Inc., Palo Alto, CA, USA). A 90-mm Helmholtz volume coil and an inductively coupled surface coil (2.5 cm diameter) were used for excitation and detection of radio frequency signals, respectively. The MRI protocol included T_2-weighted multi-echo MRI (repetition time (TR) = 3000 ms; echo times (TE) = 12-144 ms in twelve 12-ms steps; field-of-view (FOV) = 32x32 mm^2; data matrix = 256x128; 19 slices of 1 mm; number of acquisitions (NA) = 2 and a flow-sensitive alternating inversion recovery (ITS-FAIR)[112] protocol with a 2-shot gradient-echo EPI acquisition (TR = 10000 ms; TE = 4.8 ms; delay between the 46 images in the inversion curve = 150 ms; flip angle = 10°; FOV = 32x32 mm^2; data matrix = 64x64; slice thickness = 2 mm; selective inversion slab = 10 mm; NA = 16) for perfusion measurement

Manufacturer information

- Laser-Doppler flowmetry (LDF) device: type moorVMS-LDF, Moor Instruments, Devon, UK
- FSL software: 3.1.8, Flitney et al., University of Oxford, Oxford, UK
- Pentobarbital: Alfasan, Woerden, The Netherlands
- Sodium azide: Sigma-Aldrich, St. Louis, MO, USA
- Digital microscopy: Nanozoomer 2.0HT, Hamamatsu Photonics, Hamamatsu-shi, Japan

Chapter 4

Measurement of Distinctive Features of Cortical Spreading Depolarizations with Different MRI Contrasts

Umesh Rudrapatna S, Hamming AM, Wermer MJH,
Van der Toorn A, Dijkhuizen RM

NMR Biomed 2015 May; 28(5):591-600

Abstract

Growing clinical evidence suggests critical involvement of spreading depolarizations (SDs) in the pathophysiology of neurological disorders such as migraine and stroke. MRI provides powerful tools to detect and assess co-occurring cerebral hemodynamic and cellular changes during SDs. This study reports the feasibility and advantages of two MRI scans, based on balanced steady-state free precession (b-SSFP) and diffusion-weighted multi-spin-echo (DT2), heretofore unexplored for monitoring SDs. These were compared with gradient-echo MRI. SDs were induced by KCl application in rat brain. Known for high SNR, the T_2- and T_1-based b-SSFP contrast was hypothesized to provide higher spatiotemporal specificity than T_2^* math formula -based gradient-echo scanning. DT2 scanning was designed to provide simultaneous T_2 and apparent diffusion coefficient (ADC) measurements, thus enabling combined quantitative assessment of hemodynamic and cellular changes during SDs.

Procedures were developed to automate identification of SD-induced responses in all the scans. These responses were analyzed to determine detection sensitivity and temporal characteristics of signals from each scanning method. Cluster analysis was performed to elucidate unique temporal patterns for each contrast.

All scans allowed detection of SD-induced responses. b-SSFP scans showed significantly larger relative intensity changes, narrower peak widths and greater spatial specificity compared with gradient-echo MRI. SD-induced effects on ADC, calculated from DT2 scans, showed the most pronounced signal changes, displaying about 20% decrease, as against 10–15% signal increases observed with b-SSFP and gradient-echo scanning. Cluster analysis revealed additional temporal sub-patterns, such as an initial dip on gradient-echo scans and temporally shifted T_2 and proton density changes in DT2 data.

To summarize, b-SSFP and DT2 scanning provide distinct information on SDs compared with gradient-echo MRI. DT2 scanning, with its potential to simultaneously provide cellular and hemodynamic information, can offer unique information on the inter-relationship between these processes in pathologic brain, which may improve monitoring of spreading depolarizations in (pre)clinical settings.

Introduction

The occurrence of spreading depolarizations (SDs) in cerebral tissue has been implicated in the pathophysiology of various brain disorders, such as migraine, ischemic stroke, subarachnoid hemorrhage and traumatic brain injury.[117] However, the exact mode of action through which SDs affect brain tissue remains unclear. SDs are fronts of profound cellular and electrophysiological changes that propagate slowly across the cortex, regardless of functional or vascular territories. They are characterized by disruption of ion homeostasis, leading to neuronal swelling, distortion of dendritic spines, dramatic reduction in low frequency (i.e. direct current (DC)) extracellular potential and temporary silencing of brain activity (therefore often referred to as cortical spreading depression).[59, 118-120]

SDs result in drastic increase in cellular metabolism and energy requirements, leading to high demands on neurovascular coupling. Recent experimental studies have shown that complex vasomotor responses are trigged by SDs.[121] An intrinsic relationship between the propagation of vasodilation associated with SD, and the nature of the vasculature, has also been observed.[122] Thus, given that hemodynamics are strongly influenced by SDs, and that hemodynamics in turn influence tissue status[121], discerning the various vascular changes that co-occur with cellular changes during SDs can lead to improved monitoring, which may ultimately lead to development of treatment strategies that can contain or mitigate their deleterious effects.

Optical and electrophysiological measurements have provided insights into micro-circulation and neuronal signaling during and after SD propagation[123-125], and form the main basis of what is currently known about these topics. However, besides being fairly invasive, the spatial coverage of these techniques is rather limited, thereby hindering studies on the entire brain. While laser-speckle imaging can overcome this restriction to some extent[126], the recordings are mostly limited to blood flow measurements on the cortical surface. Thus, MRI with its unique repository of varied contrast mechanisms, its whole-brain coverage and its non-invasiveness is well suited to assess different features of SDs over a large spatial extent.

The strong influence SD wields on hemodynamics (i.e. increased tissue oxygenation and perfusion) has previously been exploited using T_2^*-weighted MRI[73, 127, 128], and perfusion imaging[72] in rodent and feline models. Likewise, the profound cellular changes induced by SD have been the target of diffusion-weighted MRI sequences, which allowed detection of transient cell swelling.[77, 92, 129-132]

To gain more insight into the vascular events triggered by SDs, one can use the knowledge gained by the functional MRI (fMRI) community, which seeks answers to similar questions related to the interaction between cellular and hemodynamic events, but in the context of brain function. fMRI studies have revealed that, although T_2^* contrast shows higher sensitivity to blood oxygenation changes (i.e. the BOLD effect) in comparison with T_2 contrast, it is mainly

influenced by large venous structures, especially at low field strengths. However, spin-echo MRI signals have been shown to be mostly sensitive to changes at the microvascular level, which are more closely related to neuronal changes.[133-135] For this reason, spin-echo-based fMRI studies have been suggested for improved spatial and temporal specificity.[136] As in the case of fMRI, a better understanding of the hemodynamics that accompany SDs can be obtained by measuring complementary functional contrasts under similar conditions. We therefore hypothesized that passband balanced steady-state-free-precession (b-SSFP) contrast, owing to its dependence on T_2 and T_1[137-140], would provide higher spatiotemporal specificity in comparison with gradient echo T_2^* contrast in localizing SD events.

In order to gain insight into co-occurring cellular changes during SDs, diffusion-weighted MRI can be included in the imaging protocol. Earlier MRI studies have executed more than one scan (generally T_2^*- and diffusion-weighted imaging), either in succession or in an interlaced manner, to discern the various physiological processes accompanying SDs.[73, 128, 129, 131] However, with this approach, the exact spatiotemporal relationships between the two contrasts cannot be established due to the need for spatially co-registering and temporally interpolating the separate datasets. The capacity to simultaneously acquire multiple contrasts in a single scan can yield direct information regarding the causal relationships between their representative processes. Further, if such contrasts are parametrically quantified, the information they provide can be straightforwardly compared and cross-validated between sessions, groups and other measurements.

Motivated by these ideas, a diffusion-weighted multi-spin-echo MRI scan (denoted as DT2), capable of producing T_2 and ADC maps within 10 s, was developed and deployed to elucidate the simultaneous evolution of T_2 and ADC during the propagation of cortical SDs. Such a scan would provide spatiotemporally co-localized information regarding the inter-connections between hemodynamics (BOLD) and cellular changes in brain (patho)physiology and could help understand the physiological causes behind non-quantitative contrast mechanisms such as b-SSFP.

Studies with optical and electrophysiological measurements have shown that the amount of change observed in various physiological parameters and their timing and duration during SDs are varied.[124] Thus, in this study, we analyzed the temporal characteristics, and to a limited extent the spatial characteristics, of the proposed MRI-based contrasts during SDs, to elucidate the relationships between the observed contrasts and the physiological changes that drive them.

Methods

Animal preparation

Adult male Wistar rats (*n=15*, weighing 250–300 g) were used for the experiments with approval from the Utrecht University Ethical Committee on Animal Experiments. All the procedures followed the guidelines of the European Communities Council Directive. Rats were anesthetized with 4% isoflurane for endotracheal intubation, followed by mechanical ventilation with 2% isoflurane in air/O_2 (2:1) mixture. A cranial window of 2×2 mm was opened in the skull 2 mm anterior and 2 mm lateral of lambda. The dura was carefully opened without causing injury to the underlying brain parenchyma. The exposed brain parenchyma was covered by a small cotton wad drenched in saline. In order to be able to trigger the onset of SDs inside the scanner, a nylon tube (≈1 mm diameter), pre-filled with KCl solution (1 M) was carefully glued to the skull with its opening adjacent to the cotton wad. The other end of the tubing was attached to a 1 ml syringe filled with 1 M KCl solution, which allowed delivery of KCl to the cotton wad on the cortical surface during MRI acquisition.

During MRI scanning, the animals were ventilated with 70% air and 30% O_2 mixed with 2.0–2.5% isoflurane, and body temperature was maintained at 37°C using a temperature-controlled warm water bed. Blood oxygenation and end-tidal CO_2 were monitored throughout the session.

MRI scans

MRI scans were performed on a 4.7 T/40 cm magnet (Varian, Palo Alto, CA, USA). A custom-built (2.5 cm diameter) surface coil was used for both transmission and reception of RF signals. Throughout the duration of the experiments, on a weekly basis, the stability of the scans was monitored using quality assurance measurements[141] using an agarose gel phantom. In each session, after preliminary scans for positioning, shimming and pulse power calibrations, three scans were performed to measure the onset and evolution of SDs. The first scan performed was the combined diffusion and T_2 mapping sequence (DT2). The second and the third scans were nearly equally split between a gradient-echo 3D echo-planar imaging (GE3d-EPI) scan and a b-SSFP scan. All three scanning protocols were developed in-house. The power calibration (for maximum signal-to-noise-ratio (SNR)) was separately performed for each of the scans before the induction of SDs.

DT2 scan

The DT2 scan was based on a multislice multi-spin-echo two-shot EPI sequence with provision for diffusion-weighting. The pulse-sequence diagram for this scan is given in Fig. 1. During acquisition, the diffusion-weighting was turned on only for the first echo. Five successive spin-echoes were acquired without further diffusion-weighting. Since we used a surface coil

for both signal transmission and reception, a pair of adiabatic full-passage hyperbolic-secant inversion pulses replaced the conventional refocusing pulse.[142] Though this increased the minimum achievable echo time in comparison with non-adiabatic refocusing pulses, the delay between the adiabatic pulses was efficiently used for diffusion-weighting. The diffusion gradients were straddled around the two inversion pulses (along with crusher gradients in other directions). This strategy resembles spectroscopic diffusion-weighted sequences[143] but can additionally suppress eddy-current artifacts caused by the diffusion-weighting gradients. The sequence parameters were as follows: echo time (spacing) (TE), 25 ms; repetition time (TR), 1.67 s; interleaves, two; number of echoes, six; averages, one; field of view (FOV), 32×32×12 mm; data matrix, 64×64×10; acquisition plane, axial; diffusion-weighting direction, *x* (lateral). The scan involved sinusoidal (non-cartesian) readout-based *k*-space sampling, in order to reduce the readout duration. The reconstruction was based on fast Gaussian gridding.[144] The temporal resolution of the scan (time per volume) was 3.3 s. The scan protocol changed the diffusion-weighting *b*-value to three different values (0, 300 and 500 s/mm^2), periodically.

Previous studies that assessed diffusion changes alone during SDs used maximum *b*-values in the wide range of 850–1780 s/mm^2 [77, 128, 132] and reported about 20–30% decrease in ADC during SDs. Thus, assuming a normal brain gray matter ADC of 0.65×10^{-3} mm^2/s, with a *b*-value of 500 s/mm^2, one can expect more than 7% increase in diffusion-weighted signal during SDs, compared with baseline. Thus, we decided to use a maximum *b*-value of 500 s/mm^2 and additionally acquire T_2 information. This also facilitated better spatial resolution and coverage (whole brain) with the proposed DT2 scan, compared with most previous studies.

With this scan, ADC and T_2 maps could be obtained at 9.9 s intervals. In each session, the DT2 scan lasted 40 min. The first 10 min of acquisition was used for obtaining baseline data. At the end of the 10th minute, 50 *µl* KCl was slowly dropped on the cotton wad, to trigger the onset of SDs.

Gradient-echo scan

The GE3d-EPI scan was based on EPI in two dimensions and stepped Fourier encoding in the third. As in the case of DT2 scans, the EPI part of the scan was based on non-cartesian (sinusoidal) readout of *k*-space, with reconstruction based on fast Gaussian gridding. The sequence parameters were as follows: TE, 20 ms; TR, 40 ms; interleaves, one; phase encodings (in third dimension), 28; averages, two; FOV, 32×32×14 mm; data matrix, 64×64×28; acquisition plane, axial. Prior to the start of the gradient-echo scan, the cotton wad on the rat head was refreshed with 10 *µl* KCl. The temporal resolution of the GE3d-EPI scan was 2.24 s. The total duration of the GE3d-EPI scan was 40 min.

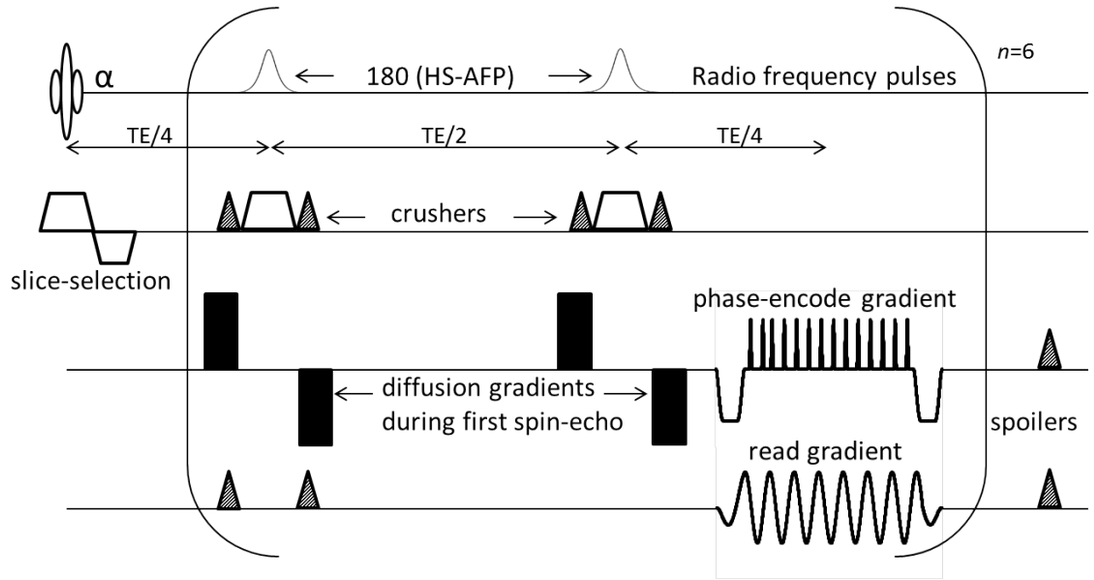

Figure 1. Pulse sequence diagram for the combined diffusion- and T_2-weighted multi-spin echo (DT2) scan with EPI readout. HS-AFP, hyperbolic secant, adiabatic full passage inversion pulse. *α*, flip angle optimized for maximum SNR. Diffusion-weighting gradients are shown in black. Crushers and spoiler gradients are shown in gray.

b-SSFP scan

The b-SSFP scan used in this study was optimized on the sole criterion of minimizing the temporal resolution. At the fastest temporal resolution achievable, the excitation flip angle that provided the highest overall SNR (in the brain region) was empirically determined by acquiring eight datasets with flip angles varying from 5 to 70°. This typically resulted in flip angles around 25–30°, and was used for the SSFP time-series acquisition. The sequence parameters were as follows: TE, 2 ms; TR, 4 ms; phase encodings (PExPE2), 64×24; averages, one; FOV, 32×32×12 mm; data matrix, 64×64×24; acquisition plane, axial. The temporal resolution of the b-SSFP scan was 6.14 s per 3D volume. The b-SSFP scan was executed contiguously without stopping after acquisition of each 3D dataset to maintain the steady-state condition. Prior to the start of the b-SSFP scan, the cotton wad on the rat head was refreshed with 10 *µl* KCl.

MRI data analysis

Processing of GE3d-EPI and b-SSFP data

The spatial resolutions of GE3d-EPI and b-SSFP scans were the same. We also analyzed these data in the same manner to compare their signal characteristics. After reconstruction, brain masks were generated and split manually into ipsilateral (KCl application side) and contralateral hemispheres. Since the rats were well anesthetized (2–2.5% isoflurane), no motion-correction had to be applied to the datasets. The temporal data from brain voxels were filtered using a robust smoothing procedure[145] and de-trended. From these data, modified *Z*-scores (0.6745*(x(t)-*median*)/*median absolute deviation* (MAD))[146] were calculated at each voxel location in the temporal dimension. The temporal changes in signals, expressed as percentages of median values, were used for statistical analyses.

Knowing that substantial signal increases are expected in gradient echo images in response to SDs,[73, 127, 128] only ipsilateral time series with a maximum *Z*-score greater than 1.64 ($p<0.05$) were further analyzed using a peak-finding algorithm.[147] For every peak detected in a time series, a 5 min window of data (2.5 min on each side of the peak) was retained for statistical analysis of peak amplitude and duration. To visualize the movement of SDs, the temporal *Z*-score evolutions were spatially filtered using a 3D Gaussian kernel with standard deviation of 0.25 mm and converted to movies.

Processing of DT2 datasets

After data reconstruction, generation of brain masks and separation into ipsilateral and contralateral hemispheres as described earlier, the DT2 datasets were processed in two stages. Given that estimation of both T_2 and ADC can be biased at low SNRs[148, 149], the first stage was used to perform spatial smoothing of the raw data. Conventional spatial smoothing can result in loss of SD-related information since SDs affect spatially specific voxels at a time. Thus, we decided to perform anisotropic spatial smoothing.[150, 151] For this study, the weights for spatial smoothing were based on the temporal correlations of T_2 and ADC among neighboring voxels. For this, estimates of the underlying ADC, T_2 and proton density were obtained from a linear least-squares fit to the DT2 data with a moving window of 120 s duration, with window shifts of 10 s. From these, the temporal correlations (of T_2 and ADC) between each voxel and its neighbors in a 3×3×3 grid were calculated.

For performing anisotropic spatial smoothing, the raw data time series at each voxel location was normalized using the median proton density (PD) (over time), to bring the signal amplitude of all voxels to the same scale. Then, in the 3×3×3 grid around every voxel location, the sum of correlations in T_2 and ADC values with those of the central voxel were assigned as spatial smoothing weights. Only those neighbors with both correlations above 0.1 were used for smoothing. Finally, the weighted sum of neighboring time series was added to the time series of the voxel under consideration, to obtain a smoother DT2 dataset.

In the second stage, these noise-reduced DT2 datasets were used to obtain temporal evolutions of ADC, T_2 and PD. In this stage, the parameters were estimated using the more accurate (but computationally more expensive) non-linear least-squares fit in a moving window manner, with window width of 70 s and step size of 10 s. The temporal evolutions of the three parameters at each voxel location were then converted to modified *Z*-scores and the relative signal changes were expressed as percentages of the median and used for all further statistical analyses. Since SDs have been shown to induce reductions in ADC[73, 128], we subjected ADC data to a valley-picking (instead of peak-picking) procedure as described above. T_2 and PD changes co-occurring in the same temporal window as ADC changes were used for all analysis (i.e., T_2 and PD did not undergo peak-picking on their own). In order to mitigate the effect of moving window temporal smoothing, the obtained ADC valley patterns were de-convolved with the moving window boxcar function using Lucy–Richardson deconvolution[152] and were separately analyzed as well. To visualize ADC, T_2 and PD evolutions, their *Z*-score data were re-sampled to isotropic 0.5 mm voxels, and converted to movies.

Statistical analysis

To compare the sensitivity of the proposed imaging protocols with SDs, and to compare their temporal characteristics, the maximum relative signal changes and the full-width at half-maximum (minimum in the case of ADC) (FWHM) were calculated for each data pattern at four different *Z*-score thresholds, 1.64, 2.33, 2.58 and 3.09 (corresponding to *p*-values 0.05, 0.01, 0.005 and 0.001, respectively) and analyzed using *t*-tests. Further, to quantify the effect of different scans on the signal changes, robust, non-parametric Cliff's δ effect sizes[153, 154], which are valid under non-normality and variance heterogeneity, were estimated.

In order to discern if different temporal evolutions were found in the different contrasts, *k*-means clustering was performed on the peak waveforms obtained from GE3d-EPI and b-SSFP signals and the parameters (ADC, T_2 and PD) obtained from the DT2 scans with data obtained at a *Z*-threshold of 2.33. This was performed after up-sampling all the waveforms to 1 s resolution using spline interpolation, and aligning their peak (valley) positions. Since the target of cluster analysis was to separate temporal profiles of the signals rather than their actual magnitudes, the waveforms were scaled to unit height before clustering. For example, if $x(t)$ represents the peak waveform in terms of percentage of baseline, then the scaling was performed as $(x(t)-100)/(max(x(t))-min(x(t)))$. In order to obtain robust results, clustering was repeated 200 times (replicates) for each dataset, with different starting cluster centroid positions.

The SNR obtained with the three scanning protocols in the contralateral (to the site of KCl application) dorsal cortex was assessed by taking the temporal median of the ratio between the mean signal average (in the dorsal cortex) and the standard deviation of manually delineated noise-only voxels.

The movies created from the three scans were analyzed to calculate the speed of travel of SD waves across the cortex from the site of KCl application to the tip of the cortex.

Results

From the 15 animals used in this study, data from 21 DT2 sessions (four animals were scanned twice and one animal was scanned three times), 13 GE3d EPI sessions and 15 b-SSFP sessions of 40 min duration each contributed towards the analysis.

Example movies created to visualize the movement of SDs on the rat brain's cortical surface are provided as supplementary information (Movies 1–3), with one dataset from each scan. They represent modified *Z*-scores in the range of 1.5–4 (1–3 for DT2 contrasts). Movies from most datasets revealed clearly distinguishable waves of signal intensity changes in b-SSFP and GE3d-EPI scans and ADC changes in DT2 scans, propagating from the region of KCl application, up to the frontal cortex. The frequency of occurrence of SD events during a 40 min observation window was assessed by manually counting the SD events in the movies (summarized in supplementary information Table S2). Most datasets contained three or four SD events. The time taken by SD waves to travel over the cortex (approximately 12 mm in length) was also assessed from the same movies, and was found to be around 4–4.5 min (see supplementary information Fig. S1), thereby indicating a travel speed of around 2.7–3 mm/min. This compares well with earlier reports.[120]

Fig. 2 shows representative voxel time series data obtained using the three different scans in different rats, where the effect of SDs on the signals is clearly visible. The top and middle time series in Fig. 2 represent signal amplitudes in a voxel of GE3d-EPI and b-SSFP scans. Peaks in signal intensity reflect the passage of SD through that voxel. The bottom time series in Fig. 2 represents ADC changes induced by SD in a voxel in one of the DT2 datasets, where ADC declines mark occurrences of SD. One can appreciate the high SNR afforded by the b-SSFP scan, albeit at a lower temporal resolution than the GE3d-EPI scan. In fact, the SNR was high enough to detect the traversal of SDs without any processing in the b-SSFP datasets, unlike the case for GE3d-EPI datasets. Results from the SNR analysis on the three different datasets (summarized in supplementary information Fig. S2) revealed that, while GE3d-EPI datasets had an average SNR of around 25 (at each time point), b-SSFP datasets had an average SNR of 64. After normalization for varying temporal resolutions (2.24 s for GE3d-EPI and 6.14 s for b-SSFP), the b-SSFP datasets seemed to have about 50% higher SNR than GE3d-EPI datasets.

Fig. 3 shows representative SD-related *Z*-score activation maps from GE3d-EPI, b-SSFP and DT2 (ADC) datasets, overlaid on their corresponding anatomical images. The bright yellow regions represent strong positive T_2^*, T_2-weighted signal increases relative to baseline, during the passage of SD in the case of GE3d-EPI and b-SSFP datasets, respectively. ADC changes in the DT2 dataset are presented with a change in sign for easier visualization. The corresponding changes in T_2 and PD in the same dataset were relatively small, and hence have not been shown. Such signal/parameter changes were found mainly in the ipsilateral

hemisphere (i.e. on the side where KCl was applied) and propagated over the cortex anteriorly, posteriorly, medially and laterally. Supplementary Figures S3, S4 and S5 portray the spatial traversal of SD as captured in representative GE3d-EPI, b-SSFP and DT2 (ADC) datasets.

The number of peak (valley in the case of ADC) waveforms collected from the three different scanning protocols at four *Z*-thresholds are summarized in supplementary information Table S1, and indicates that a large number of samples (6000–70 000) were available for amplitude change and FWHM analysis. Estimates of these parameters at two (out of the four) *Z*-thresholds are presented in Fig. 4. Higher signal increases were found in b-SSFP scans in comparison with GE3d-EPI scans at all *Z*-thresholds. DT2 data revealed even stronger responses to SDs, as decreases in ADC significantly exceeded the increase in signals observed with both GE3d-EPI and b-SSFP. Also, smaller FWHMs were observed in b-SSFP and deconvolved ADC signals in comparison with GE3d-EPI signals at all *Z*-thresholds. b-SSFP and deconvolved ADC waveforms showed similar FWHMs.

From the knowledge of the total number of peak waveforms detected under different contrasts at different *Z*-thresholds (Table S1), and by the estimated number of SDs contributing to these waveforms (by visual counting of SD events), we estimated that the average number of voxels highlighted in response to a single SD event under b-SSFP scans was restricted to about 75% of the volume highlighted with GE3d-EPI scanning. Moreover, increasing *Z*-threshold during peak-detection (from 2 to 4.7 in seven steps) revealed a greater drop-out rate for GE3d-EPI waveforms than b-SSFP, thereby hinting at possible lower spatial specificity in GE3d-EPI responses.

Table 1 summarizes the Cliff's δ effect size estimates obtained by pairwise comparisons of signal change and FWHM among contrasts at two *Z*-scores. Cliff's δ is a non-parametric measure of effect size that ranges from -1 to 1 and represents the degree of overlap (0 indicating complete overlap and ±1 indicating no overlap) in the populations of the samples being compared. While we find significant differences in peak amplitude changes across scans, in particular between GE3d-EPI and ADC (deconv.) and b-SSFP and ADC (deconv.), the effects are much smaller in the case of FWHM measurements. We find minimal differences in FWHM between b-SSFP and ADC (deconv.), and the biggest differences were between GE3d-EPI and ADC (deconv.).

To study the temporal profiles of various signals and parameters in detail, peak waveform examples at a *Z*-threshold of 2.33 were chosen. Fig. 5 (A)–(E) summarizes the results obtained from different contrasts as a plot of median ± median absolute deviation (MAD) of the corresponding peak waveforms. Although the b-SSFP signal response (Fig. 5B) is narrower and slightly elevated in comparison with GE3d-EPI signals (Fig. 5 (A)), the shapes of the temporal profiles look similar. The PD changes (Fig. 5 (E)) resemble ADC changes (Fig. 5C). However, T_2 changes (Fig. 5D) seemed less specific.

Results from the *k*-means cluster analysis are presented in Fig. 5(F)–(J), showing the median temporal waveform corresponding to the first three major clusters. The percentage of total peak waveforms contributing to each cluster under different contrasts is summarized in supplementary Table S3. We found that in all the contrasts the first three major clusters were able to account for 72% or more contributing waveforms. Fig. 5(F) and (G) reveals several sub-patterns within GE3d-EPI and b-SSFP scans, respectively. In particular, two clusters in b-SSFP (clusters 1 and 2), and more predominantly cluster 2 corresponding to GE3d-EPI scans, indicate an initial signal dip with respect to the baseline. This indication was also evidenced by patches of negative *Z*-scores preceding the arrival of the signal peak in several voxel locations in the movies of GE3d-EPI *Z*-scores. Fig. 5(H) reveals that ADC changes also showed distinct modes, with cluster 1 showing a pronounced increase in ADC before the decrease associated with SD, while cluster 3 shows a post-SD overshoot. Similarly, Fig. 5(J) also indicates possible patterns of increased relative PD before (cluster 3) or after (cluster 1) the onset of the main response. Most of these patterns were visible in movies of the corresponding parameters. The minima in clusters 1 and 3 occur a few seconds before or after the minimum in ADC. Although in Fig. 5(I) T_2 signals from the three clusters look dissimilar at the outset, they show similar patterns at different time points; i.e., they seem to represent certain phenomena taking place with various lags.

Table 1. Cliff's δ estimates for comparisons of maximum percent signal change (PSC) and FWHM between scans. Boxplots of the corresponding data are depicted in Fig. 4.

	Z=2.33		Z=3.09	
	PSC	FWHM	PSC	FWHM
GE3d-EPI vs b-SSFP	0.18	-0.12	0.18	-0.16
GE3d-EPI vs ADC (deconv.)	-0.64	0.17	-0.57	0.08
b-SSFP vs ADC (deconv.)	-0.43	0.013	-0.35	-0.1

Table S1. Number of peak waveforms at various Z-thresholds detected using a peak-picking algorithm. These waveforms were used in the analysis reported in Fig. 4.

	Z-threshold			
Scan	1.64	2.33	2.58	3.09
GE3D-EPI	61081	33774	27726	19246
b-SSFP	44545	23594	18931	12320
DT2	70531	24116	15536	6140

Table S2. Frequency table of number of spreading depolarization events observed (in 40min) from 28 combined GE3d-EPI and b-SSFP datasets, visually observed to contain 73 SD events in all.

# SD	%
1	17.4
2	8.7
3	34.8
4	26.1
5	8.7
7	4.35

Table S3. Percentage of samples contributing to various clusters reported in Fig. 5.

	Cluster Number				
Scan	1	2	3	4	5
GE3D-EPI	32	31	23	12	3
b-SSFP	39	25	22	10	4
ADC (DT2)	25	25	22	21	8
T2 (DT2)	26	25	22	14	14
PD (DT2)	28	26	25	12	9

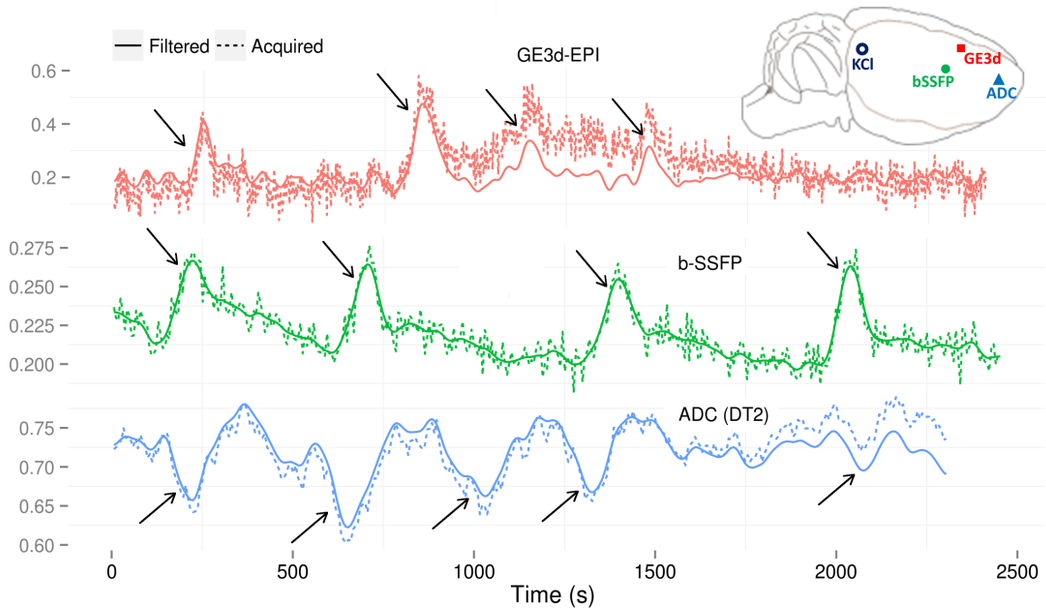

Figure 2. Example time-series of different MRI contrasts (from different datasets) and their filtered versions. The *y*-axis scales are arbitrary for b-SSFP and GE3d-EPI, while ADC is in 10^{-3} mm²/s. The arrows point to instances of passage of SD. The locations corresponding to the site of KCl application, and the regions from which the time series were sampled from the datasets are marked on the inset rat brain schematic diagram.

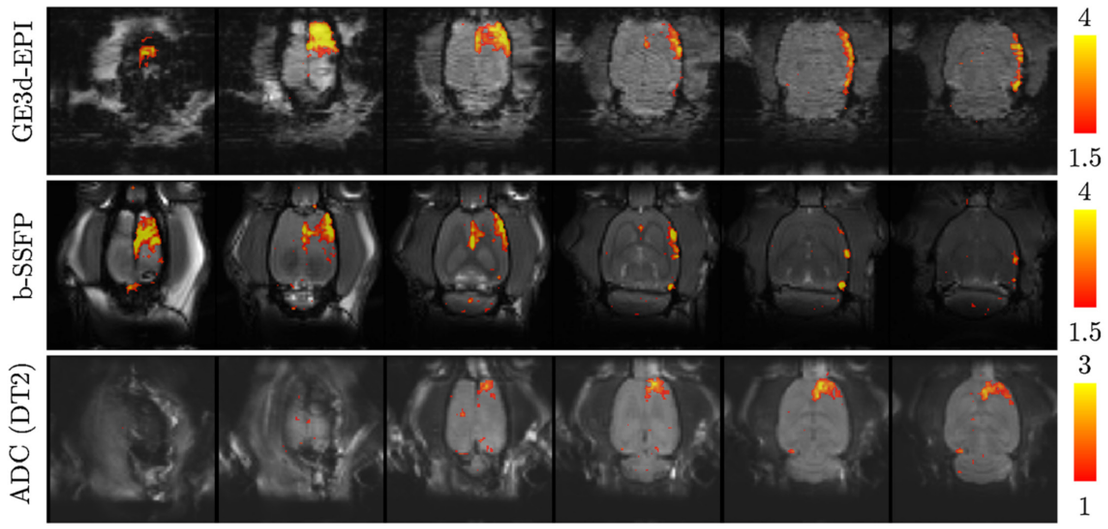

Figure 3. *Z*-score activation maps from gradient echo, b-SSFP and DT2 scans (from different animals) highlighting the passage of a single SD event, overlaid on corresponding anatomical slices (in axial orientation, left to right: top to bottom slice).

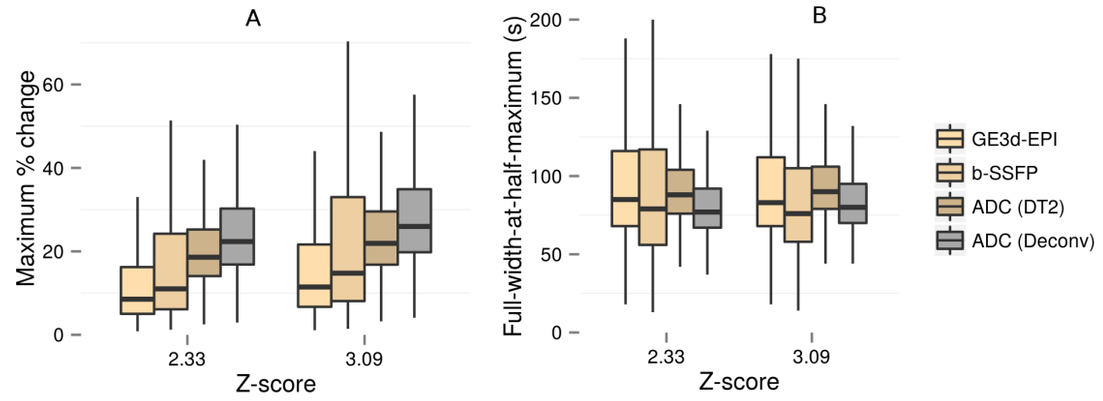

Figure 4 (above). Maximum peak deviations from baseline (A) and FWHM (B) of SD-related peak waveforms obtained from GE3d-EPI, b-SSFP and ADC (DT2) and deconvolved ADC patterns. GE3d-EPI and b-SSFP signal changes were increases, while ADC (DT2 and deconv.) represent reductions from baseline. Most *t*-tests between pairs of measurements revealed significant ($p<0.05$) differences in peak deviations and in FWHM at all *Z*-thresholds.

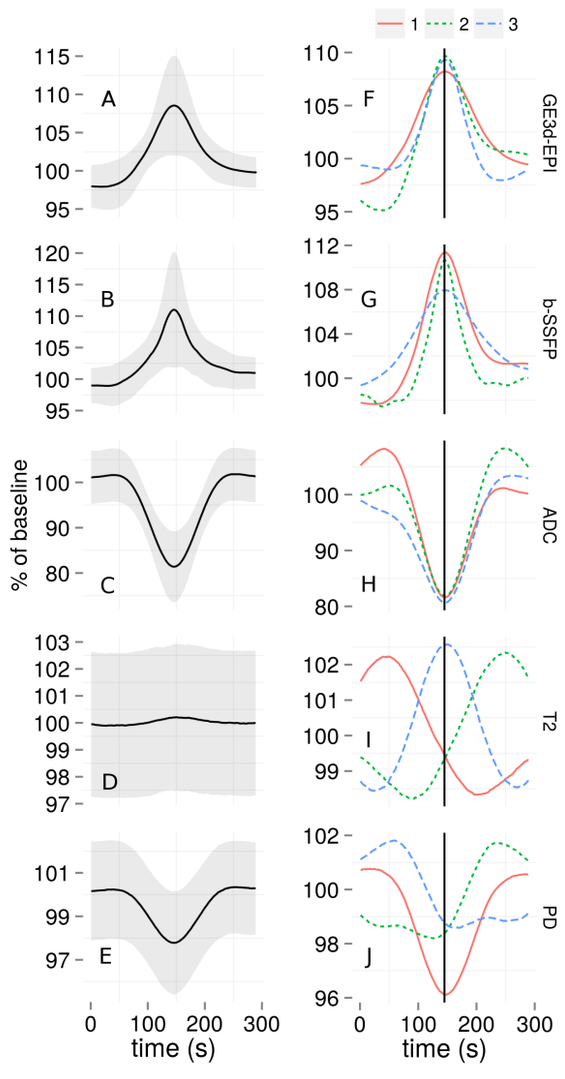

Figure 5. (A)–(E) Temporal evolution of various contrasts during SDs as measured from GE3d-EPI (33 774 waveforms) (A), b-SSFP (23 594 waveforms) (B) and DT2 (24 116 waveforms) ADC (C), T_2 (D) and proton density (E), expressed as median ± median absolute deviation (MAD). GE3d-EPI and b-SSFP peaks had $Z>2.33$ and ADC (DT2) minima satisfied $Z<-2.33$. (F)–(J) Median temporal evolution of the first three major clusters obtained from *k*-means cluster analysis of the same data: GE3d-EPI (F), b-SSFP (G), ADC (H), T_2 (I) and PD (J).

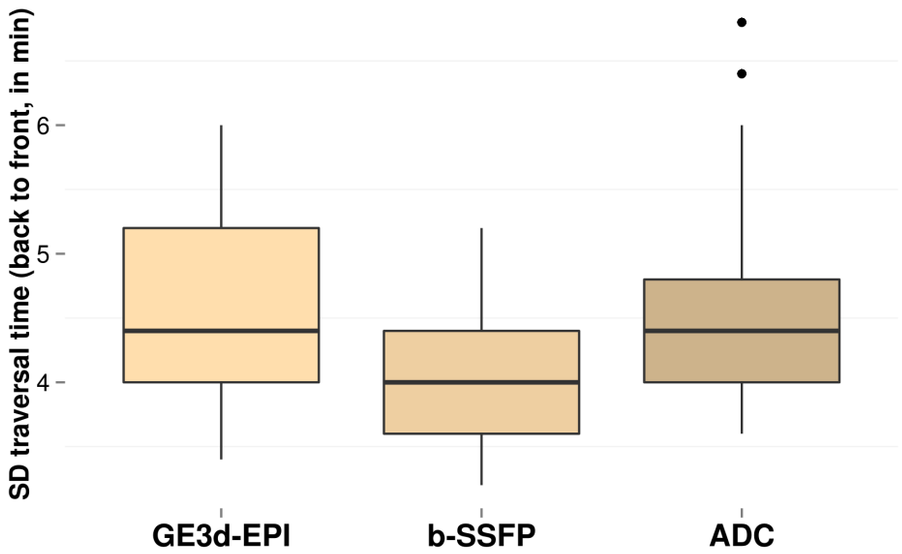

Figure S1. Estimated time for traversal of spreading depolarization events on the cortex (posterior to anterior) in min, as observed from the three scans.

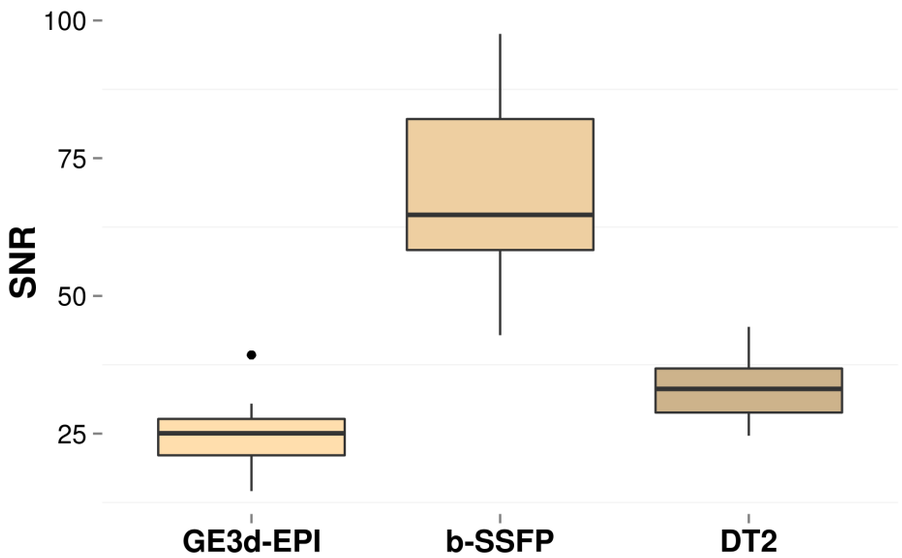

Figure S2. Estimated SNR (mean signal/noise-SD) in the contralateral side of dorsal cortex (median over time) obtained from the three scans. Regions containing CSF were excluded from the analysis.

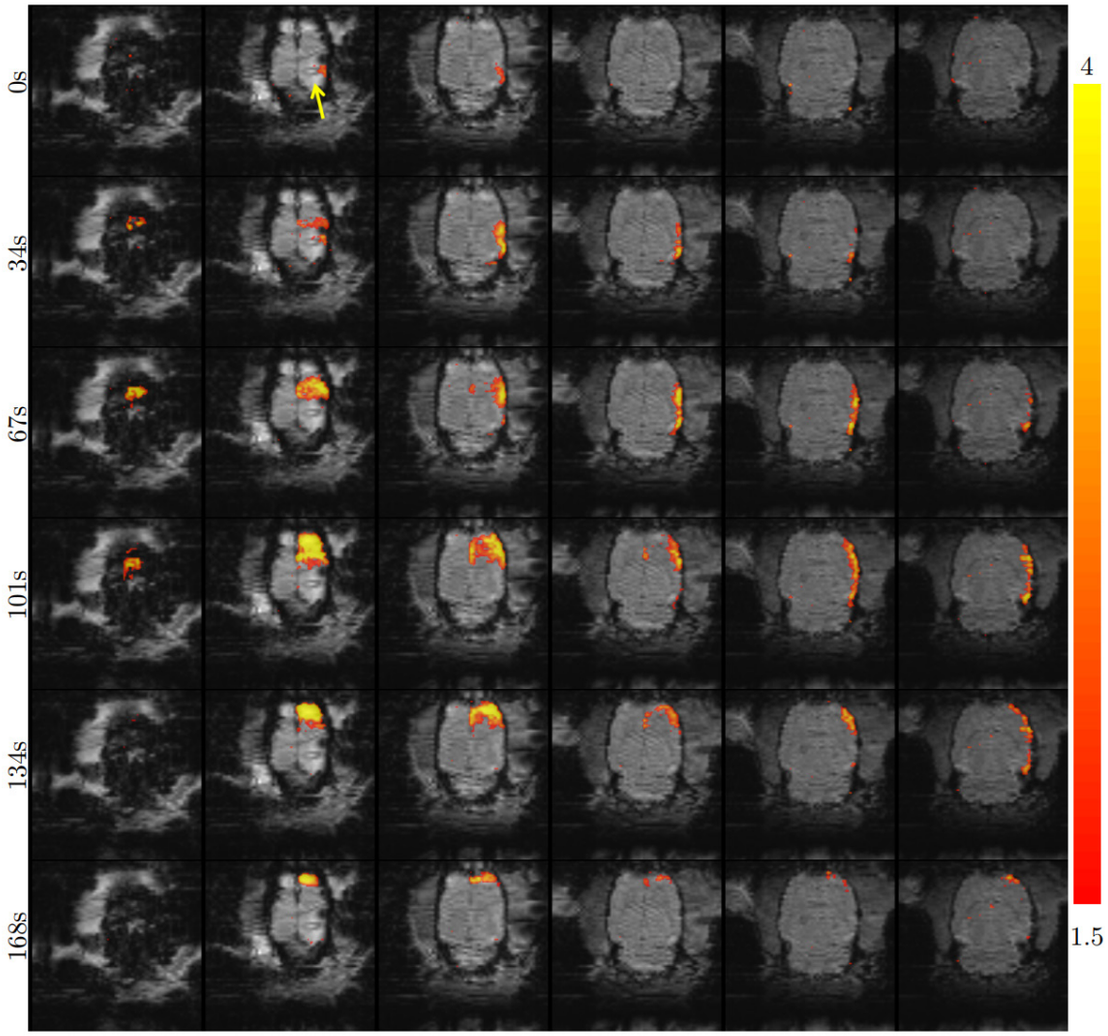

Figure S3. Representative images from six axial slices (left to right: top slice to bottom slice) of one of the GE3d-EPI datasets at different time points depicting the movement of a spreading depolarization (the yellow arrow points to the induction site). The sets of images (top to bottom) were captured with a difference of 33.6s each and cover a span of 168s. Relative time stamps are marked on the left side of each set.

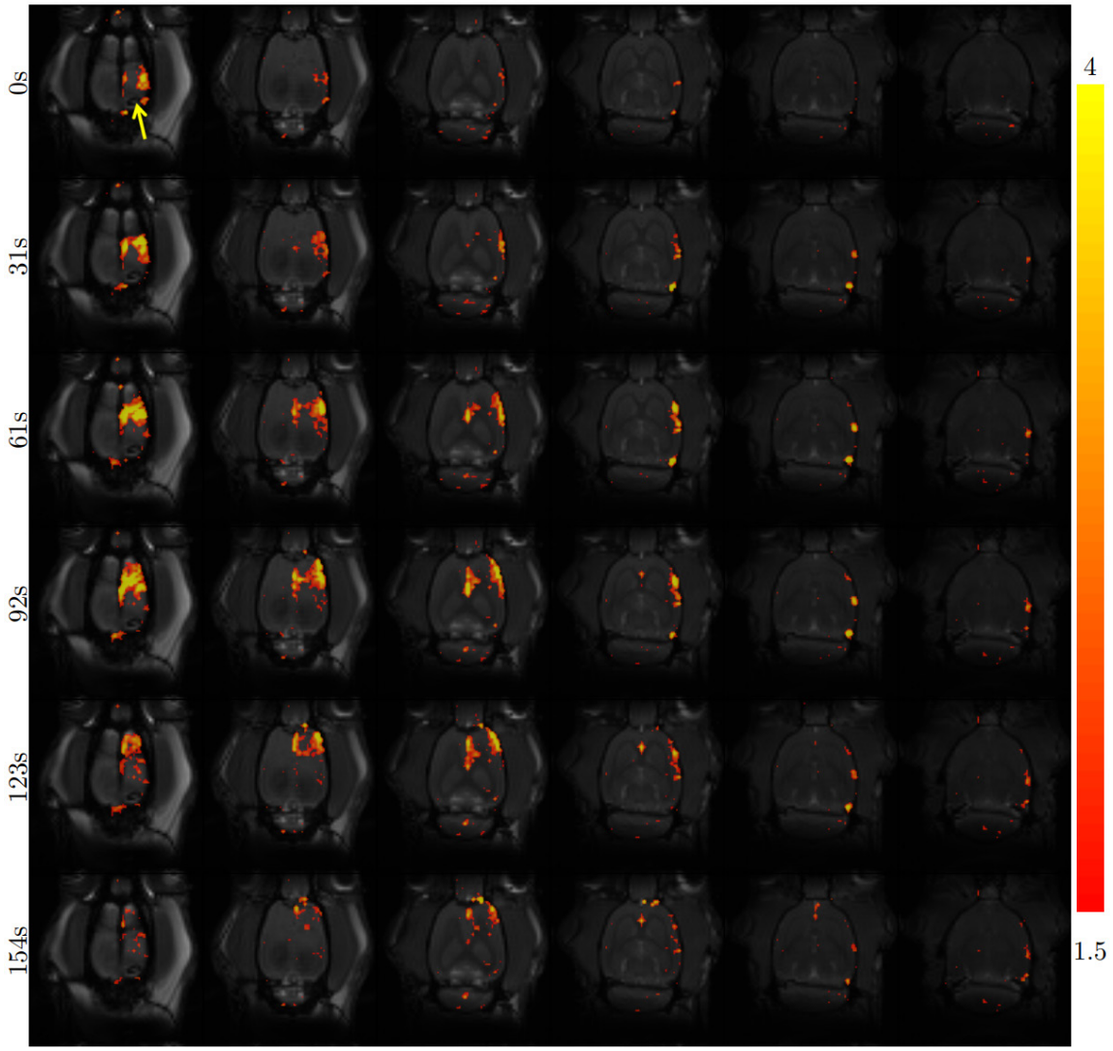

Figure S4. Representative images from six axial slices (left to right: top slice to bottom slice) of one of the b-SSFP datasets at different time points depicting the movement of a spreading depolarization (the yellow arrow points to the induction site). The sets of images (top to bottom) were captured with a difference of 30.7s each and cover a span of 154s. Relative time stamps are marked on the left side of each set.

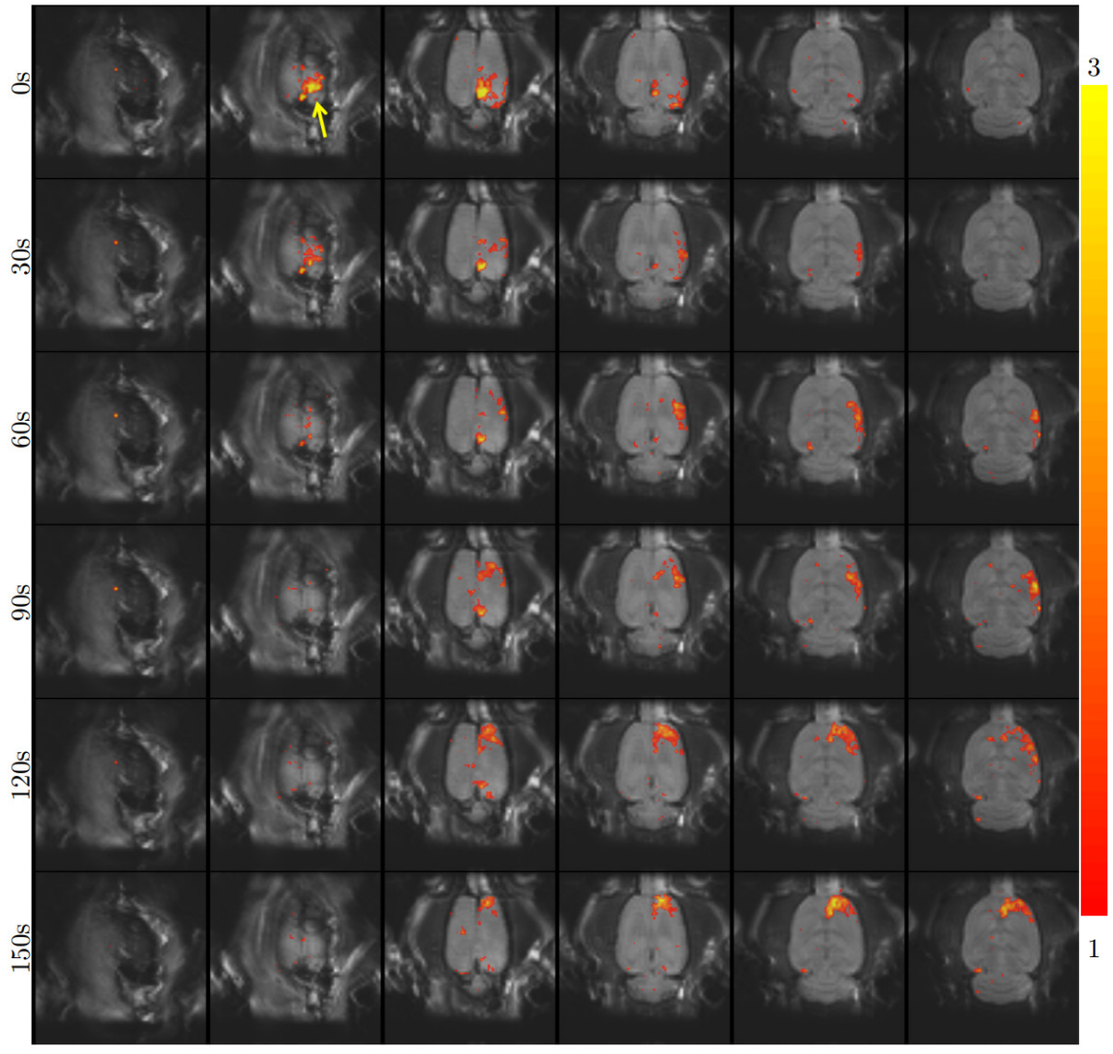

Figure S5. Representative images from six axial slices (left to right: top slice to bottom slice) of one of the DT2 (ADC) datasets at different time points depicting the movement of a spreading depolarization (the yellow arrow points to the induction site). The sets of images (top to bottom) were captured with a difference of 30s each and cover a span of 150s. Relative time stamps are marked on the left side of each set.

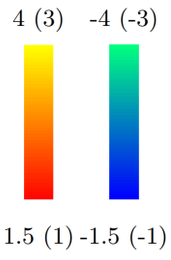

Figure S6.
Colour scales for videos. The number in the brackets corresponding to those of DT2 video and those outside depict the scale for GE3d-EPI and b-SSFP datasets.
Videos: https://doi.org/10.1002/nbm.3288

Discussion

Assessing the impact of SDs on both hemodynamics and cellular changes can help identify routes to tackle their deleterious effects. MRI is well suited to study such phenomena non-invasively over large spatial scales. We have presented two novel approaches to detect SDs using MRI, namely b-SSFP, which is expected to provide predominantly T_2-related contrast, and a diffusion-weighted multi-spin-echo (DT2) scan, which allows for simultaneous acquisition of T_2 and ADC maps, which broadly represent hemodynamic and cellular changes. We compared results from these scans with results obtained from a more conventional gradient-echo MRI sequence.

Overall, the temporal characteristics, namely, the speed of travel of SDs estimated from the scans (2.7–3 mm/min) and the duration of SDs (around twice the FWHM estimates) are in the typical range reported in the literature.[124, 155] Also, the spatial movement of SD-related changes followed the often reported patterns. These observations clearly demonstrate the suitability of b-SSFP and DT2 for visualization of SD-related changes.

b-SSFP-based detection of SDs

To the best of our knowledge, application of b-SSFP to detect SDs has not been reported. However, the growing wealth of literature on its value for fMRI[138, 139, 156-158] supports its suitability. We used a pass-band b-SSFP technique, which, at the short repetition time used in this study, is mostly influenced by changes in T_2 [138, 140], and mostly reflects oxygenation changes in capillary beds and arterioles.

Results from our comparisons between b-SSFP and GE3d-EPI data reveal the superior sensitivity (in terms of increased signal changes) and sharper temporal profile (lower FWHM) of b-SSFP signals in our experiments. Besides, the more restricted response regions observed with b-SSFP scanning (about 75% of GE3d-EPI scans), combined with the lower fall-off rate of number of detected peak waveforms with increasing *Z*-threshold, may indicate that b-SSFP scanning provides better spatial specificity than GE3d-EPI for localizing SDs. This possibility is in agreement with fMRI studies, which have shown that spin-echo sequences, which are more sensitized to microvascular signal changes, allow better co-localization with functionally activated brain regions.[136] Gradient-echo MRI approaches are sensitive to less specific changes in remote draining veins as well, and may overestimate the spatial extent of the effect of SD on neuronal tissue. Therefore, spin-echo-based techniques, such as the b-SSFP, may allow more accurate monitoring and identification of regions where SDs can cause tissue damage, e.g. secondary ischemic injury following stroke.

Moreover, at short repetition times, distortions and signal drop-outs in b-SSFP images are typically less in comparison with EPI images, since the increased pass-band minimizes the banding artifacts usually associated with b-SSFP.[138] Besides, hardware demands (on gradients)

are generally lower in b-SSFP in comparison with EPI. Above all, b-SSFP can provide the highest possible SNR per unit time compared to all other scans.[137] In our experiments, b-SSFP scans had nearly 50% greater SNR than the GE3d-EPI scans. Though b-SSFP in this study was used in pass-band mode, it is a highly configurable sequence with myriad contrast options that can reveal complementary information about tissue oxygenation status.[138] Thus, in our perspective, measurement of hemodynamic changes during SDs can benefit substantially by the use of b-SSFP.

During tissue depolarization, due to high energy demands, tissue uptake of oxygen increases drastically, resulting in initial blood deoxygenation.[159] This could perhaps explain the initial dip we see in both b-SSFP and GE3d-EPI responses. In order to satisfy this energy demand, a hyperemic response is triggered, whereby blood oxygenation eventually supersedes the demand (BOLD effect). This is a natural explanation for the signal increases we observed in our b-SSFP scans during SDs. However, the exact source of b-SSFP contrast in this study may need more careful evaluation, given the observed small T_2 changes (≈2%), but large (≈10%) changes in T_2-dependent b-SSFP contrast. Pass-band 3D b-SSFP signal is principally insensitive to T_1 changes and inflow.[137] From spin-echo fMRI studies, it has been observed that T_2-weighted BOLD changes (and thus T_2 changes) are typically small (≈2%)[133, 160], in contrast with gradient-echo BOLD signal changes (≈7%). A b-SSFP-based fMRI study in humans has shown that the signal increases at short TR (4 ms) in response to visual stimuli are expected to be less than 1%.[157] A recent study of SDs in rats[161] reports 3–4% spin-echo BOLD signal changes in a restricted region of interest. This again is much lower than the b-SSFP signal changes observed in this study.

Thus, from both our DT2 results and existing literature, despite the fact that SDs may elicit stronger vascular responses than fMRI activation, it seems unlikely that the large changes in b-SSFP contrast observed in our study are entirely T_2 related. We conjecture that, apart from T_2-related changes, the b-SSFP signal increases observed during SDs could have been influenced by the ADC changes as well. This is supported by the ≈20% drop in ADC values as measured with DT2. The b-SSFP sequence, like all others, possesses a certain inherent diffusion weighting, depending on the strength of the imaging gradients used. Although this topic was addressed earlier[162], to our knowledge no clear analytical solutions are available to estimate the inherent diffusion-weighting of b-SSFP scans. However, unlike a conventional diffusion-weighted spin-echo sequence, it is known that very small unbalanced diffusion-weighting gradients can provide significant diffusion-weighting in b-SSFP scans.[163] The b-SSFP sequence used in this study used relatively large imaging gradients, which were active for most of the repetition time. Thus, we suspect that the b-SSFP scan used in our study had a relatively high inherent diffusion-weighting. Given these facts, a decrease in tissue ADC during SD could have contributed to significant signal increases in b-SSFP contrast.

DT2-based detection of SDs

The design of the DT2 sequence reported here is similar to the PFG-CPMG sequence reported in[164], but with important modifications, namely, the use of adiabatic refocusing pulses, split-gradient diffusion-weighting and EPI readouts. Other scans for combined T_2 and ADC measurements have been proposed in the context of structural imaging.[155, 165-167] Also, scans have been proposed for combined T_2^* and ADC measurements.[168, 169] In the context of fMRI, Song et al.[170] have reported on a combined T_2^* and ADC scan protocol that can better localize regions related to neuronal activation. While the temporal dynamics of BOLD signals have been extensively studied and characterized in fMRI literature, hemodynamic changes associated with SDs and their relationship with co-occurring cellular changes remain largely unexplored.

The observed 20% decline in tissue ADC during SDs is in line with earlier observations[73, 128 92 171] and has been attributed to transient cell swelling due to the temporarily altered ion homeostasis.[119] This is purported to reduce the mobility of tissue water molecules and leads to subsequent decrease in ADC.[73, 128]The apparent non-specificity of T_2 changes in DT2 data (Fig. 5I) prompted us to verify them by performing only T_2 fits to $b=0$ data. These results (not shown) were nearly identical, indicating the robustness of the observations. Dynamic changes in T_2-based signals are typically attributed to hemodynamics (BOLD effect). In Fig. 5(I), cluster 3 seems to represent the expected hyperemic response associated with SDs. This response shows an initial dip (compared with baseline) in T_2, which corroborates our observations from the GE3d-EPI and b-SSFP datasets. The other two clusters seem to show a similar response except for a lead or lag. Thus, our data may point to the varied oxygenation status of different tissue compartments during the passage of SDs. Though at present we do not have a clear understanding of these signals or the changes in PD (Fig. 5(J)), they may eventually provide new insights into the multitude of physiological processes co-occurring during SDs. If verified, the possible contribution of diffusion-related signal changes to b-SSFP scanning during SDs (as discussed earlier) could be an important example to illustrate the strength of DT2 scanning in disentangling the possible confounds in contrast mechanisms.

Study limitations

In our experiments, a surface coil was used for RF transmission and reception. This reduced the SNR achievable in lower parts of the brain drastically in all the scans, apart from increasing echo time (TE) in DT2. Performing these experiments with a volume-transmit/surface-receive coil set-up can drastically improve the SNR in all the scans. Although the effect of temporal smoothing on DT2-derived parameters has been largely addressed by deconvolution processing, direct measurements would be desirable.

It has been observed that the choice of anesthesia impacts the rate of occurrence and propagation of SD events.[172 173] These rates may be lower under isoflurane anesthesia than under other types of anesthesia. However, the complete effect of anesthesia on the nature of

temporal evolution of MRI contrasts during SDs has not been fully characterized yet and may have to be taken into consideration in future studies.

On the data modeling front, given the fact that our model does not take into account either the massive influx of extracellular water into intracellular space during SD-triggered cell swelling or the possible changes in diffusivity and T_2 in the two pools [174], a cellular association with the observed T_2 changes cannot be ruled out. Similarly, a rigorous interpretation of reduction in ADC and any associated changes in PD may have to consider the water exchange between various compartments and associated changes in membrane properties and diffusivities.[174]

Our study demonstrates the potential of specific MRI approaches to monitor and assess distinctive SD-associated changes in whole-brain tissue. Nevertheless, cross-validation with other modalities such as electrocorticography and laser-Doppler flowmetry are necessary to further elucidate the underlying physiological mechanisms of the observed imaging contrasts.

Sources of Funding

We thank the following funding programs/agencies for supporting this research: the Utrecht University High Potential program, and the Brain Foundation of the Netherlands (Project 2011(1)-102).

Chapter 5

Spreading depolarization-modulating drugs and delayed cerebral ischemia in patients with subarachnoid hemorrhage

A hypothesis-generating retrospective clinical study

Hamming AM[1], Mulder IA[1], Gathier CS, van den Bergh WM, Dankbaar JW, Hoff RG, Vandertop WP, Verbaan D, Ferrari MD, Rinkel GJE, Algra A, Wermer MJH

[1] These authors contributed equally to the manuscript

J Neurol Sci 2016 Jul 15; 366:224-228

Abstract

Background

Delayed cerebral ischemia (DCI) occurs in approximately one-third of patients with aneurysmal subarachnoid hemorrhage (aSAH). A proposed underlying mechanism for DCI is spreading depolarization(SD). Our aim was to, retrospectively, investigate the influence of the use of SD-modulating drugs on the occurrence of DCI.

Methods

We, retrospectively, combined data from four cohorts of aSAH patients with data on the use of home medication prior to hospital admission, occurrence of DCI, and clinical outcome. Home medication was classified as “SD-inhibiting”, “SD-facilitating”, or “SD-neutral based” on a comprehensive literature review. We defined subgroups “likely”, “possibly” and “weak” concerning the amount of evidence in literature. We performed Cox and Poisson regression analysis and calculated hazard ratios (HR) and risk ratios (RR) for the influence of “SD-modulating” drugs on primary outcome measure DCI and secondary outcome measure poor clinical outcome (modified Rankin Scale ≥ 3) three months after aSAH. We adjusted for age, sex and clinical condition on admission (aHR/aRR).

Results

DCI occurred in 343 (29%) of 1,194 patients. Patients using SD-inhibiting home medication had an aHR for DCI of 0.66 (95%CI: 0.42-1.06) and an aRR for poor outcome of 1.13 (95%CI: 0.90-1.41). Patients using SD-facilitating drugs had an aHR for DCI of 1.24 (95%CI:0.83-1.87) and an aRR for poor outcome of 1.19 (95%CI: 0.95-1.50). When comparing patients using SD-inhibiting drugs with patients using SD-facilitating drugs, the aHR was 0.54 (95%CI: 0.29-0.99) for DCI and the aRR 0.97 (95%CI: 0.71-1.32) for outcome.

Conclusions

In this exploratory study chronic use of SD-inhibiting drugs tended to reduce DCI but did not result in a better clinical outcome. Additional research is needed to investigate the specific effects of SD-modulation on DCI and outcome and to further explore its effectiveness in preventing DCI after aSAH.

Introduction

Delayed cerebral ischemia (DCI) after aneurysmal subarachnoid hemorrhage (aSAH) occurs in approximately one-third of patients after aSAH and is an important cause of poor outcome.[22] It has long been assumed that DCI is caused by cerebral vasospasm, however, not all DCI patients have vasospasm and not all aSAH patients with vasospasm develop DCI.[175] Another proposed mechanism for DCI is the occurrence of waves of self-propagating neuronal depolarization, called spreading depolarization (SD). SDs are the underlying mechanism of migraine aura but have also been found after trauma, stroke and aSAH.[59, 176] In healthy brain, SDs appear to be benign phenomena often followed by hyperperfusion, but in injured brain SDs may cause hypoperfusion and ischemia.[59] In aSAH patients, a correlation between SDs and DCI was found.[66, 177] Therefore, SDs may be a target for prevention or reduction of DCI.
In animals, SDs can be inhibited by several drugs, such as migraine prophylactics and calcium-antagonists, especially when treatment is started weeks before the event.[36] Migraine prophylactic drugs often need chronic administration to achieve efficacy on experimental SDs.[36] Drugs that suppress SDs after brief treatment probably increase in efficiency by longer treatment duration.[36] Until now, nimodipine is the only proven drug for the risk reduction of DCI in humans. It has been suggested that this beneficial effect is partly based on SD-inhibition.[85, 106, 178] Because a randomized trial with pre-treatment of SD inhibitors several weeks before stroke onset is not possible in patients we, retrospectively, investigated large cohorts of aSAH patients. Our aim was to investigate the possible influence of chronic use of SD-modulating drugs at the time of aSAH on the occurrence of DCI and clinical outcome.
Drugs were categorized for their influence on SD based on literature, where most evidence was based on animal studies.

Materials ans Methods

Cohorts

We performed a retrospective study for which we included four cohorts of aSAH patients who were admitted to the University Medical Center Utrecht (UMCU) or the Academic Medical Center (AMC) Amsterdam and for whom the use of medication on admission was known as well as whether DCI had developed and what the clinical outcome was. These cohorts included participants of the DECIDE study,[179, 180] the OPTICA study,[181] the MASH (1 and 2)[182, 183] studies and a combined observational cohort of patients from the UMCU and AMC. Home medication was gathered from the patients' clinical records. Based on the assumption that 10% of the patients would use SD-inhibiting drugs at time of aSAH and 25% of these patients would develop DCI versus 35% of the unexposed patients, power analysis showed that the ~1,300 patients included in the four studies would be sufficient to detect a RR of 0.7 with accurate confidence intervals. Details of all studies, including in- and exclusion criteria, are listed in table 1. Patients who participated in more than one study were included only once.

All aSAH patients received nimodipine upon admission. After admission, home medication was usually continued or substituted, except for anticoagulants and most antihypertensive drugs. All trials and cohorts were approved by the Medical Ethical Committee of the local hospitals.

Literature study

To classify SD-modulating effects of home medication we conducted a comprehensive literature study using PubMed and WebOfKnowledge. We used the search-terms *"spreading depression" OR "cortical spreading" OR "anoxic depolarization" OR "spreading depolarization" AND (name of drug). For the name of the drug, when available, a* MeSH-term was used. Other clinically used drugs of the same functional group were also included in our search to assess group effects for drugs with no relevant hits. For each drug, the number of hits was stated. For every useful hit, the experimental method (species, dose, route, pre-treatment, SD induction and SD monitoring) was assessed, as well as the influence of the drug treatment on SD susceptibility, speed, duration and amplitude. The effect of each drug on SDs was scored first for each published article and thereafter a total score for each drug was given based on the summary of all articles independently by two researchers (A.M.H and I.A.M). When both researchers gave a different score a definite conclusion was reached by consensus. We scored drugs that inhibit or facilitate SDs as:

- *Likely*: Studies in mammals, with concentrations that did not deviate strongly from human therapeutic range with a clear influence on susceptibility, duration or amplitude of SDs, or two distinct references classified as "possibly".
- *Possibly*: Evidence for SD-modulating effects of the drug in the literature but not meeting the criteria for likely.
- *Weak evidence*: SD-modulating effects were described in drugs of the same pharmacological group but no literature about the effects on SDs of this particular drug was found.

If studies described absence of drug-specific effects on SD susceptibility, duration or amplitude, the drug was classified as '*no SD effect'*. Drugs without (useful) hits were classified as '*no available data*' and drugs with conflicting study results were categorized as '*no consistent data*'. Drugs in the class '*no SD effect*', '*no available data*' or '*no consistent data'* were combined and classified as '*SD-neutral drugs'*. The complete list of drugs is listed in the web appendix.

Patients

We classified patients according to their home medication. Patient classes were use of SD-inhibiting drugs *('likely'*, '*possibly'* and *'weak'),* SD-facilitating drugs *('likely'*, '*possibly'* and *'weak')*, SD-neutral drugs or no use of home medication. Patients using a combination of both inhibiting and facilitating drugs were excluded from the study.

Outcome measures

The primary outcome was development of DCI. In the DECIDE, OPTICA and MASH-2 studies, DCI was defined as a decline in neurological function without any other possible explanation such as hydrocephalus, infections or metabolic disturbances, based on CT and blood examination results. In the MASH-1 and the AMC and UMCU cohort studies, DCI was defined as a new spontaneous hypodense lesion as revealed by a CT scan compatible with clinical features of DCI (gradually developed focal deficits, decreased level of consciousness, or both). The secondary outcome measure was poor clinical outcome defined as a score of ≥ 3 on the modified Rankin Scale (mRS)[184] three months after onset of aSAH.

Data analysis

Cox (for DCI as outcome measure) and Poisson (for the dichotomous mRS outcome measure) univariable and multivariable regression analyses were done to calculate hazard ratios (HR) and risk ratios (RR) including 95% confidence intervals (CI). We calculated HRs and RRs for the primary and secondary outcome measures for the use of SD-inhibitors (likely, possibly, weak and all combined) and the use of SD-facilitators (likely, possibly, weak and all combined) compared with patients without use of SD-modulating medication (SD-neutral and no home medication). The same analyses were performed comparing only patients who used SD-inhibitors with patients who used SD-facilitators. Adjustments (aHR/aRR) were made for age, sex and clinical condition on admission (assessed by means of World Federation of Neurosurgical Societies (WFNS) SAH grading scale[185]) on admission. A Kaplan-Meier survival curve was constructed with DCI as the outcome measure. Patients with unknown mRS score at three months were excluded from analyses of the clinical outcome.

Results

Patients and literature study

In total 1,289 potentially eligible patients were identified. Complete datasets on medication and DCI were available for 1,209 patients. A total of 848 articles was reviewed, yielding 386 different drugs, of which 52 were classified as SD-inhibiting and 32 as SD-facilitating (Table 2 and tables A.1, A.2 and A.3 of the appendix).

Fifteen patients were excluded because they used both SD-inhibiting and SD-facilitating medications. The remaining 1.194 patients were included in the present study and 155 (13%) of these used SD-modulating medication before admission: 89 (57%) SD-inhibiting drugs and 66 (43%) SD-facilitating drugs. Patients' characteristics are shown in table 3.

SD-modulation in relation with DCI

DCI occurred in 343 (29%) patients (table 3). Kaplan-Meier analysis showed a trend towards less DCI in the group using inhibiting drugs and more DCI in the group using facilitating drugs compared with patients not using SD-modulating drugs (Figure 1).

After adjustment for age, sex and WFNS the aHR was 0.66 (95% CI: 0.42-1.06) for patients using inhibiting drugs and 1.24 (95% CI: 0.83-1.87) for patients using facilitating drugs compared to patients without use of SD-modulating medication (table 4). When comparing patients using SD-inhibiting drugs with patients using SD-facilitating drugs, a HR of 0.56 (95% CI: 0.31-1.02) and an aHR of 0.54 (95% CI: 0.29-0.99) was found for the occurrence of DCI.

SD-modulation in relation with clinical outcome

Clinical outcome was poor in the 423 (47%) of the 909 patients with a known mRS score after three months. The aRR for a poor outcome was 1.13 (95% CI: 0.90-1.41) for patients using SD-inhibiting home medication and 1.19 (95% CI: 0.95-1.50) for patients using SD-facilitating home medication compared to patients without use of SD-modulating medication (table 4). When comparing patients using inhibiting drugs with patients using SD-facilitating drugs, a RR of 0.97 (95% CI: 0.70-1.33) and an aRR of 0.97 (95% CI: 0.71-1.32) was found for the clinical outcome.

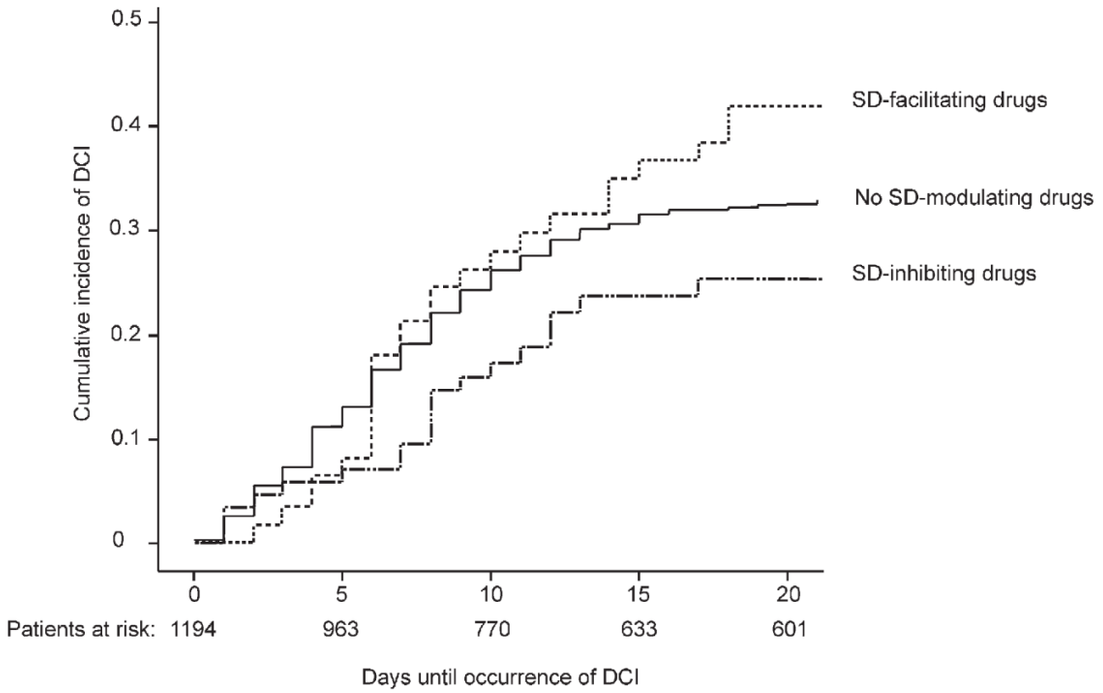

Figure 1. Kaplan-Meier curve of the cumulative incidence of delayed cerebral ischemia grouped by drug usage.

Table 1. Characteristics of four cohorts of aSAH patients#

	Number of patients	Inclusion period	Study design	Aim of the study	Cohort specific inclusion criteria	Cohort specific exclusion criteria
DECIDE	128	2007-2009	Clinical imaging studies	To evaluate CT-perfusion imaging for the diagnosis of DCI	Admission <72hrs; imaging at time of deterioration or <14 days after aSAH in clinically stable patients	Creatinine >200 µmol/L or other contraindications for contrast-enhanced CT scans
MASH (1+2)	419 (201 + 218)	2000-2006	Randomized controlled trials	To investigate Mg (and aspirin for MASH-1) for prevention of DCI	Randomisation within 4 days after aSAH	Creatinine >150 µmol/L. Weight <50kg (MASH-2)
OPTICA	96	2006-2007	Controlled trial	To investigate the effect of fluid management on hypovolemia	Admission within 72hrs after aSAH	Accompanying head injury, liver or renal failure or indicator dye allergy
AMC/ UMCU	464/183	1997-2011	Cohort study	AMC: cohort of admitted patients. UMCU: cohort of admitted patients 1997-2006	AMC: All aSAH patients. UMCU: Admission within 72hrs after aSAH and CT performed upon admission	-

aSAH - aneurysmal subarachnoid hemorrhage; DCI - delayed cerebral ischemia

- all patients were 18 years or older

Table 2. Results of the drug literature search

Drug category		Number
SD-inhibiting		52
	Likely	15
	Possibly	13
	Weak	24
SD-facilitating		32
	Likely	1
	Possibly	8
	Weak	23
SD-neutral		302
	No SD effect	38
	No consistent data	12
	No available data	252

Table 3. Baseline characteristics and outcomes of 1,194 patients with aSAH

	Total	No SD modulating drugs	SD-Inhibiting drugs	SD-Facilitating drugs
N	1,194	1,039 (87%)	89 (7%)	66 (6%)
Women	765 (64%)	657 (63%)	58 (65%)	50 (76%)
Mean age (years (±st.dev.))	55.8 (13.3)	55.0 (13.2)	62.4 (12.8)	58.9 (13.4)
WFNS 1-3	788 (66%)	688 (66%)	53 (60%)	47 (71%)
DCI	343 (29%)	299 (29%)	19 (21%)	25 (38%)
Days until occurrence of DCI (mean (±st.dev.))	6.9 (4.4)	6.8 (4.3)	7.5 (4.5)	8.9 (4.7)
mRS at 3 months after aSAH*				
0-2	486 (53%)	437 (55%)	27 (44%)	22 (42%)
3-6	423 (47%)	359 (45%)	34 (56%)	30 (58%)

Values are number (percentage).

* Patients with unknown mRS at three months (n=285) were left out.

WFNS - The World Federation of Neurosurgeons SAH grading scale

Table 4. Crude and adjusted effect estimates for DCI and poor outcome according to drug used.

	DCI + (n (%))	Crude HR (95% CI)	Adjusted HR (95% CI)	mRS ≥3 (n (%))	Crude RR (95% CI)	Adjusted RR (95% CI)
No SD-modulating drugs	299/1,039 (29%)	ref.	ref.	359/796 (45%)	ref.	ref.
SD-inhibiting drugs	19/89 (21%)	0.70 (0.44-1.12)	0.66 (0.42-1.06)	34/61 (56%)	1.24 (0.98-1.57)	1.13 (0.90-1.41)
Likely	3/21 (14%)	0.50 (0.16-1.56)	0.46 (0.15-1.42)	10/16 (63%)	1.39 (0.94-2.04)	1.25 (0.86-1.82)
Possibly	6/18 (33%)	1.06 (0.47-2.39)	1.00 (0.44-2.24)	7/12 (58%)	1.29 (0.80-2.10)	1.31 (0.87-1.97)
Weak	10/50 (20%)	0.65 (0.35-1.22)	0.62 (0.33-1.18)	17/33 (52%)	1.14 (0.81-1.60)	1.00 (0.72-1.40)
SD-facilitating drugs	25/66 (38%)	1.26 (0.84-1.89)	1.24 (0.83-1.87)	30/52 (58%)	1.28 (1.00-1.63)	1.19 (0.95-1.50)
Likely	1/1 (100%)	7.56 (1.06-54.07)	5.03 (0.70-36.26)	1/1 (100%)	2.22 (2.05-2.39)	1.32 (1.18-1.48)
Possibly	11/36 (31%)	1.01 (0.55-1.84)	1.03 (0.56-1.88)	12/29 (41%)	0.92 (0.59-1.42)	0.89 (0.60-1.34)
Weak	13/29 (45%)	1.47 (0.84-2.56)	1.41 (0.81-2.45)	17/22 (77%)	1.71 (1.35-2.18)	1.53 (1.20-1.97)

Left columns: Cox-regression analysis with DCI as the outcome variable. Adjustments were made for age, sex and WFNS. DCI + were patients who developed DCI after aSAH within the follow-up period of 21 days. Right columns: Poisson-regression analysis with dichotomous mRS as the outcome variable (n=285 missing). Adjustments were made for age, sex and WFNS. The group of patients with no SD-modulating drugs is composed of 624 (60%) patients without the use of home medication and 415 (40%) patients using non-SD-modulating drugs.

Discussion

Our exploratory analysis suggest a trend towards a protective effect of SD-inhibiting drugs on the development of DCI but this did not result in a better clinical outcome. In contrast, our data suggest a neutral, or even detrimental, influence of SD-modulating drugs on clinical outcome. The suggestion of a possible protective effect of SD-inhibition on DCI supports recent findings that SDs play a role in the development of secondary ischemia after aSAH.[33, 59, 66, 177] In 2009, SDs were detected with electrocorticography in a small series of aSAH patients. In almost all SAH patients SDs were present, and a correlation between the occurrence of SDs and the development of DCI was found.[66, 177] The association between SDs and progression of cerebral ischemia has also been described in animals and patients.

In an ischemic stroke model in rats, SD-waves have been found to circle around and enlarge ischemic brain lesions.[109] In addition, SDs have been shown to occur in the penumbra of patients with ischemic stroke.[176] In injured brain tissue the vascular response to SDs may be a paradoxical vasoconstriction or vasospasm.[102] Decreased delivery of oxygen and metabolites in injured brain tissue may explain why SDs cause no damage in normal brain tissue, but might cause (progression of) ischemia after aSAH or ischemic stroke.[66, 177]

We have no good explanation for the absence, or possible negative effect, of both SD-modulating drugs on clinical outcome. Our crude RRs for outcome changed considerably after adjustment for age, sex and WFNS score, however, we cannot exclude residual confounding. Unfortunately, because of lack of information we were not able to adjust for the amount of extravasated blood measured with the modified Fisher score, which has been suggested to be another predictor for DCI and clinical outcome.[23, 186, 187]

Our study has several limitations. First, our main assumption, based on animal studies, was that prolonged drug treatment is needed for effective SD-inhibition and that SDs generally develop early after aSAH.[36, 66, 87, 177] Although we assumed that most drugs were in chronic use at the time of hemorrhage, and were continued during admission, we did not check this in every patient. In addition, we did not include possible effects of drugs that were started during admission. All patients used nimodipine during their hospital course. Because several studies suggest that the protective effect of nimodipine is partly based on SD inhibition, the standard use of nimodipine might have diluted our effect estimates.[85, 90, 106, 188] Part of our study population participated in the MASH trials and were randomized between magnesium or placebo treatment. We did not take this treatment into account because magnesium was not found to be effective and randomization in the MASH trial was considered independent of SD-modulating home medication.[182, 183] Second, because SDs can only be measured with invasive corticography we were not able to directly measure the effect of the SD inhibiting drugs on the occurrence of SDs. Many of the drugs used in the study have multiple mechanisms of action which hampers interpretation of our data. Third, we classified the SD-effect of drugs by assessing whether the

dose used in animals correlated plausibly with the human therapeutic range. This could possibly have diluted the effect estimates. Also, there were no data on 252 drugs at the time the literature search was performed. We assumed that these drugs did not have any SD-modulating effects.

Besides that, confounding may have occurred because the included patients were taking their SD-modulating drugs for diseases such as migraine or epilepsy, which themselves may have an effect on the occurrence of DCI. Because of a possible hyperexcitability of the brain one could hypothesize that patients with these diseases are more susceptible to develop DCI. However, in a recent study a history of migraine was not a predictor for the occurrence of DCI.[23] In addition, drugs used for migraine or epilepsy were mostly classified as SD-inhibiting drugs. Therefore, even despite a possibly higher risk of DCI in these patients, there still was a positive trend in our study for a beneficial effect of SD-inhibition.

Strong points of this study, which is the first to study the effect of SD-modulating drugs on DCI in humans, are the large number of patients investigated and the extensive literature study on SD-drugs. This study also includes a pre-treatment effect as the drugs were already used before admission to hospital. The need for a long pre-treatment phase could also, in part, explain why many trials on neuroprotective therapies for prevention of DCI after aSAH have not been successful.

Conclusion

Although no firm conclusions can be drawn from our study, it suggests a possible protective role of SD-inhibiting drugs against DCI, which provides opportunities for new research on preventing DCI. However, more insight is needed from epidemiological and experimental studies into the possible detrimental effects on clinical outcome before SD-inhibition is studied further for preventing DCI in humans.

Sources of Funding

This study was supported by a grant of the Dutch Brain Foundation (project 2011(1)-102). Dr. Wermer was supported by a personal grant from the Netherlands Organisation for Scientific Research (ZonMW Veni grant) and the Netherlands Heart Foundation (2011T055).

Supplementary data

The results of the literature study can be found in Tables A1 and A2.

Table A1. Results of the literature search.

Human dose route is per os, unless mentioned otherwise.

Subgroup	Drug Mesh term	Hits fo	SD categ	Species	Comments	Monitor	Human dose	Dose, route	Pretreatment	SD induction	Susceptibility	Speed	Duration	Amplitude	Reference
Anti-depressants															
Serotonine manipulators	Methysergide	5	ip	Rat		DC	1-6 mg/day	10 mg/kg, i.p.	105 min	E	↔	nd	↔	↔	Marrannes book 1 (review Ayata)
(oa. SSRIs)				Rat		DC		10 mg/kg/day, p.o.	5 days	M	↔	↔	nd	↔	Hansen, book (review Ayata)
				Rat		DC		0.1-1 mg/kg/day, i.p.	≥ 6 weeks	KCl	↓	↔	↔	↔	Ayata, Ann Neurol 2006
				Chicken	retina	DC		100 μM, CM	nd	KCl	nd	↓δ	↓δ	↓	Wiedemann, Naunyn-Schmiedebergs Arch Pharmacol 1996
	Pizotyline	2	na	Rat		DC	1.5-4.5 mg/day	10 mg/kg, i.p.	105 min	E	↔	nd	↔	↔	Marrannes, book 1 (review Ayata)
	Fluoxetine	1	ip	Rat		DC	20-60 mg/day	10-40 mg/kg/day, s.c.	≥ 25 days	KCl	nd	↓δ	↔	↓δ	dos Santos, Exp Neurol 2006
	Citalopram	2	ip	Rat		DC	20-40 mg/day	20 mg/kg/day, i.p.	1 week	KCl	nd	↓	↔	↓δ	Guedes, Nutr Nrsc 2002
TCAs	Amitriptyline	1	ncd	Rat		DC	50-300 mg/day	20 mg/kg, i.p.	60 min	E, KCl	↔	↔	↔	↔	Ayata, Ann Neurol 2006
				Rat		DC		10-20 mg/kg/day, i.p.	≥ 4 weeks	E, KCl	↓	↓	↔	↔	Ayata, Ann Neurol 2006
AEDs															
	Valproic Acid	21	il	Rat		DC	10-60 mg/kg/day	200 mg/kg, i.v.	60 min	E, KCl	↔	↔	↔	↔	Hoffmann, Cephalalgia 2011
				Rat		DC		200 mg/kg, i.p.	5 weeks	E, KCl	↓	↓	↓	↔	Hoffmann, Cephalalgia 2012
				Rat		DC		200 mg/kg, i.p.	4 weeks	KCL	↓	↓	↓	↔	Bogdanov, Neurobiol Dis 2011
				Cat		LDF, SUA		3.5-7 mg/kg, i.v.	60 min	Ischemia	↔	↔	nd	↔	Kaube, Eur Neurol 1994
				Rat		DC		100-200 mg, i.p.	60 min	E, KCl	↔	nd	nd	nd	Ayata, Ann Neurol 2006
				Rat		DC		200 mg/kg/day, i.p.	1 week	E, KCl	↔	↔	↔	↔	Ayata, Ann Neurol 2006
				Rat		DC		25-200 mg/kg/day, i.p.	4-16 weeks	E, KCl	↓δ	↓	↔	↔	Ayata, Ann Neurol 2006
				Rat		DC, LDF		200mg/kg, i.p.	60 min	KCL	↔	nd	nd	↑ (LDF) ↔ (DC)	Peeters, J Pharmacol Exp Ther 2007
				Mouse	hippocampal slices	DC		1 mM, aCSF	na	E	↑	nd	nd	nd	Abdelmalik, Neurobiol Dis 2007
	Topiramate	19	il	Cat		LDF, SUA	25-200 mg/day	10-30 mg/kg, i.v.	30 min	M	↓	↔	↔	nd	Akerman, Neuroreport 2005
				Rat		LDF, SUA		10-30 mg/kg, i.v.	30 min	M	↓	↔	↔	nd	Akerman, Neuroreport 2005
				Rat		DC		60-80 mg/kg, i.p.	60 min	E, KCl	↔	nd	nd	nd	Ayata, Ann Neurol 2006
				Rat		DC		80 mg/kg/day, i.p.	1 week	E, KCl	↔	↔	↔	↔	Ayata, Ann Neurol 2006
				Rat		DC		60-80 mg/kg/day, i.p.	≥ 4 weeks	E, KCl	↓δ	↓	↔	↔	Ayata, Ann Neurol 2006
				Rat		DC, LDF		50-600 mg/kg/day, p.o.	6 weeks	KCl	↓δ	↓δ	nd	↔	Unekawa, Cephalalgia 2012
				Rat		DC, LDF		50-600 mg/kg/day, p.o.	60 min	KCl	↔	↔	nd	↓ (LDF) ↔ (DC)	Unekawa, Cephalalgia 2012
	Carbamazepine	2	ip	Mouse		Optical	10-60 mg/kg/day	0.35-0.5 mM, local	15 min	E	↓	nd	nd	nd	Chen, J Neurophysiol 2005
	Etiracetam	2	iw	Rat	neocortical slices	DC	500-3000 mg/day	32-100 μM, CM	20, 100 min	KCl	nd	nd	↔	↔	Margineanu, Seizure 2009
	Phenytoin	10	ip	Cat		DC, SUA	150-400 mg/day	1-2 mg/ml, local	0.5-2 min	Paw stimulation	↑	↔	nd	↓	Harris, Exp Neurol 1978
				Rat		DC		80 mg/kg, i.p.	45, 120 min	E	↔	nd	↔	↔	Marrannes, Brain Res 1988
				Rat		DC		30-90 mg/kg, nd	nd	E	↓	nd	nd	nd	Reid, Physiol Bohemoslov 1988 (abstract)
				Chicken	retina	Optical		nd	nd	nd	↓	↓δ	nd	nd	Chebabo, Braz J Med Biol Res 1988 (abstract)
				Mouse	hippocampal slices	DC		50 μM, CM	na	E	↓	nd	nd	nd	Abdelmalik, Neurobiol Dis 2007
				Chicken	retina	DC		0-100 μM, CM	20 min	KCl	↓	↓	↓	↔	Chebabo, Brain Res 1991
				Rat	caudate nuclei	DC		100 μM, CM	na	hypoxie/hypoglyce	↓	nd	↑	nd	Toner, Neuroscience 1997
				Guinea pig	hippocampal slices	DC		10.7 μM, CM	90 min	Veratridine, KCl	↓ (onset) ↔ (# of SDs)	nd	↔	↑	Ashton, Brain Res 1997
				Cat		DC		nd	nd	KCL	nd	nd	↑	nd	Somjen, Fed Proc 1976
	Lamotrigine	4	il	Guinea pig	hippocampal slices	DC	50-500 mg/day	8.8 μM, CM	90 min	Veratridine, KCl	↓ (onset) ↔ (# of SDs)	nd	↔	↔	Ashton, Brain Res 1997
				Rat		DC, ECoG		15 mg/kg, i.p.	4 weeks	KCL	↓	↑	↓	↓	Bogdanov, Neurobiol Dis 2011
	Oxcarbazepine	1	na	Rat		DC	600-2400 mg/day	200 mg/kg, p.o.	90 min	E, KCl	↔	↔	↑	↔	Hoffmann, Cephalalgia 2011
				Rat		DC		50 mg/kg, p.o.	5 weeks	E, KCl	↔	↔	↔	↔	Hoffmann, Cephalalgia 2011
	Gabapentin	8	il	Rat		DC	900-3600 mg/day	100-200 mg/kg, i.v.	60 min	E, KCl	↓δ	↔	nd	nd	Hoffmann, J Cereb Blood Flow Metab 2010
				Mouse		DC, ECoG		50-400 mg/kg, i.v.	60 min	MCAo	↔	nd	↔	nd	Hoffmann, J Cereb Blood Flow Metab 2011
	Riluzole	2	ip	Guinea pig	hippocampal slices	DC	100 mg/day	1-1.95 μM, CM	90 min	Veratridine, KCL	↓ (onset) ↔ (# of SDs)	nd	↔	↑	Ashton, Brain Res 1997
	Phenobarbital	5	fp	Cat		Fluorometric	100-250 mg	20-80 mg/kg, i.c.	na	E	nd	↔	↑δ	nd	LaManna, Brain Res 1975
				Cat		DC		nd	nd	KCl	nd	nd	↑	nd	Somjen, Fed Proc 1976 (abstract)
	Barbital	1	fp	Chicken	retina	DC	650-970 mg	800 μM, CM	na	KCl	nd	↑δ	↔	↑	Wiedemann, Naunyn-Schmiedebergs Arch Pharmacol 1996
				Chicken	retina	Optical		800 μM, CM	na	M	nd	↑	nd	↑	Brand, Naunyn-Schmiedebergs Arch Pharmacol 1998
Benzodiazepines															
	Diazepam	6	fp	Rat	chronically epileptic	DC	6-40 mg/day	5-10mg/kg, i.v.	na	KCl	↑	nd	↔	↑	Guedes, Epilepsy Res 1997
				Rat		DC		40 mg/kg, i.p.	30 min	E	↔	nd	↑	↔	Marrannes, Brain Res 1988
	Clonazepam	1	na	Cat		LDF, SUA	2-4 mg/day	15-45 μg/kg, i.v.	60 min	ischemia	↔	↔	nd	↔	Kaube, Eur Neurol 1994
	Midazolam	2	il	Mouse	hippocampal slices	DC	7.5-15 mg/day	10 nM, CM	na	E	↓	nd	nd	nd	Abdelmalik, Neurobiol Dis 2007
				Human	trauma	DC		avg 22.3 mg, i.v.	varying	spontaneous	↑δ	nd	nd	nd	Hertle, Brain 2012
Anti-hypertensives															
Beta blockers	Propranolol	16	il	Rat		DC	120-320 mg/day	20 mg/kg, i.p.	105 min	E	↔	nd	↔	↔	Marrannes, book 1 (review Ayata)
				Rat		DC		20 mg/kg, p.o. b.i.d.	5 days	M	↔	↔	nd	↔	Hansen, book (review Ayata)
				Rat		DC		20 mg/kg, i.p.	60 min	E, KCl	↔	↔	↔	↔	Ayata, Ann Neurol 2006
				Rat		DC		20 mg/kg/day, i.p.	≥ 4 weeks	E, KCl	↓	↓	↔	↔	Ayata, Ann Neurol 2006
				Rat		DC, LDF		250-1000 μmol/L, CM	na	M, KCl	↔	↓δ			Richter, J Cereb Blood Flow Metab 2005
				Chicken	retina	DC		700 μM, CM	nd	KCl	nd	↓δ	↓	↓	Wiedemann, Naunyn-Schmiedebergs Arch Pharmacol 1996 (abstract)
				Rat		DC, LDF		20 mg/kg, i.p.	30-60 min	KCl	↔	nd	nd	↔	Peeters, J Pharmacol Exp Ther 2007
				Rat		ECoG, [14C]iap		1.5 mg/kg, i.v.	10 min	E	nd	nd	nd	↔	Duckrow, J Cereb Blood Flow Metab 1991
	Metoprolol		na	Cat		LDF, SUA	100-400 mg/day	25 mg/kg, i.v.	60 min	ischemia	↔	↔	nd	↔	Kaube, Eur Neurol 1994
				Rat		DC, ECoG		5 mg/kg, i.v.	na	KCl	↔	↔	nd	↔	Alemdar, Cephalalgia 2007
Calcium antagonists	Nimodipine	24	il	Rat		LDF, DC	360 mg/day	2 μg/kg/min, i.v.	60 min	KCl	↓	nd	↓	↔	Dreier, Neurosurgery 2002
				Rat		LDF, DC		2 μg/kg/min, i.v.	60 min	ischemia	↓	nd	nd	nd	Dreier, J Cereb Blood Flow Metab 1998
				Guinea pig	hippocampal slices	DC		7.27 μM, CM	90 min	Veratridine, KCl	↓ (onset) ↔ (# of SDs)	nd	↔	↔	Ashton, Brain Res 1997
				Rat	SHRSP	nd		nd	na	na	↓	nd	nd	nd	Kawasaki, Calcium Ion Modulators 1998 (book)
				Rat		DC		10^{-5} M, CM	60 min	KCl	↓	nd	nd	↓	Richter, Neurosci Lett 2002
	Nifedipine	11	iw	na	organotypic cultures	DC, optical	30-120 mg/day	10 μM, CM	na	E	↔	nd	nd	nd	Kunkler, Hippocampus 2004
	Diltiazem	2	iw	Guinea pig	hippocampal slices	DC	200-300 mg/day	2.77 μM, CM	90 min	Veratridine, KCL	↓ (onset) ↔ (# of SDs)	nd	↔	↑	Ashton, Brain Res 1997
	Verapamil	10	ncd	Guinea pig	hippocampal slices	DC	320-720 mg/day	1.27 μM, CM	90 min	Veratridine, KCL	↓ (onset) ↔ (# of SDs)	nd	↔	↑	Ashton, Brain Res 1997
Central acting BPLs	Clonidine	5	ip	Rat		DC	0.1-1.5 mg/day	1.25-10 mg/kg, i.p.	105 min	E	↔	nd	↑	↔	Marrannes, book 1 (review Ayata)
				Rat		DC		0.56 μmol/L, CM	na	M, KCl	↓	nd	nd	nd	Richter, J Cereb Blood Flow Metab 2005
				Chicken	retina	DC		100-500 μM, CM	na	KCl	nd	↔	↔	↔	Wiedemann, Naunyn-Schmiedebergs Arch Pharmacol 1996
Diuretics	Amiloride	6	fl	Human	slices	DC	5-10 mg/day	50 μmol/L, CM	5 hrs	KCl, amiloride	↑	nd	nd	nd	Gorji, Brain Res 2001
Other				Guinea pig	hippocampal slices	DC		25-200 μmol/L, CM	5 hrs	KCl	↑	↔	↔	↔	Gorji, Cephalalgia 2009
Diuretics (non antihyper	Furosemide	11	ncd	Cat		DC, LDF	20-1500 mg/day	0.2-20 mg/kg, i.v.	5-30 min	KCl	↓ δ	↔	↓ δ	↔	Read, Cephalalgia 1997
				Rat	hippocampus	DC		2 mM, CM	15 min	E	↑	nd	↑	↓	M¨uller Neuroscience 2000
Mannitol				Rat	hippocampus	DC, Optical		2 mM, CM	15 min	E	↑	nd	nd	↓	M¨uller, J Neurophysiol 1999
		13	na	Rat		DC	1500-2000 mg/kg, i.v.	20% solution, 1 mL i.v.	na	KCl	nd	↔	nd	nd	Batinga, Neurosci Lett 2011
NSAIDs															
Acetaminophen		6	fp	Chicken	retina	DC	1500-2000 mg/kg	10 mM, CM	na	KCl	nd	↓ δ	↓	↓ δ	Wiedemann, Naunyn-Schmiedebergs Arch Pharmacol 1996
				Rat		DC, LDF, FOSir		200 mg/kg, i.p.	60 min	KCl	↔	nd	↔	↑	Supornsilpchai, Cephalalgia 2010 (1)
Indomethacin				Rat		DC, LDF, FOSir		200 mg/kg/d, i.p.	30 days	KCl	↑	nd	↔	↔	Supornsilpchai, Cephalalgia 2010 (2)
		13	fp	Rat		DC, LDF	75-200 mg/day	5 mg/kg, i.v.	20 min	KCl	nd	nd	nd	↓	Shimizu, Neuroreport 2000
				Rat		DC, LDF		5 mg/kg, i.v.	20 min	KCl	nd	nd	↔	↔	Shimizu, Brain Res 2002

Table A1 (continued).

Subgroup	Drug Mesh term	Hits fo	SD categ	Species	Comments	Monitor	Human dose	Dose, route	Pretreatment	SD induction	Susceptibility	Speed	Duration	Amplitude	Reference
				Rabbit		Optical		15 mg/kg, i.v.	na	KCl	nd	nd	nd	↑	Meng, am J Physiol 1995
				Rat		ECoG, [14C]iap		5 mg/kg, i.v.	10 min	E	nd	nd	nd	↑	Duckrow, J Cereb Blood Flow Metab 1991
				Rat		DC		10 mg/kg, i.v.	15 min	M	nd	nd	nd	nd	Lauritzen, Acta Neurol Scand 1987
				Rabbit		DC, LDF		5-10 mg/kg, i.v.	30 min	KCl	nd	nd	nd	↑	Shibata, am J Physiol 1991
				Rabbit		DC, LDF		5-7 mg/kg, i.v.	30 min	KCl	nd	↔	nd	↑	Shibata, Brain Res 1992
				Rabbit		DC, LDF		5-10 mg/kg, i.v.	30 min	KCl	↔	↔	↔	↑	Shibata, Brain Res 1990
Immune suppressants															
Glucocorticoids	Dexamethasone	9	il	Rat		IHC	0.5-24 mg/day	2 mg/kg, i.p.	60 min	KCl	↓	nd	nd	nd	Caggiano, J Comp Neurol 1996 (1)
				Rat		IHC		2 mg/kg, i.p.	60 min	KCl	↓	nd	nd	nd	Caggiano, J Comp Neurol 1996 (2)
				Rat		IHC		1.5-5 mg/kg, i.p.	30 min	KCl	↓	nd	nd	nd	Miettinen, Proc Natl Acad Sci USA 1997
				Rat	in vivo + slices	DC, NB, ICC		1.5 mg/kg, i.p.	30 min	KCl	↔	nd	nd	nd	Koponen, Neuroscience 1999
				Chicken	retina	Optical		0.1-3 mM, CM	60 min	M	nd	nd	↑	↓	Dahlem, Brain Res 2005
Other	Cyclosporine	4	il	Rat	ECoG, LDF	2.5-15 mg/kg/day		0.1 mmol/L, CM	na	M	↔ (ECoG)	nd	↓ (CBF)	nd	Piilgaard, J Cereb Blood Flow Metab 2011
Opiates															
	Morphine	9	na	Human	trauma	DC	< 10 mg/day	avg. 8 mg	varying	Ischemia	↔	nd	nd	nd	Hertle, Brain 2012
	Sufentanil	1	na	Human	trauma	DC	10-20 μg/hour, epidural	avg. 0.06 mg	varying	Ischemia	↔	nd	nd	nd	Hertle, Brain 2012
	Fentanyl	3	na	Human	trauma patient	DC	0.2-0.8 mg	avg. 0.15 mg	varying	Ischemia	↔	nd	nd	nd	Hertle, Brain 2012
	Naloxone	11	ncd	Rat		DC	0.1 mg, i.v.	10 mg/kg/d, s.c.	7-28 days	KCl	nd	↓	nd	nd	Rocha-de-Melo, Neurosci Lett 2008
				Rat		DC		40 mg/kg, i.p.	10 min	KCl	↔	nd	nd	nd	Sprick, Brain 1981
Antidiabetics															
	Insulin	36	ncd	Rat		nd	0.5-1.0 IU/kg, i.v.	nd	40-70 min	nd	nd	↑	nd	nd	Ximenes-da-Silva, Braz J Med Biol Res 1991
			Rat	hypoglycaemic		DC		2 IU/kg, i.p.	na	KCl	nd	nd	↑	↔	Gid¨o , J Cereb Blood Flow Metab 1993
				Rat	hypoglycaemic	DC		3 U/kg/day, s.c.	3 days	KCl	↑	↑	nd	nd	Costa-Cruz, Neurosci Lett 2001
				Cat		Optical		1.5-4.5 mU/kg/min, i.v.	nd	Ischemia	↑	nd	nd	nd	hopwood,J Cereb Blood Flow Metab 2005
				Rat	hippocampal slices	DC, optical		400 μg/mL, CM	0,3,7 days	E	↓	nd	nd	nd	Grinberg, J Neurochem 2012
				Rat		DC		0.3 U/100 g, i.v.	na	KCl	nd	↑ (day) ↔ (night)	↓ (day) ↔ (night)	nd	Batinga, Neurosci Lett 2011
				Rat		DC		2.7-3.7 IU/kg, i.p.	30 min	KCl	↔	nd	↑	↔	Koistinaho, Stroke 1999
	Glyburide	2	nd	Rat		DC, LDF	2,5-15 mg/day	10-6, 10-5, 10-4M, CM	na	KCl	nd	nd	nd	↑ (LDF)	Shimizu, Neuroreport 2000
	Tolbutamide	4	na	Rat	hippocampal slices	DC	0,5-2 g/day	200 μM, CM	20 min	Hypoxia	↔	nd	nd	nd	Hepp, J Neurophysiol 2005
Antibiotics															
	Penicillins	33	il	Rat		DC	1. 2 * 10^6 IE, i.v.	nd	na	KCl	↓	↑	↓	↓	Ueda, Electroencephalogr Clin Neurophysiol 1977
				Rat		DC		10 M, topical	na	E	↓	nd	nd	nd	Koroleva, Electroencephalogr Clin Neurophysiol 1985
				Rat		DC		nd	20 min	KCl		nd	↓	↓	Koroleva, Electroencephalogr Clin Neurophysiol 1980
				Rat		DC		nd, topical	na	KCl	↓	nd	nd	nd	Bures, Epilepsia 1975
				Rat		DC		0.5 mg, topical	na	E	ncd	nd	nd	nd	Koroleva, Exp Brain Res 1983
	Ceftriaxone	1	nd	Rat	hippocampus	DC	1-4 g/day, i.v.	200 mg/kg, i.p.	5 days	OGD	↓	nd	nd	nd	Lipski, Neuroscience 2007
Narcotics															
	Ketamine	29	il	Human	trauma + sih	DC	40-240 mg/d	2-3 mg/kg/h, i.v.	na	Spontaneous	↓	nd	nd	nd	Sakowitz, Stroke 2009
				Rat		DC		40,80 mg/kg, i.p.	15 min	E	↓	↓	↑	↔	Marrannes, Brain Res 1988
				Rat		DC		10 mg/kg, i.p.	15 min	E	↔	↓	↔	↔	Marrannes, Brain Res 1988
				Human	trauma	DC		avg 200 mg, nd	varying	Spontaneous	↓ δ	nd	nd	nd	Hertle, Brain 2012
				Rat		DC		> 12mg/kg, i.p.	10-40 min	K-acetate	↓	nd	↔	↓−δ	Hernandez-Caceres, Brain Res 1987
				Rat		DC		50 mg/kg, i.p.	15-75 min	KCl	↓−δ	nd	nd	↓	Rashidy-Pour, Brain Res 1995
				Rat		DC		50 mg/kg, i.v.	30 min	E	↓	nd	nd	nd	Martin, Neurosci Lett 1994
				Rat		DC		100 mg/kg, i.p.	150-250 min	K-acetate	↓−δ	nd	↑	↓−δ	Amemori, Brain Res 1990
				Rat		DC		30-100 mg/kg, i.p.	5 min	K-acetate	↓−δ	nd	nd	↓−δ	Gorelova, Electroencephalogr Clin Neurophysiol 1987
	Propofol	6	il	Human	trauma	DC	avg 150 mg, i.v.	avg 150 mg, i.v.	varying	Spontaneous	↓	nd	nd	nd	Hertle, Brain 2012
				Mice		DC		120-200 mg/kg, i.p.	15 min	KCl	↓	↓	nd	↔	Dhir, Neurosci Lett 2012
	Pentobarbital	39	na	Rat		ECoG, [14C]iap	100-200 mg	40 mg/kg, i.v.	30 min	E	nd	↔	nd	↓	Duckrow, J Cereb Blood Flow Metab 1991
				Rat		DC		1.0 MAC	nd	KCl	↔	nd	↔	↔	Kitahara, J Neurosurg Anesthesiol 2001
Vitamins & minerals															
	Vitamin B2	7	fp	Rat		DC	3-10 mg/d	10 mg/kg, i.p.	4 weeks	KCl	↑	↓	↑	↔	Bogdanov, Neurobiol Dis 2011
	Ascorbic Acid	10	fp	Rat	well- and malnourished	DC, ECoG	50-500mg/day	60 mg/kg/d, p.g.	7-28 days	KCl	nd	↑	nd	↑	Monte-Guedes, Neurosci Lett 2011
	Magnesium Sulfate	15	ncd	Chicken	retina	Optical	500-1500mg/day, i.v.	0-4 mM, CM	na	M, optical	↓	↓	nd	nd	Martins-Ferreira, J Neurophysiol 1974
				Rat	SAH	DC		90 mg/kg, i.v.	na	Ischemia	nd	nd	↓	nd	Van den Bergh, J Neurosurg 2002
				Rat		DC		90 mg/kg, i.v.	90min post KCl	KCl	↓	nd	nd	nd	Van der Hel, Neuroreport 1998
Anticoagulants															
	Dipyridamole	2	il	Rat	hippocampus	DC	200mg/day	100 μM, CM	120 min	KCl	↓	nd	nd	↔	Hada, Eur J Pharmacol 1996
				Rat	hippocampus	DC		100 μM, CM	120 min	KCl	↓	nd	nd	nd	Kaku, Brain Res 1994
	Acetylsalicylic acid	3	na	Cat		LDF, SUA	1-8g/day	30 mg/kg, i.v.	60 min	Ischemia	↔	↔	nd	↔	Kaube, Eur Neurol 1994
Antipsychotics															
	Haloperidol	4	ip	Rat		DC	0.5-20mg/day	Intracerebral infusion	na	NMDA infususion	↓	nd	nd	nd	Svensson, Brain Res 1994
Hormones															
	Progesterone	8	ncd	Rat	neocortical slices	DC	na	0.1-50 μmol/L, CM	na	KCl	↑	↔	↑	↑	Sachs, Neurobiol Dis 2007
	Estrogens	55	ncd	Rat	neocortical slices	DC	na	0.1-50 μmol/L, CM	na	KCl	↑	↔	↑	↑	Sachs, Neurobiol Dis 2007
				Rat	WAR	DC		na	na	KCl	ncd	↔	nd	nd	Guedes, Epilepsy Res 2009
				Mice		nd		nd	nd	nd	ncd	nd	nd	nd	Brennan, Ann Neurol 2007
				Mice	FHM1	DC		na	na	KCl	ncd	ncd	ncd	ncd	Eikermann-Haerter, Ann Neurol 2009
				Rat		DC	0.025-0.075 mg, s.c. pellet	21 days release	na	KCl	ncd	ncd	ncd	ncd	Eikermann-Haerter, J Clin Invest 2009
				Rat	ovariectomized	DC		na	na	KCl	nd	↑	↑	ncd	Accioly, Int J Dev Neurosci 2012
	Melatonin	8	ip	Rat		LDF	2mg/day	20-40 mg/kg, i.p.	30 min	KCl	↓	nd	nd	↓	Le Grand, Neuroreport 2006
				Chicken	retina	Optical		0.3-1.4 mM, CM	na	M	nd	↓	nd	nd	Ebert, Neurosci Lett 1999
	Norepinephrine	17	ip	Rat		DC, LDF	2-4 μg/min	0.1-1 mmol/L, CM	na	M, KCl	↓	nd	nd	nd	Richter, J Cereb Blood Flow Metab 2005
	Propylthiouracil	2	nd	Rat		nd	75-150mg/day	8 mg/kg/day, nd	na	nd	nd	↓	nd	nd	Guedes, Braz J Med Biol Res 1993 (abstract)
	Somatostatin	6	nd	Rat	cortical slices	DC	3.5 μg/kg/h, i.v.	1 μM, CM	nd	E	↓	nd	nd	nd	Ben-Ari, Neurosci 2003
Local acting agents															
	Miconazole	1	na	Rat		DC, LDF	na	10-6, 10-5 M, CM	na	KCl	↔ (CBF)	nd	↔	↔	Shimizu, Brain Res 2002
	Benzocaine	1	na	Chicken	retina	DC	na	1-4 mM, CM	30 min	nd	↓	↓ δ	↓	↓	Chebabo, Exp Brain Res 1993
Parasympatihicolytics															
	Atropine	17	nd	Rat		ECoG, [14C]iap	0,3-0,6 mg, s.c./i.m.	0.3 mg/kg, i.v.	10 min	E	nd	nd	nd	↔	Duckrow, J Cereb Blood Flow Metab 1991
Migraine prophylactics															
	Flunarizine	26	il	Rat		DC	10mg/day	20-40 mg/kg, i.p.	105 min	E	↔	nd	↔	↔	Marrannes, book 1 (review Ayata)
				Rat		DC		20 mg/kg, p.o. b.i.d.	36 hrs	E	↔	nd	↓	↔	Marrannes, book 1 (review Ayata)
				Rat		DC		20 mg/kg/day, p.o.	5 days	M	↔	↔	nd	↔	Hansen, book (review Ayata)
				Rat		DC		30 mg/kg, p.o.+ 10 mg/k	24 hrs	M, E	↓	nd	nd	nd	Reid, Drug Dev Res 1987
				Rat		DC		40 mg/kg, i.p.	60 min	M	↓	nd	nd	nd	Wauquier, Cephalalgia 1985
				Rat		DC		10-20 mg/kg, i.p.	105 min	E	↔	nd	↓	nd	Marrannes, book 2 (review Ayata)
				Rat		DC		20 mg/kg, p.o. b.i.d.	36 hrs	KCl	↓	nd	↓	nd	Marrannes, book 2 (review Ayata)
				Rat		DC		30+10 mg/kg, nd	nd	E	↔	nd	nd	nd	Reid, Physiol Bohemoslov 1988 (abstract)
				Rat		DC		1-2 mg/kg i.p.+40 μM, tc	nd	KCl	↓	nd	nd	nd	Richer, Neurosci Lett 2005
				Rat		LDF		1 mg/kg, i.v.	5 min	KCl	nd	nd	nd	↓ (CBF)	Shimazawa, Br J Pharmacol 1995
Migraine treatment															
	Ergotamine	13	na	Rat		DC	1-4mg/week, supp	0.31-20 mg/kg, i.p.	105 min	E	↔	nd	↑	↔	Marrannes, book 1 (review Ayata)
				Chicken	retina	DC		10-20 μM, CM	nd	KCl	nd	↔	↔	↔	Wiedemann, Naunyn-Schmiedebergs Arch Pharmacol 1996
	Dihydroergotamine	14	na	Cat		LDF, SUA	1-3/attack, max 6mg/wk	15 μg/kg, i.v.	60 min	Ischemia	↔	↔	nd	↔	Kaube, Eur Neurol 1994

Table A1 (continued).

Subgroup	Drug Mesh term	Hits fo	SD categ	Species	Comments	Monitor	Human dose	Dose, route	Pretreatment	SD induction	Susceptibility	Speed	Duration	Amplitude	Reference
				Mice		Optical		0.03-0.15 mg/kg, nd	nd	KCl	↓	nd	nd	↓	Zyuzin, Headache 2012
	Sumatriptan	69	na	Cat		MRI	50-300mg/day	0.3 mg/kg, i.v.	15 min	KCl	↔	↔	↔	nd	Bradley, Exp Neurol 2001
				Cat, rat		DC		0.3 mg/kg, i.v.	15 min	KCl	↔	nd	nd	↔	Read, Brain Res 2000
				Rat		DC		0.3 mg/kg, i.v.	30 min	KCl	↔	nd	↓	↔	Moskowitz, J Neurosci 1993
				Rat		DC		0.3 mg/kg, i.v.	15 min	KCl	↔	nd	nd	nd	Read, Brain Res 2001
				Chicken	retina	DC		1.5 mM, CM	nd	KCl	nd	↓ *δ*	↓	↓ *δ*	Wiedemann, Naunyn-Schmiedebergs Arch Pharmacol 1996
				Rat		DC,LDF		2mg/kg, i.v.	-5 min	Ischemia	↓	nd	↓	nd	Mies, J Stroke Cerebrovasc Dis 1998
				Rat	hippocampal slices	nd		10M, CM	nd	hypoxia	↔	nd	nd	nd	Takagi, Nihon Yakurigaku Zasshi 1998
				Chicken	retina	DC		0.05-2mM, CM	na	M	↓	↓ *δ*	nd	nd	Maranhao-Filho, Cephalalgia 1997
Dementia drugs															
	Memantine	6	il	Rat		DC, LDF	10-20mg/day	3-10 mg/kg, i.p.	60 min	KCl	↓	nd	nd	↓	Peeters, J Pharmacol Exp Ther 2007
Membrane stabilizers															
	Lidocaine	23	na	Cat		LDF, SUA	200-300mg/hour, i.v.	5 mg/kg, i.v.	60 min	Ischemia	↔	↔	nd	↔	Kaube, Eur Neurol 1994
				Chicken	retina	DC		3-7mM, CM	30 min	nd	↓	↓ *δ*	↓	↓	Chebabo Exp Brain Res 1993
				Rat	caudate nucleus	DC		200 μM, CM	na	hypoxie/hypoglyce	↓	nd	↑	nd	Toner, Neuroscience 1997
				Gerbil	hippocampal slices	DC		10,50,100 μM, CM	10 min	Ischemia	↓	nd	↔	↓	Liu, Anesthesiology 1997
				Rat		DC, LDF		10μg, local	20 min	M, KCl	↔	nd	nd	nd	Lambert, Cephalalgia 2011
Anti-arrhythmics															
	Quinidine bisulfate	2	ip	Rat	cortical slices	DC	200-1600 mg/day	100-200 μM, CM	na	KCl	nd	↓	↓ *δ*	↓	Margineanu, Brain Res Bull 2006
Gastric antispasmodic															
	Papaverine	7	ip	Rat		LDF, DC	300-600mg/day	100 μmol/L, CM	nd	KCl	↓ (CSI ↔CSD)	nd	nd	nd	Dreier, J Physiol 2001
				Rat		LDF		100 μM, CM	nd	KCl	↔	nd	nd	nd	Scheckenbach, Exp Neurol 2006
Nitrates															
	Nitroglycerin	16	ip	Mice		DC, optical	0,4-1,2mg, s.l.	0.5-10 mg/kg, i.p.	30,60 min	E	nd	↔	↔	↑	bates, Cephalalgia 2010
				Cat		DC, LDF		0.25 μg/kg/min, i.v.	2 hrs	KCl	nd	nd	↓	↔	Read, Cephalalgia 1997
Muscle relaxants															
	Baclofen	5	na	Chicken	Retina	nd	30-80mg/day	100 μm, CM	na	KCL	↔	nd	nd	nd	Sheardown, Brain Res 1993
Pulmonary hypertension															
	Sildenafil	4	na	Rat		DC	20-60mg/day	100 μg, CM	100-200 min pos	E	nd	nd	↔	↔	Wang, Brain Res 2004
Ungrouped															
	Theophylline	4	fp	Rat	hippocampus	DC	5-900mg/d	1 mM, CM	120 min	KCl	↑	nd	nd	nd	Hada, Eur J Pharmacol 1996
				Rat	hippocampus	DC		1 mM, CM	120 min	KCl	↑	nd	nd	↓	Kaku, Brain Res 1994
	Lithium	12	ncd	Rat		DC	800-1600mg/d	50mg/kg, i.p.	1x 15-30 days	KCL	nd	↓	nd	nd	de Aguiar, Nutr Nrsc 2011
				Rat		nd		1.5 g/kg, nd	nd	nd	nd	↓	nd	nd	Guedes, Braz J Med Biol Res 1989
	Zaprinast	1	ncd	Rat		DC	25-100mg/d	300 μg, CM	100-200 min pos	E	nd	nd	↑	↓	Wang, Brain Res 2004

Legend of tables A1 & A2

Abbreviation	Definition
↔	no effect
↓	decrease
↑	increase
δ	dose dependent increase
−δ	dose dependent decrease
TCAs	tricyclic antidepressants
AEDs	anti-epileptics
BPLs	blood pressure lowering drugs
NSAIDs	non-steroidal anti-inflammatory drugs
il	SD inhibitor likely
ip	SD inhibitor possibly
iw	SD inhibitor weak
fl	SD facilitator likely
fp	SD facilitator possibly
fw	SD facilitator weak
nd	no data
ncd	no consistent data
DC	slow extracellular potential shift
LDF	laser doppler flowmetry measuring blood flow changes
SUA	single unit spike activity
ECoG	electrocorticogram
IHC	immunohistochemistry
NB	northern blot
ICC	immunocytochemistry
14C-iap	[14C]-iodoantipyrine
E	electricatelectrically-induced SD
M	mechanical pinprick-induced SD
KCl	kaliumcloride-induced SD
OGD	oxygen glucose deprivation-induced SD
CM	culture medium
i.v.	intraveneous
i.p.	intraperitoneal
i.c.	intracortical
p.o.	per os
b.i.d.	bis in die
p.g.	per gavage
i.m.	intramusculair
s.l.	sublingual
supp	suppositorium
avg	average
sah	subarachnoidal hemorhage
sih	spontaneous intracranial hypotension
SHRSP	stroke-prone spontaneously hypertensive

Table A2. Medications with category 'no data' or without any hits.

Group	Drug Mesh term	hits	cat.
Serotonine manipulators (oa. SSRIs)	Venlafaxine	0	nd
	Paroxetine	0	nd
	Duloxetine	0	nd
	Escitalopram	2	nd
	Fluvoxamine	0	nd
	Sertraline	0	nd
TCAs	Clomipramine	1	nd
	Imipramine	1	nd
	Nortriptyline	0	nd
	Maprotiline	0	nd
Other antidepressives	Mirtazapine	0	nd
Anti-epileptics	Ethosuximide	0	iw
	Felbamate	0	iw
	Lacosamide	0	iw
	Stiripentol	0	iw
	Vigabatrin	0	iw
	Zonisamide	0	iw
	Pregabalin	1	iw
	Primidone	0	fw
Benzodiazepines	Clobazam	0	nd
	Alprazolam	0	nd
	Bromazepam	0	nd
	Chlordiazepoxide	1	nd
	Lorazepam	0	nd
	Lormetazepam	0	nd
	Prazepam	0	nd
	Oxazepam	0	nd
	Flumazenil	1	nd
	Flurazepam	0	nd
	Zopiclone	0	nd
	Zolpidem	0	nd
	Temazepam	0	nd
	Nitrazepam	0	nd
Beta blockers	Atenolol	1	nd
	Oxprenolol	0	nd
	Acebutolol	0	nd
	Betaxolol	0	nd
	Carvedilol	0	nd
	Bisoprolol	0	nd
	Celiprolol	0	nd
	Esmolol	0	nd
	Labetalol	0	nd
	Nebivolol	0	nd
	Pindolol	0	nd
	Sotalol	0	nd
ACE inhibitors	Lisinopril	0	nd
	Enalapril	0	nd
	Captopril	0	nd
	Perindopril	0	nd
	Benazepril	0	nd
	Fosinopril	0	nd
	Cilazapril	0	nd
	Quinapril	0	nd
	Ramipril	0	nd
	Trandolapril	0	nd
	Zofenopril	0	nd
Angiotensin inhibitors	Candesartan	1	nd
	Eprosartan	0	nd
	Irbesartan	0	nd
	Losartan	0	nd
	Valsartan	0	nd
	Olmesartan	0	nd
	Telmisartan	0	nd
Parasympatihicolytics	Ipratropium	0	nd
	Tiotropium	0	nd
	Atropine	17	nd
BPIs, central acting	Methyldopa	0	nd
	Moxonidine	0	nd
BPLs, diuretics	Triamterene	0	nd
	Epithizide	0	nd
	Hydrochlorothiazide	0	nd
	Chlorthalidone	0	nd
	Clopamide	0	nd
BPLs, other	Urapidil	0	nd
	Bumetanide	3	nd
	Spironolactone	2	nd
NSAIDs	Ibuprofen	3	fw
	Diclofenac	4	fw
	Aceclofenac	0	fw
	Celecoxib	0	fw
	Etoricoxib	0	fw
	Phenylbutazone	0	fw
	Naproxen	4	fw
	Rofecoxib	0	fw
	Nabumetone	0	fw
	Meloxicam	1	fw
H2r-antagonists	Cimetidine	1	nd
	Ranitidine	3	nd
	Famotidine	0	nd
	Nizatidine	0	nd
Proton pump inhibitors	Omeprazole	0	nd
	Esomeprazole	0	nd
	Pantoprazole	0	nd
	Lansoprazole	0	nd
	Rabeprazole	0	nd
Urine retention drugs	Tamsulosin	0	nd
	Doxazosin	0	nd
	Alfuzosin	0	nd
	Dutasteride	0	nd
	Finasteride	0	nd
	Terazosin	0	nd
Lipid lowering agents	Simvastatin	0	nd
	Atorvastatin	0	nd
	Fluvastatin	0	nd
	Pravastatin	0	nd
	Rosuvastatin	0	nd
	Cerivastatin	0	nd
	Colesevelam	0	nd
	Ezetimibe	0	nd
	Ciprofibrate	0	nd
Glucocortcoids	Prednisolone	1	iw
	Prednisone	1	iw
	Cortisone	0	iw
	Hydrocortisone	2	iw
	Methylprednisolone	1	iw
	Triamcinolone	1	iw
Opiates	Alfentanil	3	fw
	Buprenorphine	0	fw
	Dextromoramide	0	fw
	Dextropropoxyphene	0	fw
	Hydromorphone	0	fw
	Methadone	0	fw
	Nicomorphine	0	fw
	Oxycodone	0	fw

Table A2 (continued).

Group	Drug Mesh term	hits	cat.
	Pentazocine	1	fw
	Meperidine	1	fw
	Piritramide	0	fw
	Remifentanil	0	fw
	Tramadol	0	nd
	Codeine	0	nd
Antibiotics	Amoxicilin	0	nd
	Clarithromycin	0	nd
	Clavulanic Acids	0	nd
	Floxacillin	0	nd
	Norfloxacin	0	nd
	Ciprofloxacin	0	nd
	Trimethoprim	0	nd
	Cotrimoxazole	0	nd
	Cefazolin	0	nd
	Doxycycline	0	nd
	Erythromycin	0	nd
	Nitrofurantoin	0	nd
	Clindamycin	0	nd
Antiviral agents	Acyclovir	0	nd
	HAART	0	nd
	Zidovudine (HAART1)	0	nd
	Lamivudine (HAART2)	0	nd
	Lopinavir (HAART3)	0	nd
	Tenofovir (HAART4)	0	nd
	Emtricitabine (HAART5)	0	nd
	Efavirenz (HAART6)	0	nd
Histamine antagonists	Promethazine	1	nd
	Cetirizine	0	nd
	Acrivastine	0	nd
	Trimeprazine (Alimemazine)	0	nd
	Clemastine	0	nd
	Cyproheptadine	1	nd
	Desloratadine	0	nd
	Dexchlorpheniramine	0	nd
	Dimethindene	0	nd
	Ebastine	0	nd
	Fexofenadine	0	nd
	Hydroxyzine	0	nd
	Ketotifen	0	nd
	Levocetirizine	0	nd
	Loratadine	0	nd
	Mebhydroline	0	nd
	Mizolastine	0	nd
	Oxatomide	0	nd
	Rupatadine	0	nd
	Cinnarizine	1	nd
	Terfenadine	0	nd
	Sulfamethoxazole	0	nd
Vitamins & minerals	Vitamin B Complex	7	nd
	Thiamine (VitB1)	0	nd
	Niacinamide (VitB3)	0	nd
	Pantothenic Acid (VitB5)	1	nd
	Pyridoxine (VitB6)	0	nd
	Biotin (VitB7)	4	nd
	Folic Acid (VitB9)	1	nd
	Vitamin B12	0	nd
	Vitamin D	0	nd
	Iron fumarate	0	nd
	Calcium Carbonate	3	nd
	Cholecalciferol	0	nd
Laxatives	Bisacodyl	0	nd
	Magnesium Hydroxide	0	nd
	Lactulose	0	nd
	Polyethylene Glycols	0	nd
	Magnesium Oxide	1	nd
	Psyllium	0	nd
Immune suppressants	Mycophenolate mofetil	0	nd
Anticoagulants	Warfarin	0	nd
	Acenocoumarol	0	nd
	Phenprocoumon	0	nd
	Clopidogrel	0	nd
	Heparin	3	nd
	Dalteparin	0	nd
	Nadroparin	0	nd
	Danaproid	0	nd
	Enoxaparin	0	nd
	Fondaparinux	0	nd
	Tinzaparin	0	nd
Antipsychotics	Clozapine	0	nd
	Pimozide	0	nd
	Risperidone	0	nd
	Perphenazine	0	nd
	Olanzapine	0	nd
Anti-diabetics	Metformin	0	nd
	Glimepiride	0	nd
	Gliclazide	0	nd
Calcium antagonists	Mepirodipine	0	iw
	Felodipine	0	iw
	Lacidipine	0	iw
	Nicardipine	3	iw
	Lercanidipine	0	iw
	Isradipine	1	iw
	Nitrendipine	0	iw
	Amlodipine	0	iw
Hormone and -inhibitors	Tamoxifen	3	nd
	Deamino Arginine	0	nd
	LH	3	nd
	Thyroxine	0	nd
	Methimazole	0	nd
	Potassium Iodide	1	nd
	Carbimazole	0	nd
	Medroxyprogesterone	0	nd
	Vasopressin	0	nd
Vertigo drugs	Betahistine	0	nd
Local acting agents	Indacaterol	0	na
	Povidone	0	na
	Albuterol	0	na
	Tiotropium	0	na
	Formoterol	0	na
	Salmeterol	0	na
	Ephedrine	0	na
	Terbutaline	0	na
	Fluticasone	0	na
	Beclomethasone	0	na
	Budesonide	0	na
	Ciclesonide	0	na
	Miconazole	0	na
	benzocaine	1	na
	Chloramphenicol	0	na
	Latanoprost	0	na
	Acetylcysteine	0	na
	Dorzolamide	0	na
	Betamethasone	0	na

Table A2 (continued).

Group	Drug Mesh term	hits	cat.
	Dexamethasone	0	na
	Fusidic Acid	0	na
	Timolol	3	na
Migraine prophylactics	Methysergide	0	nd
	Pizotyline	0	nd
	Topiramate	0	nd
Migraine treatment	Almotriptan	1	nd
	Eletriptan	1	nd
	Rizatriptan	4	nd
	Naratriptan	2	nd
	Frovatriptan	0	nd
	Zolmitriptan	6	nd
Dementia drugs	Rivastigmine	0	nd
Gastric antispasmodic	Mebeverine	0	nd
	Scopolaminebutyl	0	nd
Nitrates	Isosorbide Dinitrate	0	nd
	Isosorbide-5-mononitrate	0	nd
	Nitroprusside	11	nd
Dopamine antagonists	Domperidone	0	nd
	Metoclopramide	1	nd
	Droperidol	0	nd
	Alizapride	0	nd
Hemostatics	Tranexamic Acid	0	nd
MS drugs	Interferon beta-1b	0	nd
	Interferon beta-1a	0	nd
	Interferons	6	nd
	Copolymer 1 (Glatirameer)	0	nd
Muscle relaxants	Atracurium	0	nd
	Botulinum Toxins	14	nd
	Dantrolene	3	nd
	Hydroquinidine	0	nd
	Pramipexol	0	nd
	Ropinirole	0	nd
	Rotigotine	0	nd
	Tizanidine	0	nd
Parkinson drugs	Levodopa	0	nd
	Amantadine	0	nd
	Benserazide	1	nd
Claudicatio intermittens	Ginkgo biloba	0	nd
	Pentoxifylline	0	nd
Gout drugs	Allopurinol	0	nd
	Colchicine	1	nd
Calcium regulators	Etidronic Acid	0	nd
	Alendronate	0	nd
	Risedronic acid	0	nd
Rheumatoid arthritis	Methotrexate	0	nd
	Infliximab	0	nd
	Azathioprine	0	nd
	TNFR-Fc fusion protein	0	nd
	Hydroxychloroquine	0	nd
Pulmonary hypertension	Tadalafil	0	nd
Ib shorten action potential	Flecainide	0	nd
	Propafenone	0	nd
	Disopyramide	0	nd
Antipsychotics	Haloperidol	4	ip
Ungrouped	Sucralfate	0	nd
	Misoprostol	0	nd
	Acetylcysteine	0	nd
	Montelukast	0	nd
	Potassium Chloride	»	ncd
	Mesna	0	nd
	Naltrexone	0	nd
	Gemfibrozil	0	nd
	Tolterodine	0	nd
	Thalidomide	0	nd
	Sulfasalazine	0	nd
	Solifenacin	0	nd
	Digoxin	1	nd
	Nevirapine	0	nd
	Pancreatin	0	nd

Legend of tables A1 & A2

Abbreviation	definition
↔	no effect
↓	decrease
↑	increase
δ	dose dependent increase
$-\delta$	dose dependent decrease
TCAs	tricyclic antidepressants
AEDs	anti-epileptics
BPLs	blood pressure lowering drugs
NSAIDs	non-steroidal anti-inflammatory drugs
il	SD inhibitor likely
ip	SD inhibitor possibly
iw	SD inhibitor weak
fl	SD facilitator likely
fp	SD facilitator possibly
fw	SD facilitator weak
nd	no data
ncd	no consistent data
DC	slow extracellular potential shift
LDF	laser doppler flowmetry measuring blood flow changes
SUA	single unit spike activity
ECoG	electrocorticogram
IHC	immunohistochemistry
NB	northern blot
ICC	immunocytochemistry
14C-iap	[14C]-iodoantipyrine
E	electricatelectrically-induced SD
M	mechanical pinprick-induced SD
KCl	kaliumcloride-induced SD
OGD	oxygen glucose deprivation-induced SD
CM	culture medium
i.v.	intraveneous
i.p.	intraperitoneal
i.c.	intracortical
p.o.	per os
b.i.d.	bis in die
p.g.	per gavage
i.m.	intramusculair
s.l.	sublingual
supp	suppositorium
avg	average
sah	subarachnoidal hemorhage
sih	spontaneous intracranial hypotension
SHRSP	stroke-prone spontaneously hypertensive

Chapter 6

Circle of Willis variations in migraine patients with ischemic stroke

Hamming AM, Van Walderveen MAA, Mulder IA, van der Schaaf AC,
Kapelle LJ, Velthuis BK, Ferrari MD, Terwindt GM,
Visser MC, Schonewille W, Algra A, Wermer MJH,
On behalf of the Dutch acute Stroke Trial (DUST) investigators

Brain Behav 2019 Mar 9(3):e01223

Abstract

Objectives

Migraine is a risk factor for stroke, which might be explained by a higher prevalence in anatomical variants in the circle of Willis (CoW). Here, we compared the presence of CoW-variants in patients with stroke with and without migraine.

Materials and Methods

Participants were recruited from the prospective Dutch acute Stroke Trial. All participants underwent CT-angiography on admission. Lifetime migraine history was assessed with a screening questionnaire and confirmed by an interview based on International Classification of Headache Disorders criteria. CoW was assessed for incompleteness/ hypoplasia (any segment<1mm), for anterior cerebral artery asymmetry (difference>1/3) and for posterior communicating artery (Pcom) dominance (Pcom-P1 difference>1/3). Odds ratios with adjustments for age and sex (aOR) were calculated with logistic regression.

Results

We included 646 participants with stroke, of whom 52 had a history of migraine. Of these, 45/52 (87%) had an incomplete or hypoplastic CoW versus 506 (85%) of the 594 participants without migraine (aOR:1.47; 95%CI:0.63-3.44). There were no differences between participants with and without migraine in variations of the anterior or posterior CoW, anterior cerebral artery asymmetry (aOR:0.86; 95%CI:0.43-1.74), or Pcom dominance (aOR:0.64; 95%CI:0.32-1.30). There were no differences in CoW-variations between migraine patients with or without aura.

Conclusion

We found no significant difference in the completeness of the circle of Willis in acute stroke patients with migraine compared to those without.

Introduction

The circle of Willis (CoW) is an important structure for collateral cerebral blood flow. Anatomical variations of the CoW are common in the general population. CoW variants may be congenital but can also be acquired when patients get older.[189] Some[190-193], but not all[56, 194, 195] studies report a higher frequency of incomplete CoW in migraine patients compared with controls in particular for the posterior circulation and in patients with migraine with aura.

Migraine with aura is associated with a two-fold risk of ischemic stroke.[52] In addition, migraine with aura is strongly associated with subclinical infarctions in the posterior circulation.[196] Variation in the anatomy of the CoW, notably in the posterior circulation, might contribute to the increased risk of stroke in migraine patients like in patients with cardiovascular disease.[18, 197, 198] An incomplete CoW might hamper collateral blood flow through the CoW in case of an ischemic event and might also affect cerebral perfusion, possibly facilitating spreading depolarizations (SDs).[192] SDs are the electrophysiological correlate for migraine aura, and most commonly affect the visual cortex in the posterior circulation territory.[41, 190] Higher susceptibility to SDs decreases the threshold for cerebral ischemia.[49, 59, 176] Thus the combination of SDs and CoW variations might be a risk factor for stroke in migraine.

The relationship between migraine and CoW-variants has thus far only been investigated in population or out-patient based migraine cohorts.[190-192, 195] One would expect, however, that if there is a real relationship between variation in the CoW and migraine, this should be more pronounced in patients with stroke. In the present study we tested this hypothesis.

Materials and methods

Patients

Participants were included from the Dutch acute Stroke Trial (DUST), a large prospective multicenter cohort study performed between May 2009 and August 2013 in the Netherlands (ClinicalTrials.gov NCT00880113).[199] The aim of DUST was to investigate the value of CT perfusion (CTP) and CT angiography (CTA) for predicting outcome after ischemic stroke.[199] Inclusion criteria were: age ≥ 18 years, onset of stroke symptoms < 9 h, and NIHSS ≥ 2 or ≥1 if intravenous thrombolysis was indicated. Exclusion criteria were: other diagnosis than ischemic stroke on CT scan, known renal failure or known contrast allergy. Between February 2011 and August 2013, 10 of the 14 participating hospitals (University Medical Center Utrecht (UMCU), Alysis, Catharina Ziekenhuis, St Radboud Nijmegen, Gelre Hospital Apeldoorn, Leiden University Medical Center (LUMC), Medisch Centrum Haaglanden (MCH), St Elisabeth Ziekenhuis, VU Medical Center (VUmc) and St Antonius Ziekenhuis) included patients in the migraine side-study.

Demographic data, medical history, cardiovascular risk factors and NIHSS score on admission were prospectively recorded. Stroke territory was assessed by the treating physician with access to clinical and radiological data. DUST was approved by the medical ethical committee of the participating hospitals. Written informed consent was obtained from all patients for use of their data.

Migraine assessment

Lifetime migraine history was assessed in a uniform way by the DUST research nurses with the short 5-item migraine in stroke screener (MISS). The MISS questionnaire was validated in a previous study and has a high negative predictive value (0.99) but a moderate positive predictive value (0.80) in patients with stroke.[200] Therefore, all patients who answered positively to any of the questions were contacted by a research assistant, trained by a migraine neurologist (G.M.T), for an extensive migraine interview to verify the migraine diagnosis. The migraine interview was based on the International Classification of Headache Disorders (ICHD)-II criteria[201] which are comparable to the recently updated ICHD-III beta criteria[202]. Migraine diagnoses were divided in two subtypes: 1) migraine with aura and 2) migraine without aura. Patients who had both migraine attacks with and without aura, were included in the migraine with aura group. Patients who fulfilled the criteria for migraine without aura but had probable or possible aura symptoms were classified as migraine without aura. Patients who refused to participate in the telephone interview or were lost to follow-up were excluded from the analysis.

Assessment of anatomical variations in the circle of Willis

All patients underwent non-contrast CT, CTP and CTA on admission with standardized scan protocols between centers. Scan parameters of the non-contrast CT (NCCT) were: 120 kVp, 300 mAs and 1 mm reconstructed slice thickness. For CTA 60–80 mL of contrast agent (300 mg I/mL) was injected into the antecubital vein (18-gauge needle) at a rate of 6 mL/s followed by a 40 mL saline flush at a rate of 6 mL/s. The scan parameters for the CTA were: 120 kVp, 150 mAs and 1 mm reconstructed slice thickness. Radiologic parameters were assessed by one of three neuroradiologists with at least 5 years of experience in stroke imaging.[203]

Our primary endpoint was incompleteness of the CoW. Segments of the CoW were considered normal if they had a diameter of ≥ 1 mm. Segments < 1 mm were classified as hypoplastic or invisible. The anterior CoW was classified as incomplete if the anterior communicating artery or one of the A1 segment(s) of the anterior cerebral artery were hypoplastic or invisible. The posterior CoW was classified as one-sided incomplete if one of the posterior communicating arteries (Pcom) or P1 segments of the posterior cerebral artery was hypoplastic or invisible. If a hypoplastic or invisible Pcom or P1 segment was present on both sides, the posterior CoW was classified as two-sided incomplete.

A1 asymmetry was considered present if the diameter of the left and right A1 segments differed by more than one-third. The Pcom was considered dominant if the Pcom diameter exceeded the ipsilateral P1 diameter by more than one-third. Additional variants of the CoW were noted, such as a median artery corpus callosi (MACC, three A2 segments) and an azygos anterior cerebral artery. Patients with incomplete radiological data on the CoW anatomy were excluded. For a subgroup analysis excluding patients with large vessel disease, we excluded all patients with with a stenosis >70% or occlusion in a large vessel (common and internal carotid, basilar an vertebral arteries) as visible on CT-angiography.

Data analysis

Anatomical variations of the CoW were compared between stroke patients with and without a history of migraine. Within the patients with migraine we compared CoW variations in patients with and without aura. Odds ratios (OR) and 95% confidence intervals (CI) were calculated with univariable and multivariable (aOR, adjusted for age and sex) logistic regression analyses. Data were analysed with IBM SPSS Statistics for Windows, Version 20.0.

Results

Patients

In total 866 DUST patients were included in the participating hospitals during the period of collecting the MISS migraine questionnaire. Of those, 707 (82%) participants filled in the questionnaire. In total 32 were lost to follow-up, 25 refused to participate in the telephone interview and in 4 the radiological data on the CoW were incomplete for technical reasons. We therefore included 646 patients in our study; 52 with a history of migraine and 594 without migraine. Of the 52 patients with migraine, 29 (56%) had migraine with aura and 23 (44%) had migraine without aura.

Stroke patients with migraine were in general younger, more often female and had less often hypertension compared with stroke patients without migraine (Table 1). Migraine with aura patients more often had ischemia in the posterior circulation compared to migraine without aura patients and patients without migraine. Stroke subtypes were scored according to the etiological TOAST classification (as introduced in the Trial of Org 10172 in Acute Stroke Treatment).[10] Stroke subtypes were comparable between the groups except that small vessel disease was more often found to be the cause of stroke in migraine patients with aura.

Variants of the circle of Willis

Forty-five (87%) of the 52 migraineurs had an incomplete CoW versus 506 (85%) of the 594 participants without migraine (OR 1.12; 95% CI 0.49-2.56) (Table 2). After adjustment for age and sex the aOR was 1.47 (95% CI 0.63-3.44). There were also no differences between the two groups when the anterior and posterior CoW were analyzed separately. Asymmetry of the A1 segment of the anterior cerebral artery (aOR 0.86; 95% CI 0.43-1.74) and dominance of the posterior communicating artery (aOR 0.64; 95% CI 0.32-1.30) were also not different in migraineurs. Migraine with aura patients more often had an incomplete anterior CoW compared with participants without migraine (aOR 3.22; 95% CO 1.21-8.59). There were no differences in posterior of total CoW incompleteness between migraine with aura and participants without migraine.

In total 23 (79%) of migraine with aura patients had an incomplete CoW versus 22 (96%) migraine without aura patients (aOR 0.14; 95% CI 0.01-1.58) (Table 3). There was no difference in A1 asymmetry or Pcom dominance between the two subtypes of migraine. Additional variants (most commonly the MACC) were found in 4% of all patients and were not more frequent in migraineurs.

In patients with ischemia in the posterior circulation, incompleteness of the posterior CoW was not more common in migraineurs than in patients without migraine (aOR 0.81; 95%CI 0.16-4.14).

In a subgroup analysis excluding patients with large vessel disease, no significant differences were found between participants with versus no migraine, nor in participants with migraine with aura versus no migraine in unadjusted nor adjusted odds ratios, comparing total, anterior and posterior completeness, A1 asymmetry nor Pcom dominance (supplementary tables 2b and 3b).

Table 1. Baseline characteristics of the 646 participants.

	No migraine N=594	Migraine N=52	MA N=29	MO N=23	*P*-value (migraine vs no migraine)
Age (mean, ±SD)	67 (± 13)	60 (± 11)	58 (± 8)	64 (± 13)	0.0003
Women	221 (37%)	29 (56%)	12 (41%)	17 (74%)	0.01
Smoker (N=615)	168 (30%)	23 (45%)	13 (45%)	10 (45%)	0.03
Alcohol use (N=496)	263 (62%)	26 (72%)	14 (70%)	12 (75%)	0.46
NIHSS (median, N=642)*	5 (7)	5 (9)	5 (9)	4 (7)	0.36
Stroke/TIA history (N=641)	138 (23%)	14 (27%)	7 (24%)	7 (30%)	0.57
Hypertension (N=639)	284 (48%)	20 (38%)	10 (34%)	10 (43%)	0.29
Stroke territory					
ACA (N=596)	23 (4%)	1 (2%)	0 (0%)	1 (6%)	0.56
ACM (N=595)	426 (77%)	29 (67%)	17 (65%)	12 (71%)	0.15
Posterior territory (N=616)	98 (17%)	11 (23%)	8 (30%)	3 (14%)	0.32
Stroke type (N=416)					0.99
Large vessel disease	169 (44%)	13 (42%)	7 (47%)	6 (38%)	
Cardiac embolus	96 (25%)	8 (26%)	3 (20%)	5 (31%)	
Small vessel disease	78 (20%)	7 (23%)	4 (27%)	3 (19%)	
Dissection	22 (6%)	2 (6%)	1 (7%)	1 (6%)	
Other	20 (5%)	1 (3%)	0 (0%)	1 (6%)	

* parentheses: interquartile range

MA = migraine with aura. MO = migraine without aura. NIHSS = National Institutes of Health Stroke Scale. ACA = anterior cerebral artery. ACM = middle cerebral artery. Smokers only include current smokers. Alcohol use is any degree of alcohol consumption. Hypertension refers to a history of hypertension prior to the stroke. Stroke territory was scored by the treating physician, with access to radiological data. Posterior stroke territory includes both the posterior cerebral artery (PCA), basilar and vertebral artery territories. Stroke type is according to TOAST classification, with dissections specified from other causes. (N) = The number of patients for the particular variable in case there are missing data. *P*-values, for migraine versus no migraine, are calculated with an independent samples Student's *t*-test for age, a Mann-Whitney U test for NIHSS and a Chi-square test for the other variables. Characteristics with *P*-values < 0.05 do not have to be confounders whereas characteristics with *P*-values >0.05 may still be confounders. We considered age and sex to be confounders and adjusted for them in our analyses.

Table 2. CoW-variants in stroke patients with and without migraine.

	Migraine	MA	no Migraine	Migraine vs. no Migraine		MA vs. no Migraine	
	(N=52)	(N=29)	(N=594)	OR (95% CI)	aOR (95% CI)	OR (95% CI)	aOR (95% CI)
CoW incomplete	45 (87%)	23 (79%)	506 (85%)	1.12 (0.49-2.56)	1.47 (0.63-3.44)	0.67 (0.26-1.68)	0.88 (0.34-2.29)
Anterior incomplete	8 (15%)	6 (21%)	61 (10%)	1.59 (0.71-3.53)	2.06 (0.90-4.73)	2.28 (0.89-5.82)	3.22 (1.21-8.59)
Posterior incomplete							
- One-sided	16 (31%)	7 (24%)	183 (31%)	1.00 (0.54-1.84)	0.95 (0.51-1.78)	0.71 (0.30-1.70)	0.70 (0.29-1.67)
- Two-sided	28 (54%)	15 (52%)	318 (54%)	1.01 (0.57-1.79)	1.22 (0.68-2.20)	0.93 (0.44-1.96)	1.12 (0.52-2.39)
A1 asymmetry (N=645)	11 (21%)	6 (21%)	156 (26%)	0.75 (0.38-1.50)	0.86 (0.43-1.74)	0.73 (0.29-1.83)	0.82 (0.32-2.07)
Pcom dominance	11 (21%)	6 (21%)	173 (29%)	0.65 (0.33-1.30)	0.64 (0.32-1.30)	0.63 (0.25-1.59)	0.67 (0.26-1.72)

OR = odds ratio (with the 95% confidence interval); aOR = odds ratio adjusted for age and sex (with the 95% confidence interval); MA = migraine with aura; CoW = Circle of Willis; Pcom = posterior communicating artery; (N) = The number of patients for the particular variable in case there are missing data.

Table 3. CoW-variants in migraine patients with and without aura.

	MA	MO	MA vs. MO	
	(N=29)	(N=23)	OR (95% CI)	aOR (95% CI)
CoW incomplete	23 (79%)	22 (96%)	0.17 (0.02-1.57)	0.14 (0.01-1.58)
Anterior CoW incomplete	6 (21%)	2 (9%)	2.74 (0.50-15.09)	4.18 (0.58-30.00)
Posterior CoW incomplete				
- One-sided	7 (24%)	9 (39%)	0.49 (0.15-1.63)	0.45 (0.12-1.67)
- Two-sided	15 (52%)	13 (57%)	0.82 (0.27-2.48)	0.85 (0.24-2.97)
A1 asymmetry	6 (21%)	5 (22%)	0.94 (0.25-3.58)	0.93 (0.21-4.17)
Pcom dominance	6 (21%)	5 (22%)	0.94 (0.25-3.58)	1.55 (0.35-6.81)

OR = odds ratio (with the 95% confidence interval); aOR = odds ratio adjusted for age and sex (with the 95% confidence interval); MA = migraine with aura; MO = migraine without aura; CoW = Circle of Willis; Pcom = posterior communicating artery; (N) = The number of patients for the particular variable in case there are missing data

Table 4. Studies reporting CoW anatomy in migraine populations.

	Cucchiara 2013[192]	Cavestro 2011[191]	Bugnicourt 2010[221]	Schoonman 2010[56]	Ikeda 2009[195]	Ezzatian-Ahar 2014[194†]	This study
Design	CC	CC?	CC	CC	CC?	CC	CC
Data collection	Pro	Pro	Pro	Retro	Retro	Retro	Pro
Controls	Age and sex matched Pt	Pt with no headache	Pt with other neurol diseases	Non-migraine Pt	Unknown	Healthy controls	Non-migraine stroke Pt
N	170	429	124	44	173	84	646
- **Non-migraine**	53	159	77	12	100	37	594
- **Migraine (% MA)**	117 (48%)	204 (32%)	47 (51%)	32 (27%)	73 (42%)	48 (0%)	52 (56%)
Mean age (St.dev)	33.3 (6.6)	44.8 (14.9)	38.7 (14.8)	42.9 (9.3)	33.2 (8.9)	28 (MO), 25 (C)	66 (13)
Women	132 (78%)	314 (73%)	86 (69%)	25 (78%)	122 (71%)	84 (100%)	250 (39%)
Imaging	MR	MR	MR	MR	MR	MR	CT
Incomplete posterior CoW‡							
Migraine	71 (61%) *	82 (30%) *	23 (49%) *	16 (50%)	28 (38%) *	n/a	44 (85%)
MA	36 (64%) *	24 (36%)*	14 (61%)	n/a	6 (19%) *	n/a	22 (76%)
MO	35 (57%)	58 (28%) *	9 (38%)	n/a	22 (52%) *	20 (43%)	22 (96%)
Control	22 (41%)	26 (16%)	14 (18%)	8 (67%)	55 (55%)	15 (41%)	501 (84%)
Anterior CoW							
Migraine	31 (26%) *	26 (10%) *	3 (6%)	3 (9%)	n/a	n/a	8 (15%)
MA	18 (32%) *	6 (9%)	2 (9%)	n/a	n/a	n/a	6 (21%)
MO	13 (21%)	20 (10%) *	1 (4%)	n/a	n/a	n/a	2 (9%)
Control	7 (13%)	8 (5%)	4 (5%)	2 (17%)	n/a	n/a	61 (10%)

Percentages are percentage incomplete posterior CoW as detected on MR or CT angiogram

Pt = patients; C = controls; M = Median; Pro = prospective; Retro = retrospective; CC = Case-control study; C = cohort study; MA = migraine with aura; MO = migraine without aura; * Statistically significant difference compared with controls. Note that in this table, in contrast to table 2, both MA and MO patients were compared with controls rather than with each other. Also note that Ikeda found a lower prevalence of incomplete CoW compared with controls; † Ezzatian-Ahar *et al.* did not discriminate between anterior and posterior incompleteness of the CoW; ‡ A part of this table is derived from the paper of Cucchiara et al.

Discussion

In our ischemic stroke cohort, anatomical variations of the CoW were equally common in patients with or without a history of migraine and in migraineurs with or without aura.

Several studies have reported an increased prevalence of CoW variants in people with migraine in comparison to the controls, in particular in migraineurs with aura and in the posterior circulation.[190-193] However, in most studies, the frequency of CoW variants in the control group was less than 50% which is considerably lower than expected from population based studies[204-208] and the 85% we found (Table 4).

Some of the variation in frequency of CoW anomalies among previous studies may have been due to differences in scoring criteria. We used a cut-off of 1 mm for incompleteness because it is known from previous autopsy and flow model studies that segments below this diameter significantly compromise blood flow.[209-212] For the same reason we chose a one-third difference for A1 asymmetry and Pcom dominance.[210, 211] Most other MRI studies used a cut-off of 0.8 mm. Also the age and sex distribution of the study populations varied between studies. Our stroke cohort consisted of relatively old persons which may account for the relatively high proportion of CoW variants as CoW variation is more common in elderly.[206] Our results suggest more frequent incompleteness of the anterior circle in migraine patients with aura compared to stroke patients without migraine. We feel this finding should be interpreted with caution because it was not reported in previous studies, it was based on only 6 migraine with aura patients and a pathophysiological explanation for the difference is lacking.

This is the first study that investigated the association between CoW variants and migraine in a stroke population. The strengths of our study are the prospective data collection, the large number of participants, the verified migraine diagnosis and the detailed investigation of the CoW by trained neuroradiologists. However, our study also has limitations. Not all DUST patients answered the MISS migraine questionnaire and 8% of the patients could not be contacted for a telephone interview. Because of the etiological nature of the study, we tried to avoid misclassification bias and only included patients with a negative questionnaire or a verified migraine diagnosis. Therefore, the exact prevalence of migraine in our stroke population cannot be derived from our study. In addition, we cannot exclude that some patients who reported on the MISS screener not to have a migraine history might not have accurately recalled their migraine symptoms when asked about it many years later. Furthermore, we cannot exclude that CoW morphology changed because of the stroke, given the plastic nature of CoW anatomy.[213] However, since all patients in our study had a stroke we feel that it is unlikely that this affected the internal validity of our study. In addition, all patients were scanned in the first hours after onset excluding chronic adaptations of the CoW after stroke. Also, chronic changes to the CoW may have occurred because of atherosclerotic changes related to ageing.[214] To address this problem we corrected for age. In addition, we performed a subgroup analyses in which we

excluded patients with large vessel stenosis or occlusions. In this subgroup analyses our results stayed essentially the same. An ultimate future study would focus on the longitudinal relation between migraine symptoms and CoW morphology."

While there is radiological and genetic evidence for a relationship between CoW variants and stroke, causality is debated.[197, 215-217] In a prospective follow-up study in patients with atherosclerotic disease, an incomplete (<0.8 mm or absent segment) anterior and posterior CoW was related to future anterior circulation stroke.[198] An incomplete CoW might decrease the possibilities for collateral blood flow and might cause shear induced platelet aggregation and possibly facilitates SDs.[218, 219,220] However, other studies also suggested that the CoW mainly functions as a pressure absorber.[18] In case the CoW is a redundancy mechanism where a secondary route takes over perfusion of the brain when the primary route is blocked, an incomplete circle may contribute to the chance of developing ischemia.[212] It can be hypothesized that patients with an incomplete posterior CoW with migraine are more susceptible for ischemia in the posterior territories. However, in our patients with posterior ischemia, there were no differences in completeness of posterior CoW in migraineurs compared with patients without migraine. We did not investigate the influence of pial and leptomeningeal collaterals. Future studies are needed to assess their role in the vascularization of the posterior circulation in patients with migraine and to assess the longitudinal relationship between migraine and CoW morphology.

Acknowledgements

The authors would like to acknowledge all Dutch acute Stroke Trial (DUST) investigators. The Dutch acute Stroke Trial (DUST) investigators are: Academic Medical Center, Amsterdam, The Netherlands (Majoie CB, Roos YB); Catharina Hospital, Eindhoven, The Netherlands (Duijm LE, Keizer K); Erasmus Medical Center, Rotterdam, The Netherlands (van der Lugt A, Dippel DW); Gelre Hospitals, Apeldoorn, The Netherlands (Droogh - de Greeve KE, Bienfait HP); Leiden University Medical Center, Leiden, The Netherlands (van Walderveen MA, Wermer MJ); Medical Center Haaglanden, The Hague, The Netherlands (Lycklama à Nijeholt GJ, Boiten J); Onze Lieve Vrouwe Gasthuis, Amsterdam, The Netherlands (Duyndam D, Kwa VI); Radboud University Nijmegen Medical Centre, Nijmegen, The Netherlands (Meijer FJ, van Dijk EJ); Rijnstate Hospital, Arnhem, The Netherlands (Kesselring FO, Hofmeijer J); St. Antonius Hospital, Nieuwegein, The Netherlands (Vos JA, Schonewille WJ); St. Elisabeth Hospital, Tilburg, The Netherlands (van Rooij WJ, de Kort PL); St. Franciscus Hospital, Rotterdam, The Netherlands (Pleiter CC, Bakker SL); VU Medical Center, Amsterdam, The Netherlands (Bot J, Visser MC); University Medical Center Utrecht, Utrecht, The Netherlands (Velthuis BK, van der Schaaf IC, Dankbaar JW, Mali WP, van Seeters T, Horsch AD, Niesten JM, Biessels GJ, Kappelle LJ, Luitse MJ, van der Graaf Y).

Chapter 7

Discussion

Over the past decades, evidence has accumulated that spreading depolarization (SD) plays a relevant role in brain lesion development after subarachnoid hemorrhage (SAH). In this thesis the role of SD as a cause and potential therapeutic target of brain tissue damage after SAH was investigated.

SDs and delayed cerebral ischemia in the experimental SAH model

One of the most important findings of this thesis is the establishment of a direct association between SD and lesion growth after SAH in a relevant rat model as reported in **chapter 2** and supported by findings in **chapter 3**. After induction of SDs with KCl application, SAH-induced brain lesions enlarged more than when no SDs were induced. Establishing such a direct association between SD and lesion growth after SAH is only feasible in animal models, as it would be unethical to subject humans to experimental induction of SD after SAH. The use of an animal model is both a strength and a limitation, because findings in these animal studies eventually need to be translated to SAH patients. This was taken in consideration when selecting the animal model for our studies. There are various rat models for SAH that involve either an injection of blood in the subarachnoid space[222] or endovascular puncture of the intracranial bifurcation of the internal carotid artery.[223] In contrast to the relatively mild blood injection model, the artery puncture model used in the studies in **Chapters 2** and **3**, is known to often cause ischemia, mortality and increase in intracranial pressure[115], thus making it more comparable to the pathophysiology of human SAH patients.

In the study in **Chapter 2** we found MRI-detectable lesions in only a minority of the rats in the control group in which SAH was induced without subsequent SD induction. In contrast, in earlier MRI studies using the same rat SAH model, lesions were observed more frequently.[63, 93] A difference between our study and the previous studies is that the animals in our study formed the control group of the treatment study in chapter 3, and therefore received four weeks pretreatment of daily intraperitoneal saline injections. Perhaps stress from the injections preconditioned[224] the rats to be less susceptible to lesion development after SAH. Another possible explanation for the lower lesion incidence is the use of a rat strain with lower susceptibility to cerebral ischemia, for example due to more collateral vessels. However, both in the experiments described in this thesis and in experiments where SAH resulted in high lesion incidences,[63, 93] Wistar rats were used, be it from different suppliers (Harlan *versus* Charles River).[225] The study in **Chapter 6** on variations in the arterial circle of Willis, a roundabout which, when complete, interconnects the main cerebral arteries for redundancy, demonstrated in humans a well-known variability in cerebral vascular anatomy. This variability has also been found in rats[226] and, more specifically, between suppliers.[225] Such variations in vascular anatomy, with better collateral vessels, may therefore explain why in the rat strain used in this thesis there is a lower lesion incidence. Unfortunately, the imaging protocol did not include an angiogram to assess the vascular anatomy.

Comparison of the vascular response to SD with human SAH patients

In 2006, it was shown in patients that brain damage after SAH is associated with spreading depolarization (SD).[33] While earlier studies had sought to establish such an association in animal models,[63, 90, 227] this was the first study to do so in SAH patients. The investigators used an elegant technique of placing a strip of electrodes on the brain surface of patients who were selected for cranial surgery, for example for clipping of the aneurysm that caused the hemorrhage. In the patients, every case of delayed cerebral ischemia (DCI) was preceded by an SD, sometimes by prolonged SDs with refractory periods of over an hour.[33] Later, this electrode strip technique was improved for a second group of patients by adding optodes to the strip that allow optical measurement of the perfusion response.[66] The findings from that study supported the notion that there is a spectrum ranging from normal-duration SDs (refractory period lasting a few minutes) to prolonged “intermediate depolarizations” (lasting up to several hours) and ultimately terminal depolarization (permanent).[59] It was hypothesized that DCI may be caused by cortical spreading ischemia, which is an SD followed by an inverse, paradoxical hemodynamic response.[228, 229] This hypoperfusion could result in a large disbalance between increased demand and decreased supply in oxygen and nutrients and ultimately a permanent terminal depolarization.[59] In the experimental SAH model of **Chapters 2** and **3** we confirmed the occurrence of such spreading hypoperfusions.

Translation of our rat model to SAH patients

Notwithstanding the advantage of animal SAH models that allow a controlled setting, such models are at best a proxy of the human condition. Our rat model of endovascular SAH followed by experimental SD induction has several limitations.

First, the timescale of lesion development differs between the rodent model and patients. In rats the lesions typically develop in the acute phase (within hours) after SAH induction.[63] This contrasts to the time frame of 4-10 days in which DCI develops in humans.[24] This discrepancy is partially offset by a markedly higher metabolism in rats[78], but translating such time frames from small animals to humans is inherently imperfect and in future research a longer follow-up could provide new insights.[31] It is unclear whether differences between species in metabolism are a sufficient explanation for the different time frames of lesion onset between rats and patients or if different mechanisms are involved such as a changing blood flow in the endovascular puncture SAH model caused by temporary reduced flow through the internal carotid artery or possible increased perfusion pressure thereafter caused by closing the external carotid artery. To specifically assess delayed mechanisms of post-SAH brain injury, we calculated subacute lesion growth, rather than lesion size, as the primary outcome measure in our model. We observed cases of new lesions at day 3 post-SAH in brain regions in which no lesions were visible at day 1 post-SAH. We found such lesions in the SD as well as no-SD groups, albeit with a lower incidence in animals without SD. Although spontaneous SD may have contributed to these secondary lesions in the no-SD groups, we were not able to identify this

as the cause. Secondary lesions formed only a small part of the total lesion volume compared to the initial lesion that developed within a day after SAH. The additional secondary lesions may potentially provide a valid representation of DCI, but their low incidence, small volume and unknown underlying cause hampers the translational value.

Second, in the rat model not all new lesions occurred in the cortex where SDs were induced. This may be explained by occurrence of spontaneous SD.[63] Even for the subcortical lesions, a direct effect of SD cannot be ruled out, since SD may occur in subcortical regions.[230-232] The experimentally induced SDs may nevertheless have contributed to subcortical and ipsilateral lesions through indirect mechanisms, such as disruption of the blood-brain barrier[117], edema formation[117], inflammation[30], excitotoxicity caused by glutamate[233] and vasoconstrictor receptor upregulation.[32]

Third, it is difficult to measure subtle effects on functional outcome in rats. We used a crude measure of neurological outcome that showed no significant differences between groups. Future studies should include more extensive testing, such as the modified Garcia score, which includes assessment of spontaneous activity, (a)symmetry in the movement of all four limbs, forepaw outstretching, climbing, body proprioception, and response to whisker touch and is considered a standard for determining neurological deficit in rodents.[234-236] Nevertheless behavioral assessments in rats remain a partial approximation of a full neurological examination in human patients.[237]

Future perspectives on our animal model

Despite the limitations discussed in **Chapters 2** and **3** and above, our animal model of SAH followed by KCl application, has the advantage of allowing the characterization of the direct association between SDs and brain injury. While the occurrence of spontaneous SDs have been reported in rats after SAH[63], experimental SD induction may provide a new, controllable model for future research on lesion development after SAH and the pathophysiological role of SD. This can be combined with longitudinal three-dimensional recording of SD using in vivo MRI, with techniques discussed in **Chapter 4** which are also applicable in patient studies. Future animal studies on lesion growth after SAH should strive for even more direct control of and insight into the mechanisms responsible for how, when and where brain lesions develop after SAH. For example, it is poorly understood what invokes the paradoxical hypoperfusion response to SD.[26] However, this more direct control and insight of underlying mechanisms should be balanced against comparability with human patients, where DCI occurs spontaneously, in one-third of the patients and at seemingly unpredictable locations and moments.[28] Perhaps future research could benefit from involving multiple research groups, multiple rat strains or even multiple animal species. Either way, future research will benefit from adequate translational techniques for recording SD and its effects after SAH.

Recording of spreading depolarizations

We reported the application of two MRI techniques that are novel in measuring SDs (**Chapter 4**). One, balanced-steady-state-free-precession (b-SSFP), improved the sensitivity and a spatial specificity compared to conventional gradient-echo MRI techniques, while the other, diffusion-weighted multi-spin-echo (DT2) allowed for simultaneous recording of cellular and hemodynamic changes. Both techniques were found to have additional value in the evaluation of SDs. While these MRI techniques were compared with the frequently applied gradient echo BOLD MRI technique, they were not compared with the ultimate gold standard for SD detection, electrocorticography (ECoG), which excludes accurate evaluation of the detection specificity and sensitivity. This may be assessed in future experiments as electrocorticographical SD recordings in animals while inside an MRI scanner have been shown to be feasible.[238, 239] Prolonged measurement of SDs in SAH patients may provide useful insights. For example monitoring the direct effects of interventions on SDs could inform on the therapeutic mode of action. However, despite the translational value of MRI, it is impractical for prolonged bedside monitoring of SAH patients. Previously, prolonged recording of SDs seemed only possible in humans with ECoG, for which part of the skull had to be removed for a clear signal. However, a study with combined ECoG and non-invasive electroencephalography (EEG) in five SAH patients found that more than 70% of the SDs could be detected on EEG as a slow potential change.[240] This was supported by another study in traumatic brain injury patients in whom SDs were detected as depressions of high-amplitude delta activity on EEG.[65] These depressions could last over a day after a cluster of SDs. Therefore, detection sometimes required reviewing the EEGs on a highly compressed timescale. These have been the first studies to show the propagation of electrophysiological SDs across large brain areas in humans.

Future perspectives on clinical recording of spreading depolarizations

While an association between EEG and ECoG findings on SD was found by the studies described in the previous section, and while it may be possible to predict DCI based on EEG findings[241], it is currently not possible to detect SDs based on EEG data alone, without ECoG recordings.[64] Thus it is uncertain if EEG data provides a sufficiently robust bedside technique for recording of SDs, even with the best possible registration and processing. Furthermore, bedside monitoring of continuous EEG recordings would be labor intensive, requires continuous accounting for artefacts, further development of software processing and requires definition of cut-off values.[64, 240] Another potential noninvasive method for recording SDs may be magnetoencephalography, but its application has so far only been reported in one case of a patient with a migraine aura.[242] Other continuous monitoring techniques, such as laser Doppler flowmetry, are not feasible in humans, because the human skull is too thick.[243]

In contrast to noninvasive techniques, invasive monitoring allows for ECoG recording, and measurement of local blood flow and even tissue oxygen pressure or metabolites.[66, 244, 245] Such invasive measurements have increased our understanding of SDs in humans and may aid in comparing animal studies to human patients. However, serious limitations include complications such as hemorrhage and infection, and the craniotomy may itself be a confounding factor.[246] Therefore, invasive recording of SD and associated physiological changes will likely not become common clinical practice, but rather a means to produce insight in the mechanisms involved in SDs, DCI and brain infarct growth and a reference for non-invasive techniques such as MR imaging for detailed three-dimensional recording and EEG for bedside recording. MR imaging of SDs could involve a protocol like the b-SSFP method described in **Chapter 4**, to enable sensitive detection of subtle changes (between groups, between SD waves and/or between brain regions). Even more insightful studies will be possible with MRI techniques that record hemodynamic and cellular effects simultaneously, such as with a diffusion-weighted multi-spin-echo technique (DT2) as applied in **Chapter 4**. If SDs are a preventable culprit in lesion development after SAH, such techniques may one day become a regular part in diagnosis, monitoring or personalized treatment selection after SAH .

Spreading depolarization-modulating drugs

For our rat studies in **Chapter 3**, we selected valproate, which has the advantage in translating our findings to human patients that it is a commonly prescribed drug, also after SAH.[247] We found that valproate mitigated the lesion growth caused by cortical KCl application after SAH compared to placebo. In our epidemiological study on SAH patients using SD-inhibiting home medication (**Chapter 5**), we found a trend towards less DCI but no statistically significant difference in clinical outcome. The imperfections of drugs such as valproate may contribute to the inadequate translation of animal findings on SD modulation to human patients, which may be less of an issue with targeted drugs. Valproate is prescribed for different disorders in humans such as epilepsy, migraine, manic episodes and neurogenic pain[248], suggesting multiple mechanisms of action which could even conceivably have opposite effects on outcome.[78, 249] Such opposite mechanisms may be expressed differently in human and animal studies, and thus contribute to the translational discrepancy between the reduced lesion growth in our rat studies in **Chapter 3** and the lack of statistically significant effects in **Chapter 5**. Despite the effects of valproate in our rat studies, which were only found after cortical KCl application, we measured no significant reduction of total SD duration, further suggesting that valproate mitigated lesion growth through multiple mechanisms. For example, valproate may also decrease cerebral perfusion[250-252], which could in turn have a more detrimental effect on brain tissue in humans than in rodents.

A recent mouse study confirmed our finding of a neuroprotective effect of valproate on outcome after SAH,[110] this study does not provide a deeper understanding of the mechanisms involved by modulating a proposed mechanism, such as our KCl application. Comparison to this study is further limited by the fact that a different, less severe SAH model was used, i.e. blood injection in the subarachnoid space, with no subsequent brain lesions, in which there was no post-procedural mortality in their 48h follow-up.[110] If valproate is a double-edged sword after SAH with neuroprotective and detrimental effects, a deeper understanding could contribute to a more targeted medical prevention of brain tissue damage after SAH and ultimately a better clinical outcome.

Historically, drugs such as valproate have been clinically incorporated if they had been proven effective in improving the clinical outcome, regardless of how this was accomplished. Clinical testing of novel drugs however, is often preceded by preclinical assessment of their mechanism of action.[253] Such drugs may be more specific in inhibiting SD or otherwise preventing brain damage after SAH, without pretreatment and only have mild side effects and thus be administered prophylactically to all patients. A drug that might have these properties is SD-inhibitor tonabersat. It is approved for use in humans, but not used in clinical practice because it produced inconsistent results in three clinical trials on its effectiveness in migraine prophylaxis, presumably related to the multifactorial cause of migraine.[254-256] Tonabersat is,

however, an effective and one of the most specific inhibitors of SD in animals[257] and would therefore be an interesting candidate for future translational research.

Future perspectives on SD-modulating drugs in SAH

The central question for research expanding on this thesis will be if and how SD inhibition is a potential target for preventing DCI after a SAH. Currently, I feel that based on the findings from this thesis and the evidence in the literature, a clinical drug trial on SD inhibition in SAH, would be premature. This paragraph will summarize the necessary steps that could lead towards such a trial. *First* of all, while the research in this thesis points to a causal relationship between KCl application and lesion growth in our rat model (**Chapters 2** and **3**), and while DCI was always preceded by SDs in the few humans in which continuous monitoring was present,[33] a causal relationship between SAH-induced SDs and DCI has not (yet) been established in humans. Research establishing this causal relationship would provide a better basis for any trials on inhibiting SDs. MRI, such as described in **Chapter 4**, may contribute to identification of SD-associated tissue changes and a potential inverse, paradoxical hypoperfusion response[258] that may precede DCI . *Second*, the ultimately relevant outcome is the clinical outcome; how the patient is doing, for example three months after the SAH. Smaller trials could first be powered to measure the effect on more direct outcome measures such as the presence or volume of DCI. An additional approach would be non-invasive bedside measuring of the effects of drugs on SDs, utilizing the therapeutic window between SAH and DCI that is absent in ischemic stroke. Such trials with bedside SD recording could provide a much larger datasets than studies with invasive methods. *Third*, an effective drug should have limited side effects and require little or no pre-treatment. Based on data from trials with continuous bedside monitoring for SDs, it might also be feasible to target drug administration only at patients in whom SDs have already been detected or are predicted to occur (or to cause DCI) based on markers that are yet to be established. *Fourth*, this thesis has focused on SD inhibition with drugs, but alternatively factors that affect the susceptibility of brain tissue for SD, such as high extracellular potassium and low nitrous oxide concentrations, or vagus nerve activity may be targeted.[37, 259] While not a condition sine qua non for drug trials, more research on the physiology of SDs could increase our understanding and may lead to alternative or supplementary means for manipulating SD susceptibility other than through drugs.

Conclusion

Subarachnoid hemorrhage (SAH) is a debilitating disease with complications such as delayed cerebral ischemia (DCI) occurring right under the eyes of treating physicians, nurses and other health care providers. A process that is involved in these complications is spreading depolarizations (SD). In this thesis SD-inhibiting drugs reduced lesion growth in our animal studies. Future research should aim at improving our understanding of mechanisms through which SD affects lesion development after SAH. Such research may increase our understanding of how SD-inhibiting drugs improve outcome, opening the way for evidence-based development of new targeted drugs. In the end, succesful translation of these findings to clinical practice may contribute to improved treatment and recovery of patients with a SAH.

Addendum

References

1. Lozano R, Naghavi M, Foreman K, Lim S, Shibuya K, Aboyans V *et al.* Global and regional mortality from 235 causes of death for 20 age groups in 1990 and 2010: a systematic analysis for the Global Burden of Disease Study 2010. *Lancet* 2012; 380(9859)**:** 2095-128.

2. Murray CJ, Acharya AK. Understanding DALYs (disability-adjusted life years). *Journal of health economics* 1997; 16(6)**:** 703-30.

3. Kasner SE, Chalela JA, Luciano JM, Cucchiara BL, Raps EC, McGarvey ML *et al.* Reliability and validity of estimating the NIH stroke scale score from medical records. *Stroke* 1999; 30(8)**:** 1534-7.

4. Jauch EC, Saver JL, Adams HP, Jr., Bruno A, Connors JJ, Demaerschalk BM *et al.* Guidelines for the early management of patients with acute ischemic stroke: a guideline for healthcare professionals from the American Heart Association/American Stroke Association. *Stroke* 2013; 44(3)**:** 870-947.

5. Olivot JM, Mlynash M, Thijs VN, Kemp S, Lansberg MG, Wechsler L *et al.* Relationships between infarct growth, clinical outcome, and early recanalization in diffusion and perfusion imaging for understanding stroke evolution (DEFUSE). *Stroke* 2008; 39(8)**:** 2257-63.

6. Schramm P, Schellinger PD, Klotz E, Kallenberg K, Fiebach JB, Kulkens S *et al.* Comparison of perfusion computed tomography and computed tomography angiography source images with perfusion-weighted imaging and diffusion-weighted imaging in patients with acute stroke of less than 6 hours' duration. *Stroke* 2004; 35(7)**:** 1652-8.

7. Easton JD, Saver JL, Albers GW, Alberts MJ, Chaturvedi S, Feldmann E *et al.* Definition and evaluation of transient ischemic attack: a scientific statement for healthcare professionals from the American Heart Association/American Stroke Association Stroke Council; Council on Cardiovascular Surgery and Anesthesia; Council on Cardiovascular Radiology and Intervention; Council on Cardiovascular Nursing; and the Interdisciplinary Council on Peripheral Vascular Disease. The American Academy of Neurology affirms the value of this statement as an educational tool for neurologists. *Stroke* 2009; 40(6)**:** 2276-93.

8. Young JA, Tolentino M. Neuroplasticity and its applications for rehabilitation. *Am. J. Ther.* 2011; 18(1)**:** 70-80.

9. Wall JT, Xu J, Wang X. Human brain plasticity: an emerging view of the multiple substrates and mechanisms that cause cortical changes and related sensory dysfunctions after injuries of sensory inputs from the body. *Brain Res. Brain Res. Rev.* 2002; 39(2-3)**:** 181-215.

10. Adams HP, Jr., Bendixen BH, Kappelle LJ, Biller J, Love BB, Gordon DL *et al.* Classification of subtype of acute ischemic stroke. Definitions for use in a multicenter clinical trial. TOAST. Trial of Org 10172 in Acute Stroke Treatment. *Stroke* 1993; 24(1)**:** 35-41.

11. Bejot Y, Caillier M, Ben Salem D, Couvreur G, Rouaud O, Osseby GV *et al.* Ischaemic stroke subtypes and associated risk factors: a French population based study. *J. Neurol. Neurosurg. Psychiatry* 2008; 79(12)**:** 1344-8.

12. Schulz UG, Rothwell PM. Differences in vascular risk factors between etiological subtypes of ischemic stroke: importance of population-based studies. *Stroke* 2003; 34(8)**:** 2050-9.

13. Grau AJ, Weimar C, Buggle F, Heinrich A, Goertler M, Neumaier S *et al.* Risk factors, outcome, and treatment in subtypes of ischemic stroke: the German stroke data bank. *Stroke* 2001; 32(11)**:** 2559-66.

14. Suarez JI. Diagnosis and Management of Subarachnoid Hemorrhage. *Continuum (Minneap Minn)* 2015; 21(5 Neurocritical Care)**:** 1263-87.

15. Anderson C, Anderson N, Bonita R. Epidemiology of aneurysmal subarachnoid hemorrhage in Australia and New Zealand: incidence and case fatality from the Australasian Cooperative Research on Subarachnoid Hemorrhage Study (ACROSS). *Stroke* 2000; 31(8)**:** 1843-50.

16. Johnston SC, Selvin S, Gress DR. The burden, trends, and demographics of mortality from subarachnoid hemorrhage. *Neurology* 1998; 50(5)**:** 1413-8.

17. Wermer MJ, van der Schaaf IC, Algra A, Rinkel GJ. Risk of rupture of unruptured intracranial aneurysms in relation to patient and aneurysm characteristics: an updated meta-analysis. *Stroke* 2007; 38(4)**:** 1404-10.

18. Vrselja Z, Brkic H, Mrdenovic S, Radic R, Curic G. Function of circle of Willis. *J. Cereb. Blood Flow Metab.* 2014; 34(4)**:** 578-84.

19. Vlak MH, Algra A, Brandenburg R, Rinkel GJ. Prevalence of unruptured intracranial aneurysms, with emphasis on sex, age, comorbidity, country, and time period: a systematic review and meta-analysis. *Lancet Neurol.* 2011; 10(7)**:** 626-36.

20. van Gijn J, Kerr RS, Rinkel GJE. Subarachnoid haemorrhage. *Lancet* 2007; 369(9558)**:** 306-18.

21. Roos YB, de Haan RJ, Beenen LF, Groen RJ, Albrecht KW, Vermeulen M. Complications and outcome in patients with aneurysmal subarachnoid haemorrhage: a prospective hospital based cohort study in the Netherlands. *J. Neurol. Neurosurg. Psychiatry* 2000; 68(3)**:** 337-41.

22. Vergouwen MD, The Participants in the International Multidisciplinary Consensus Conference on the Critical Care Management of Subarachnoid Hemorrhage. Vasospasm versus delayed cerebral ischemia as an outcome event in clinical trials and observational studies. *Neurocrit. Care* 2011; 15(2)**:** 308-11.

23. de Rooij NK, Rinkel GJ, Dankbaar JW, Frijns CJ. Delayed cerebral ischemia after subarachnoid hemorrhage: a systematic review of clinical, laboratory, and radiological predictors. *Stroke* 2013; 44(1)**:** 43-54.

24. Rinkel GJ, Klijn CJ. Prevention and treatment of medical and neurological complications in patients with aneurysmal subarachnoid haemorrhage. *Pract. Neurol.* 2009; 9(4)**:** 195-209.

25. Vergouwen MD, Ilodigwe D, Macdonald RL. Cerebral infarction after subarachnoid hemorrhage contributes to poor outcome by vasospasm-dependent and -independent effects. *Stroke* 2011; 42(4)**:** 924-9.

26. Budohoski KP, Guilfoyle M, Helmy A, Huuskonen T, Czosnyka M, Kirollos R *et al.* The pathophysiology and treatment of delayed cerebral ischaemia following subarachnoid haemorrhage. *J. Neurol. Neurosurg. Psychiatry* 2014; 85(12)**:** 1343-53.

27. Macdonald RL, Higashida RT, Keller E, Mayer SA, Molyneux A, Raabe A *et al.* Randomized trial of clazosentan in patients with aneurysmal subarachnoid hemorrhage undergoing endovascular coiling. *Stroke* 2012; 43(6)**:** 1463-9.

28. Macdonald RL. Delayed neurological deterioration after subarachnoid haemorrhage. *Nat. Rev. Neurol.* 2014; 10(1)**:** 44-58.

29. Vergouwen MD, Vermeulen M, Coert BA, Stroes ES, Roos YB. Microthrombosis after aneurysmal subarachnoid hemorrhage: an additional explanation for delayed cerebral ischemia. *J. Cereb. Blood Flow Metab.* 2008; 28(11)**:** 1761-70.

30. McMahon CJ, Hopkins S, Vail A, King AT, Smith D, Illingworth KJ *et al.* Inflammation as a predictor for delayed cerebral ischemia after aneurysmal subarachnoid haemorrhage. *J. Neurointerv. Surg.* 2013; 5(6)**:** 512-7.

31. Kooijman E, Nijboer CH, van Velthoven CT, Mol W, Dijkhuizen RM, Kesecioglu J *et al.* Long-term functional consequences and ongoing cerebral inflammation after subarachnoid hemorrhage in the rat. *PLoS One* 2014; 9(3)**:** e90584.

32. Edvinsson L, Povlsen GK. Late cerebral ischaemia after subarachnoid haemorrhage: is cerebrovascular receptor upregulation the mechanism behind? *Acta Physiol. (Oxf.)* 2011; 203(1)**:** 209-24.

33. Dreier JP, Woitzik J, Fabricius M, Bhatia R, Major S, Drenckhahn C *et al.* Delayed ischaemic neurological deficits after subarachnoid haemorrhage are associated with clusters of spreading depolarizations. *Brain* 2006; 129(Pt 12)**:** 3224-37.

34. Ayata C. Pearls and pitfalls in experimental models of spreading depression. *Cephalalgia* 2013; 33(8)**:** 604-13.

35. Leão AAP. Spreading depression of activity in the cerebral cortex. *J. Neurophysiol.* 1944; 7**:** 359–390.

36. Ayata C. Spreading depression: from serendipity to targeted therapy in migraine prophylaxis. *Cephalalgia* 2009; 29(10)**:** 1095-114.

37. Petzold GC, Haack S, von Bohlen Und Halbach O, Priller J, Lehmann TN, Heinemann U *et al.* Nitric oxide modulates spreading depolarization threshold in the human and rodent cortex. *Stroke* 2008; 39(4)**:** 1292-9.

38. Herreras O, Largo C, Ibarz JM, Somjen GG, Martin del Rio R. Role of neuronal synchronizing mechanisms in the propagation of spreading depression in the in vivo hippocampus. *J. Neurosci.* 1994; 14(11 Pt 2)**:** 7087-98.

39. Basarsky TA, Duffy SN, Andrew RD, MacVicar BA. Imaging spreading depression and associated intracellular calcium waves in brain slices. *J. Neurosci.* 1998; 18(18)**:** 7189-99.

40. Largo C, Cuevas P, Somjen GG, Martin del Rio R, Herreras O. The effect of depressing glial function in rat brain in situ on ion homeostasis, synaptic transmission, and neuron survival. *J. Neurosci.* 1996; 16(3)**:** 1219-29.

41. Hadjikhani N, Sanchez Del Rio M, Wu O, Schwartz D, Bakker D, Fischl B *et al.* Mechanisms of migraine aura revealed by functional MRI in human visual cortex. *Proc. Natl. Acad. Sci. U. S. A.* 2001; 98(8)**:** 4687-92.

42. Bartleson JD, Cutrer FM. Migraine update. Diagnosis and treatment. *Minn. Med.* 2010; 93(5)**:** 36-41.

43. DeLange JM, Cutrer FM. Our evolving understanding of migraine with aura. *Curr Pain Headache Rep* 2014; 18(10)**:** 453.

44. Stewart WF, Linet MS, Celentano DD, Van Natta M, Ziegler D. Age- and sex-specific incidence rates of migraine with and without visual aura. *Am. J. Epidemiol.* 1991; 134(10)**:** 1111-20.

45. Brennan KC, Charles A. An update on the blood vessel in migraine. *Curr. Opin. Neurol.* 2010; 23(3)**:** 266-74.

46. Tottene A, Conti R, Fabbro A, Vecchia D, Shapovalova M, Santello M *et al.* Enhanced excitatory transmission at cortical synapses as the basis for facilitated spreading depression in Ca(v)2.1 knockin migraine mice. *Neuron* 2009; 61(5)**:** 762-73.

47. Eikermann-Haerter K, Dilekoz E, Kudo C, Savitz SI, Waeber C, Baum MJ *et al.* Genetic and hormonal factors modulate spreading depression and transient hemiparesis in mouse models of familial hemiplegic migraine type 1. *J. Clin. Invest.* 2009; 119(1)**:** 99-109.

48. van den Maagdenberg AM, Pietrobon D, Pizzorusso T, Kaja S, Broos LA, Cesetti T *et al.* A Cacna1a knockin migraine mouse model with increased susceptibility to cortical spreading depression. *Neuron* 2004; 41(5)**:** 701-10.

49. Eikermann-Haerter K, Lee JH, Yuzawa I, Liu CH, Zhou Z, Shin HK *et al.* Migraine mutations increase stroke vulnerability by facilitating ischemic depolarizations. *Circulation* 2012; 125(2)**:** 335-45.

50. van den Maagdenberg AM, Pizzorusso T, Kaja S, Terpolilli N, Shapovalova M, Hoebeek FE *et al.* High cortical spreading depression susceptibility and migraine-associated symptoms in Ca(v)2.1 S218L mice. *Ann. Neurol.* 2010; 67(1)**:** 85-98.

51. Donaghy M, Chang CL, Poulter N, European Collaborators of The World Health Organisation Collaborative Study of Cardiovascular D, Steroid Hormone C. Duration, frequency, recency, and type of migraine and the risk of ischaemic stroke in women of childbearing age. *J. Neurol. Neurosurg. Psychiatry* 2002; 73(6)**:** 747-50.

52. Spector JT, Kahn SR, Jones MR, Jayakumar M, Dalal D, Nazarian S. Migraine headache and ischemic stroke risk: an updated meta-analysis. *Am. J. Med.* 2010; 123(7)**:** 612-24.

53. Pavlakis SG, Phillips PC, DiMauro S, De Vivo DC, Rowland LP. Mitochondrial myopathy, encephalopathy, lactic acidosis, and strokelike episodes: a distinctive clinical syndrome. *Ann. Neurol.* 1984; 16(4)**:** 481-8.

54. Tournier-Lasserve E, Joutel A, Melki J, Weissenbach J, Lathrop GM, Chabriat H *et al.* Cerebral autosomal dominant arteriopathy with subcortical infarcts and leukoencephalopathy maps to chromosome 19q12. *Nat. Genet.* 1993; 3(3)**:** 256-9.

55. Terwindt GM, Haan J, Ophoff RA, Groenen SM, Storimans CW, Lanser JB *et al.* Clinical and genetic analysis of a large Dutch family with autosomal dominant vascular retinopathy, migraine and Raynaud's phenomenon. *Brain* 1998; 121 (Pt 2)**:** 303-16.

56. Schoonman GG, van Oosterhout WP, Ferrari MD, van der Grond J. Anatomical variations in the circle of Willis and migraine susceptibility: is there an association? *Headache* 2010; 50(1)**:** 151-2.

57. Van Harreveld A. Changes in the diameter of apical dendrites during spreading depression. *Am. J. Physiol.* 1958; 191(2)**:** 233-242.

58. Wolf T, Lindauer U, Villringer A, Dirnagl U. Excessive oxygen or glucose supply does not alter the blood flow response to somatosensory stimulation or spreading depression in rats. *Brain Res.* 1997; 761(2)**:** 290-9.

59. Dreier JP. The role of spreading depression, spreading depolarization and spreading ischemia in neurological disease. *Nat. Med.* 2011; 17(4)**:** 439-47.

60. Dreier JP, Ebert N, Priller J, Megow D, Lindauer U, Klee R *et al.* Products of hemolysis in the subarachnoid space inducing spreading ischemia in the cortex and focal necrosis in rats: a model for delayed ischemic neurological deficits after subarachnoid hemorrhage? *J. Neurosurg.* 2000; 93(4)**:** 658-66.

61. Charles A, Brennan K. Cortical spreading depression-new insights and persistent questions. *Cephalalgia* 2009; 29(10)**:** 1115-24.

62. Connolly ES, Jr., Rabinstein AA, Carhuapoma JR, Derdeyn CP, Dion J, Higashida RT *et al.* Guidelines for the management of aneurysmal subarachnoid hemorrhage: a guideline for healthcare professionals from the American Heart Association/american Stroke Association. *Stroke* 2012; 43(6)**:** 1711-37.

63. van den Bergh WM, Zuur JK, Kamerling NA, van Asseldonk JT, Rinkel GJ, Tulleken CA *et al.* Role of magnesium in the reduction of ischemic depolarization and lesion volume after experimental subarachnoid hemorrhage. *J. Neurosurg.* 2002; 97(2)**:** 416-22.

64. Dreier JP, Fabricius M, Ayata C, Sakowitz OW, William Shuttleworth C, Dohmen C *et al.* Recording, analysis, and interpretation of spreading depolarizations in neurointensive care: Review and recommendations of the COSBID research group. *J. Cereb. Blood Flow Metab.* 2016**:** 271678X16654496.

65. Hartings JA, Wilson JA, Hinzman JM, Pollandt S, Dreier JP, DiNapoli V *et al.* Spreading depression in continuous electroencephalography of brain trauma. *Ann. Neurol.* 2014; 76(5)**:** 681-94.

66. Dreier JP, Major S, Manning A, Woitzik J, Drenckhahn C, Steinbrink J *et al.* Cortical spreading ischaemia is a novel process involved in ischaemic damage in patients with aneurysmal subarachnoid haemorrhage. *Brain* 2009; 132(Pt 7)**:** 1866-81.

67. Dunn AK, Bolay H, Moskowitz MA, Boas DA. Dynamic imaging of cerebral blood flow using laser speckle. *J. Cereb. Blood Flow Metab.* 2001; 21(3)**:** 195-201.

68. Obrig H. NIRS in clinical neurology - a 'promising' tool? *Neuroimage* 2014; 85 Pt 1**:** 535-46.

69. Stern MD. In vivo evaluation of microcirculation by coherent light scattering. *Nature* 1975; 254(5495)**:** 56-8.

70. Chen S, Li P, Luo W, Zeng S, Luo Q. Using running subtraction to detect the wavefront of cortical spreading depression. *Conf. Proc. IEEE Eng. Med. Biol. Soc.* 2005; 2**:** 1446-8.

71. Martins-Ferreira H, de Castro GO. Light-scattering changes accompanying spreading depression in isolated retina. *J. Neurophysiol.* 1966; 29(4)**:** 715-26.

72. Cutrer FM, Sorensen AG, Weisskoff RM, Ostergaard L, Sanchez del Rio M, Lee EJ *et al.* Perfusion-weighted imaging defects during spontaneous migrainous aura. *Ann. Neurol.* 1998; 43(1)**:** 25-31.

73. de Crespigny A, Rother J, van Bruggen N, Beaulieu C, Moseley ME. Magnetic resonance imaging assessment of cerebral hemodynamics during spreading depression in rats. *J. Cereb. Blood Flow Metab.* 1998; 18(9)**:** 1008-17.

74. Osborn AG, Blaser SI, Salzman KL, Katzman GL, Provenzale J, Castillo M *et al. Diagnostic Imaging Brain*, 1st edn Amirsys: Salt Lake City, Utah, USA, 2004.

75. Dijkhuizen RM, Nicolay K. Magnetic resonance imaging in experimental models of brain disorders. *J. Cereb. Blood Flow Metab.* 2003; 23(12)**:** 1383-402.

76. Ogawa S, Lee TM, Kay AR, Tank DW. Brain magnetic resonance imaging with contrast dependent on blood oxygenation. *Proc. Natl. Acad. Sci. U. S. A.* 1990; 87(24)**:** 9868-72.

77. Hasegawa Y, Latour LL, Formato JE, Sotak CH, Fisher M. Spreading waves of a reduced diffusion coefficient of water in normal and ischemic rat brain. *J. Cereb. Blood Flow Metab.* 1995; 15(2)**:** 179-87.

78. Loscher W. Serum protein binding and pharmacokinetics of valproate in man, dog, rat and mouse. *J Pharmacol Exp Ther* 1978; 204(2)**:** 255-61.

79. Somjen GG, Rosenthal M, Cordingley G, LaManna J, Lothman E. Potassium, neuroglia, and oxidative metabolism in central gray matter. *Fed. Proc.* 1976; 35(6)**:** 1266-71.

80. Brand S, Fernandes de Lima VM, Hanke W. Pharmacological modulation of the refractory period of retinal spreading depression. *Naunyn Schmiedebergs Arch. Pharmacol.* 1998; 357(4)**:** 419-25.

81. Wiedemann M, de Lima VM, Hanke W. Effects of antimigraine drugs on retinal spreading depression. *Naunyn Schmiedebergs Arch. Pharmacol.* 1996; 353(5)**:** 552-6.

82. LaManna JC, Rosenthal M. Effect of ouabain and phenobarbital on oxidative metabolic activity associated with spreading cortical depression in cats. *Brain Res.* 1975; 88(1)**:** 145-9.

83. Hoffmann U, Dilekoz E, Kudo C, Ayata C. Gabapentin suppresses cortical spreading depression susceptibility. *J. Cereb. Blood Flow Metab.* 2010; 30(9)**:** 1588-92.

84. Richter F, Mikulik O, Ebersberger A, Schaible HG. Noradrenergic agonists and antagonists influence migration of cortical spreading depression in rat-a possible mechanism of migraine prophylaxis and prevention of postischemic neuronal damage. *J. Cereb. Blood Flow Metab.* 2005; 25(9)**:** 1225-35.

85. Dreier JP, Windmuller O, Petzold G, Lindauer U, Einhaupl KM, Dirnagl U. Ischemia triggered by red blood cell products in the subarachnoid space is inhibited by nimodipine administration or moderate volume expansion/ hemodilution in rats. *Neurosurgery* 2002; 51(6)**:** 1457-65.

86. Reid KH, Marrannes R, Wauquier A. Effects of phenytoin and flunarizine on the rise in extracellular potassium induced by repetitive stimulation of rat cerebral cortex. *Physiol. Bohemoslov.* 1988; 37(3)**:** 193-202.

87. Ayata C, Jin H, Kudo C, Dalkara T, Moskowitz MA. Suppression of cortical spreading depression in migraine prophylaxis. *Ann. Neurol.* 2006; 59(4)**:** 652-61.

88. Bogdanov VB, Multon S, Chauvel V, Bogdanova OV, Prodanov D, Makarchuk MY *et al.* Migraine preventive drugs differentially affect cortical spreading depression in rat. *Neurobiol. Dis.* 2011; 41(2)**:** 430-5.

89. Peeters M, Gunthorpe MJ, Strijbos PJLM, Goldsmith P, Upton N, James MF. Effects of pan- and subtype-selective N-methyl-D-aspartate receptor antagonists on cortical spreading depression in the rat: therapeutic potential for migraine. *J Pharmacol Exp Ther* 2007; 321(2)**:** 564-72.

90. Dreier JP, Korner K, Ebert N, Gorner A, Rubin I, Back T *et al.* Nitric oxide scavenging by hemoglobin or nitric oxide synthase inhibition by N-nitro-L-arginine induces cortical spreading ischemia when K+ is increased in the subarachnoid space. *J. Cereb. Blood Flow Metab.* 1998; 18(9)**:** 978-90.

91. Chen S, Feng H, Sherchan P, Klebe D, Zhao G, Sun X *et al.* Controversies and evolving new mechanisms in subarachnoid hemorrhage. *Prog. Neurobiol.* 2014; 115**:** 64-91.

92. Beaulieu C, Busch E, de Crespigny A, Moseley ME. Spreading waves of transient and prolonged decreases in water diffusion after subarachnoid hemorrhage in rats. *Magn. Reson. Med.* 2000; 44(1)**:** 110-6.

93. Tiebosch IA, van den Bergh WM, Bouts MJ, Zwartbol R, van der Toorn A, Dijkhuizen RM. Progression of brain lesions in relation to hyperperfusion from subacute to chronic stages after experimental subarachnoid hemorrhage: a multiparametric MRI study. *Cerebrovasc. Dis.* 2013; 36(3)**:** 167-72.

94. Yonemori F, Yamaguchi T, Yamada H, Tamura A. Evaluation of a motor deficit after chronic focal cerebral ischemia in rats. *J. Cereb. Blood Flow Metab.* 1998; 18(10)**:** 1099-106.

95. Jenkinson M, Smith S. A global optimisation method for robust affine registration of brain images. *Med. Image Anal.* 2001; 5(2)**:** 143-56.

96. Sugawara T, Ayer R, Jadhav V, Zhang JH. A new grading system evaluating bleeding scale in filament perforation subarachnoid hemorrhage rat model. *J. Neurosci. Methods* 2008; 167(2)**:** 327-34.

97. Stowe AM, Altay T, Freie AB, Gidday JM. Repetitive hypoxia extends endogenous neurovascular protection for stroke. *Ann. Neurol.* 2011; 69(6)**:** 975-85.

98. Hubschmann OR, Kornhauser D. Cortical cellular response in acute subarachnoid hemorrhage. *J. Neurosurg.* 1980; 52(4)**:** 456-62.

99. Leng LZ, Fink ME, Iadecola C. Spreading depolarization: a possible new culprit in the delayed cerebral ischemia of subarachnoid hemorrhage. *Arch. Neurol.* 2011; 68(1)**:** 31-6.

100. Nedergaard M, Hansen AJ. Spreading depression is not associated with neuronal injury in the normal brain. *Brain Res.* 1988; 449(1-2)**:** 395-8.

101. Shin HK, Dunn AK, Jones PB, Boas DA, Moskowitz MA, Ayata C. Vasoconstrictive neurovascular coupling during focal ischemic depolarizations. *J. Cereb. Blood Flow Metab.* 2006; 26(8)**:** 1018-30.

102. Strong AJ, Anderson PJ, Watts HR, Virley DJ, Lloyd A, Irving EA *et al.* Peri-infarct depolarizations lead to loss of perfusion in ischaemic gyrencephalic cerebral cortex. *Brain* 2007; 130(Pt 4)**:** 995-1008.

103. Bederson JB, Levy AL, Ding WH, Kahn R, DiPerna CA, Jenkins AL, 3rd *et al.* Acute vasoconstriction after subarachnoid hemorrhage. *Neurosurgery* 1998; 42(2)**:** 352-60; discussion 360-2.

104. van den Bergh WM, Schepers J, Veldhuis WB, Nicolay K, Tulleken CA, Rinkel GJ. Magnetic resonance imaging in experimental subarachnoid haemorrhage. *Acta Neurochir. (Wien.)* 2005; 147(9)**:** 977-83; discussion 983.

105. Somjen GG. Mechanisms of spreading depression and hypoxic spreading depression-like depolarization. *Physiol. Rev.* 2001; 81(3)**:** 1065-96.

106. Richter F, Ebersberger A, Schaible HG. Blockade of voltage-gated calcium channels in rat inhibits repetitive cortical spreading depression. *Neurosci. Lett.* 2002; 334(2)**:** 123-6.

107. Wang Z, Tsai LK, Munasinghe J, Leng Y, Fessler EB, Chibane F *et al.* Chronic valproate treatment enhances postischemic angiogenesis and promotes functional recovery in a rat model of ischemic stroke. *Stroke* 2012; 43(9)**:** 2430-6.

108. Dijkhuizen RM, Beekwilder JP, van der Worp HB, Berkelbach van der Sprenkel JW, Tulleken KA, Nicolay K. Correlation between tissue depolarizations and damage in focal ischemic rat brain. *Brain Res.* 1999; 840(1-2)**:** 194-205.

109. Nakamura H, Strong AJ, Dohmen C, Sakowitz OW, Vollmar S, Sue M *et al.* Spreading depolarizations cycle around and enlarge focal ischaemic brain lesions. *Brain* 2010; 133(Pt 7)**:** 1994-2006.

110. Tso MK, Lass E, Ai J, Loch Macdonald R. Valproic Acid treatment after experimental subarachnoid hemorrhage. *Acta Neurochir. Suppl.* 2015; 120**:** 81-5.

111. Hamming AM, Wermer MJ, Umesh Rudrapatna S, Lanier C, van Os HJ, van den Bergh WM *et al.* Spreading depolarizations increase delayed brain injury in a rat model of subarachnoid hemorrhage. *J. Cereb. Blood Flow Metab.* 2015 nov 30 [epub ahead of print].

112. Gunther M, Bock M, Schad LR. Arterial spin labeling in combination with a look-locker sampling strategy: inflow turbo-sampling EPI-FAIR (ITS-FAIR). *Magn. Reson. Med.* 2001; 46(5)**:** 974-84.

113. Huber PJ. The behavior of maximum likelihood estimates under nonstandard conditions. In: Berkeley CUoCP, (ed) *Proceedings of the Fifth Berkeley Symposium on Mathematical Statistics and Probability*, 1967. pp 221-233.

114. White H. A heteroskedasticity-consistent covariance matrix estimator and a direct test for heteroskedasticity. *Econometrica* 1980; 48**:** 817-830.

115. Lee JY, Sagher O, Keep R, Hua Y, Xi G. Comparison of experimental rat models of early brain injury after subarachnoid hemorrhage. *Neurosurgery* 2009; 65(2)**:** 331-43.

116. Johannessen CU, Johannessen SI. Valproate: past, present, and future. *CNS Drug Rev* 2003; 9(2)**:** 199-216.

117. Lauritzen M, Dreier JP, Fabricius M, Hartings JA, Graf R, Strong AJ. Clinical relevance of cortical spreading depression in neurological disorders: migraine, malignant stroke, subarachnoid and intracranial hemorrhage, and traumatic brain injury. *J. Cereb. Blood Flow Metab.* 2011; 31(1)**:** 17-35.

118. Reiffurth C, Kirov S, JP D. *Animal Models of Acute Neurological Injuries*, Humana Press, Springer Science, 2009.

119. Oliveira-Ferreira AI WM, Reiffurth C, Milakara D, Woitzik J, Dreier JP. Spreading depolarization, a pathophysiological mechanism of stroke and migraine aura. *Future Neurol.* 2012; 7**:** 45-64.

120. Smith JM, Bradley DP, James MF, Huang CL. Physiological studies of cortical spreading depression. *Biol. Rev. Camb. Philos. Soc.* 2006; 81(4)**:** 457-81.

121. Ayata C. Spreading depression and neurovascular coupling. *Stroke* 2013; 44(6 Suppl 1)**:** S87-9.

122. Brennan KC, Beltran-Parrazal L, Lopez-Valdes HE, Theriot J, Toga AW, Charles AC. Distinct vascular conduction with cortical spreading depression. *J. Neurophysiol.* 2007; 97(6)**:** 4143-51.

123. Takano T, Tian GF, Peng W, Lou N, Lovatt D, Hansen AJ *et al.* Cortical spreading depression causes and coincides with tissue hypoxia. *Nat. Neurosci.* 2007; 10(6)**:** 754-62.

124. Sun X, Wang Y, Chen S, Luo W, Li P, Luo Q. Simultaneous monitoring of intracellular pH changes and hemodynamic response during cortical spreading depression by fluorescence-corrected multimodal optical imaging. *Neuroimage* 2011; 57(3)**:** 873-84.

125. Chang JC, Shook LL, Biag J, Nguyen EN, Toga AW, Charles AC *et al.* Biphasic direct current shift, haemoglobin desaturation and neurovascular uncoupling in cortical spreading depression. *Brain* 2010; 133(Pt 4)**:** 996-1012.

126. Woitzik J, Hecht N, Pinczolits A, Sandow N, Major S, Winkler MK *et al.* Propagation of cortical spreading depolarization in the human cortex after malignant stroke. *Neurology* 2013; 80(12)**:** 1095-102.

127. Gardner-Medwin AR, van Bruggen N, Williams SR, Ahier RG. Magnetic resonance imaging of propagating waves of spreading depression in the anaesthetised rat. *J. Cereb. Blood Flow Metab.* 1994; 14(1)**:** 7-11.

128. James MF, Smith MI, Bockhorst KH, Hall LD, Houston GC, Papadakis NG *et al.* Cortical spreading depression in the gyrencephalic feline brain studied by magnetic resonance imaging. *J. Physiol.* 1999; 519 Pt 2**:** 415-25.

129. Kastrup A, Neumann-Haefelin T, Moseley ME, de Crespigny A. High speed diffusion magnetic resonance imaging of ischemia and spontaneous periinfarct spreading depression after thromboembolic stroke in the rat. *J. Cereb. Blood Flow Metab.* 2000; 20(12)**:** 1636-47.

130. Busch E, Gyngell ML, Eis M, Hoehn-Berlage M, Hossmann KA. Potassium-induced cortical spreading depressions during focal cerebral ischemia in rats: contribution to lesion growth assessed by diffusion-weighted NMR and biochemical imaging. *J. Cereb. Blood Flow Metab.* 1996; 16(6)**:** 1090-9.

131. Yenari MA, Onley D, Hedehus M, deCrespigny A, Sun GH, Moseley ME *et al.* Diffusion- and perfusion-weighted magnetic resonance imaging of focal cerebral ischemia and cortical spreading depression under conditions of mild hypothermia. *Brain Res.* 2000; 885(2)**:** 208-19.

132. Rother J, de Crespigny AJ, D'Arceuil H, Mosley ME. MR detection of cortical spreading depression immediately after focal ischemia in the rat. *J. Cereb. Blood Flow Metab.* 1996; 16(2)**:** 214-20.

133. Duong TQ, Yacoub E, Adriany G, Hu X, Ugurbil K, Kim SG. Microvascular BOLD contribution at 4 and 7 T in the human brain: gradient-echo and spin-echo fMRI with suppression of blood effects. *Magn. Reson. Med.* 2003; 49(6)**:** 1019-27.

134. Lee SP, Silva AC, Ugurbil K, Kim SG. Diffusion-weighted spin-echo fMRI at 9.4 T: microvascular/tissue contribution to BOLD signal changes. *Magn. Reson. Med.* 1999; 42(5)**:** 919-28.

135. Siero JC, Ramsey NF, Hoogduin H, Klomp DW, Luijten PR, Petridou N. BOLD specificity and dynamics evaluated in humans at 7 T: comparing gradient-echo and spin-echo hemodynamic responses. *PLoS One* 2013; 8(1)**:** e54560.

136. Norris DG. Spin-echo fMRI: The poor relation? *Neuroimage* 2012; 62(2)**:** 1109-15.

137. Scheffler K, Lehnhardt S. Principles and applications of balanced SSFP techniques. *Eur. Radiol.* 2003; 13(11)**:** 2409-18.

138. Miller KL. FMRI using balanced steady-state free precession (SSFP). *Neuroimage* 2012; 62(2)**:** 713-9.

139. Miller KL, Smith SM, Jezzard P, Wiggins GC, Wiggins CJ. Signal and noise characteristics of SSFP FMRI: a comparison with GRE at multiple field strengths. *Neuroimage* 2007; 37(4)**:** 1227-36.

140. Scheffler K, Hennig J. Is TrueFISP a gradient-echo or a spin-echo sequence? *Magn. Reson. Med.* 2003; 49(2)**:** 395-7.

141. Friedman L, Glover GH. Report on a multicenter fMRI quality assurance protocol. *J. Magn. Reson. Imaging* 2006; 23(6)**:** 827-39.

142. Conolly S, Nishimura D, Macovski A. A selective adiabatic spin-echo pulse. *J. Magn. Reson.* 1989; 83**:** 324–334.

143. Valette J, Giraudeau C, Marchadour C, Djemai B, Geffroy F, Ghaly MA *et al.* A new sequence for single-shot diffusion-weighted NMR spectroscopy by the trace of the diffusion tensor. *Magn. Reson. Med.* 2012; 68(6)**:** 1705-12.

144. Greengard L, Lee J. Accelerating the nonuniform fast fourier transform. *SIAM Journal of Scientific Computing* 1999; 46**:** 443–454.

145. Garcia D. Robust smoothing of gridded data in one and higher dimensions with missing values. *Comput Stat Data Anal* 2010; 54(4)**:** 1167-1178.

146. Iglewicz B, Hoaglin DC. *How to detect and handle outliers*, ASQC Quality Press: Milwaukee, Wis, 1993.

147. Peak finding and measurement. http://www.mathworks.com/matlabcentral/fileexchange/11755-peak-finding-and-measurement.

148. Miller AJ, Joseph PM. The use of power images to perform quantitative analysis on low SNR MR images. *Magn. Reson. Imaging* 1993; 11(7)**:** 1051-6.

149. Gudbjartsson H, Patz S. The Rician distribution of noisy MRI data. *Magn. Reson. Med.* 1995; 34(6)**:** 910-4.

150. Ding Z, Gore JC, Anderson AW. Reduction of noise in diffusion tensor images using anisotropic smoothing. *Magn. Reson. Med.* 2005; 53(2)**:** 485-90.

151. Nam H, Lee D, Lee JD, Park HJ. A method for anisotropic spatial smoothing of functional magnetic resonance images using distance transformation of a structural image. *Phys. Med. Biol.* 2011; 56(15)**:** 5063-77.

152. Fish D, Brinicombe A, Pike E, Walker J. Blind deconvolution by means of the Richardson-Lucy algorithm. *Journal of Optical Society of America A* 1995; 12**:** 58–65.

153. Cliff N. Dominance statistics: Ordinal analyses to answer ordinal questions. *Psychol. Bull.* 1993; 114**:** 494–509.

154. effsize: Efficient effect size computation. http://CRAN.R-project.org/package=effsize (R package version 0.5.1).

155. Hills BP, Wright KM, Snaar JE. Combined relaxation and diffusion studies of porous media using the multigrade CPMG sequence. *Magn. Reson. Imaging* 1996; 14(7-8)**:** 715-8.

156. Park SH, Kim T, Wang P, Kim SG. Sensitivity and specificity of high-resolution balanced steady-state free precession fMRI at high field of 9.4T. *Neuroimage* 2011; 58(1)**:** 168-76.

157. Kim TS, Lee J, Lee JH, Glover GH, Pauly JM. Analysis of the BOLD Characteristics in Pass-Band bSSFP fMRI. *Int J Imaging Syst Technol* 2012; 22(1)**:** 23-32.

158. Dharmakumar R, Qi X, Hong J, Wright GA. Detecting microcirculatory changes in blood oxygen state with steady-state free precession imaging. *Magn. Reson. Med.* 2006; 55(6)**:** 1372-80.

159. Hu X, Yacoub E. The story of the initial dip in fMRI. *Neuroimage* 2012; 62(2)**:** 1103-8.

160. Barth M, Meyer H, Kannengiesser SA, Polimeni JR, Wald LL, Norris DG. T_2-weighted 3D fMRI using S2-SSFP at 7 tesla. *Magn. Reson. Med.* 2010; 63(4)**:** 1015-20.

161. Autio JA, Shatillo A, Giniatullin R, Grohn OH. Parenchymal spin-lock fMRI signals associated with cortical spreading depression. *J. Cereb. Blood Flow Metab.* 2014; 34(5)**:** 768-75.

162. Le Bihan D, Turner R, MacFall JR. Effects of intravoxel incoherent motions (IVIM) in steady-state free precession (SSFP) imaging: application to molecular diffusion imaging. *Magn. Reson. Med.* 1989; 10(3)**:** 324-37.

163. McNab JA, Miller KL. Sensitivity of diffusion weighted steady state free precession to anisotropic diffusion. *Magn. Reson. Med.* 2008; 60(2)**:** 405-13.

164. van Dusschoten D, Moonen CT, de Jager PA, Van As H. Unraveling diffusion constants in biological tissue by combining Carr-Purcell-Meiboom-Gill imaging and pulsed field gradient NMR. *Magn. Reson. Med.* 1996; 36(6)**:** 907-13.

165. Morvan D, Leroy-Willig A. Simultaneous measurements of diffusion and transverse relaxation in exercising skeletal muscle. *Magn. Reson. Imaging* 1995; 13(7)**:** 943-8.

166. Ong H, Chin CL, Wehrli SL, Tang X, Wehrli FW. A new approach for simultaneous measurement of ADC and T_2 from echoes generated via multiple coherence transfer pathways. *J. Magn. Reson.* 2005; 173(1)**:** 153-9.

167. Staroswiecki E, Granlund KL, Alley MT, Gold GE, Hargreaves BA. Simultaneous estimation of T_2 and apparent diffusion coefficient in human articular cartilage in vivo with a modified three-dimensional double echo steady state (DESS) sequence at 3 T. *Magn. Reson. Med.* 2012; 67(4)**:** 1086-96.

168. Bock M. Simultaneous T_2^* and diffusion measurements with ^{3}He. *Magn. Reson. Med.* 1997; 38(6)**:** 890-5.

169. Ajraoui S, Parra-Robles J, Marshall H, Deppe MH, Clemence M, Wild JM. Acquisition of ^{3}He ventilation images, ADC, T_2^* and B(1) maps in a single scan with compressed sensing. *NMR Biomed.* 2012; 25(1)**:** 44-51.

170. Song AW, Woldorff MG, Gangstead S, Mangun GR, McCarthy G. Enhanced spatial localization of neuronal activation using simultaneous apparent-diffusion-coefficient and blood-oxygenation functional magnetic resonance imaging. *Neuroimage* 2002; 17(2)**:** 742-50.

171. Bockhorst KH, Smith JM, Smith MI, Bradley DP, Houston GC, Carpenter TA *et al.* A quantitative analysis of cortical spreading depression events in the feline brain characterized with diffusion-weighted MRI. *J. Magn. Reson. Imaging* 2000; 12(5)**:** 722-33.

172. Kudo C, Toyama M, Boku A, Hanamoto H, Morimoto Y, Sugimura M *et al.* Anesthetic effects on susceptibility to cortical spreading depression. *Neuropharmacology* 2013; 67**:** 32-6.

173. Takagaki M, Feuerstein D, Kumagai T, Gramer M, Yoshimine T, Graf R. Isoflurane suppresses cortical spreading depolarizations compared to propofol--implications for sedation of neurocritical care patients. *Exp. Neurol.* 2014; 252**:** 12-7.

174. Mulkern RV, Haker SJ, Maier SE. On high b diffusion imaging in the human brain: ruminations and experimental insights. *Magn. Reson. Imaging* 2009; 27(8)**:** 1151-62.

175. Macdonald RL, Pluta RM, Zhang JH. Cerebral vasospasm after subarachnoid hemorrhage: the emerging revolution. *Nat. Clin. Pract. Neurol.* 2007; 3(5)**:** 256-63.

176. Dohmen C, Sakowitz OW, Fabricius M, Bosche B, Reithmeier T, Ernestus RI *et al.* Spreading depolarizations occur in human ischemic stroke with high incidence. *Ann. Neurol.* 2008; 63(6)**:** 720-8.

177. Hartings JA, Bullock MR, Okonkwo DO, Murray LS, Murray GD, Fabricius M *et al.* Spreading depolarisations and outcome after traumatic brain injury: a prospective observational study. *Lancet Neurol.* 2011; 10(12)**:** 1058-64.

178. Dorhout Mees SM, Rinkel GJ, Feigin VL, Algra A, van den Bergh WM, Vermeulen M *et al.* Calcium antagonists for aneurysmal subarachnoid haemorrhage. *Cochrane Database Syst Rev* 2007; (3)**:** CD000277.

179. Dankbaar JW, de Rooij NK, Rijsdijk M, Velthuis BK, Frijns CJ, Rinkel GJ *et al.* Diagnostic threshold values of cerebral perfusion measured with computed tomography for delayed cerebral ischemia after aneurysmal subarachnoid hemorrhage. *Stroke* 2010; 41(9)**:** 1927-32.

180. Dankbaar JW, de Rooij NK, Velthuis BK, Frijns CJ, Rinkel GJ, van der Schaaf IC. Diagnosing delayed cerebral ischemia with different CT modalities in patients with subarachnoid hemorrhage with clinical deterioration. *Stroke* 2009; 40(11)**:** 3493-8.

181. Hoff R, Rinkel G, Verweij B, Algra A, Kalkman C. Blood volume measurement to guide fluid therapy after aneurysmal subarachnoid hemorrhage: a prospective controlled study. *Stroke* 2009; 40(7)**:** 2575-7.

182. van den Bergh WM, Algra A, van Kooten F, Dirven CM, van Gijn J, Vermeulen M *et al.* Magnesium sulfate in aneurysmal subarachnoid hemorrhage: a randomized controlled trial. *Stroke* 2005; 36(5)**:** 1011-5.

183. Dorhout Mees SM, Algra A, Vandertop WP, van Kooten F, Kuijsten HA, Boiten J *et al.* Magnesium for aneurysmal subarachnoid haemorrhage (MASH-2): a randomised placebo-controlled trial. *Lancet* 2012; 380(9836)**:** 44-9.

184. van Swieten JC, Koudstaal PJ, Visser MC, Schouten HJ, van Gijn J. Interobserver agreement for the assessment of handicap in stroke patients. *Stroke* 1988; 19(5)**:** 604-7.

185. Teasdale GM, Drake CG, Hunt W, Kassell N, Sano K, Pertuiset B *et al.* A universal subarachnoid hemorrhage scale: report of a committee of the World Federation of Neurosurgical Societies. *J. Neurol. Neurosurg. Psychiatry* 1988; 51(11)**:** 1457.

186. Lindvall P, Runnerstam M, Birgander R, Koskinen LO. The Fisher grading correlated to outcome in patients with subarachnoid haemorrhage. *Br. J. Neurosurg.* 2009; 23(2)**:** 188-92.

187. Harrod CG, Bendok BR, Batjer HH. Prediction of cerebral vasospasm in patients presenting with aneurysmal subarachnoid hemorrhage: a review. *Neurosurgery* 2005; 56(4)**:** 633-54; discussion 633-54.

188. Ashton D, Willems R, Wynants J, Van Reempts J, Marrannes R, Clincke G. Altered Na(+)-channel function as an in vitro model of the ischemic penumbra: action of lubeluzole and other neuroprotective drugs. *Brain Res.* 1997; 745(1-2)**:** 210-21.

189. Zaninovich OA, Ramey WL, Walter CM, Dumont TM. Completion of the Circle of Willis Varies by Gender, Age, and Indication for Computed Tomography Angiography. *World Neurosurg.* 2017; 106**:** 953-963.

190. Bugnicourt JM, Garcia PY, Peltier J, Bonnaire B, Picard C, Godefroy O. Incomplete posterior circle of Willis: a risk factor for migraine? *Headache* 2009; 49(6)**:** 879-86.

191. Cavestro C, Richetta L, L'Episcopo M R, Pedemonte E, Duca S, Di Pietrantonj C. Anatomical variants of the circle of Willis and brain lesions in migraineurs. *Can. J. Neurol. Sci.* 2011; 38(3)**:** 494-9.

192. Cucchiara B, Wolf RL, Nagae L, Zhang Q, Kasner S, Datta R *et al.* Migraine with aura is associated with an incomplete circle of Willis: results of a prospective observational study. *PLoS One* 2013; 8(7)**:** e71007.

193. Henry BM, Roy J, Ramakrishnan PK, Vikse J, Tomaszewski KA, Walocha JA. Association of migraine headaches with anatomical variations of the Circle of Willis: Evidence from a meta-analysis. *Neurol. Neurochir. Pol.* 2015; 49(4)**:** 272-7.

194. Ezzatian-Ahar S, Amin FM, Obaid HG, Arngrim N, Hougaard A, Larsson HB *et al.* Migraine without aura is not associated with incomplete circle of Willis: a case-control study using high-resolution magnetic resonance angiography. *J. Headache Pain* 2014; 15**:** 27.

195. Ikeda K, Iwamoto K, Murata K, Ito H, Kawase Y, Kano O *et al.* Incomplete posterior circle of Willis in migraineurs with aura. *Headache* Epub only, Oct 2009.

196. Kruit MC, van Buchem MA, Launer LJ, Terwindt GM, Ferrari MD. Migraine is associated with an increased risk of deep white matter lesions, subclinical posterior circulation infarcts and brain iron accumulation: the population-based MRI CAMERA study. *Cephalalgia* 2010; 30(2)**:** 129-36.

197. Hartkamp MJ, van Der Grond J, van Everdingen KJ, Hillen B, Mali WP. Circle of Willis collateral flow investigated by magnetic resonance angiography. *Stroke* 1999; 30(12)**:** 2671-8.

198. van Seeters T, Hendrikse J, Biessels GJ, Velthuis BK, Mali WP, Kappelle LJ *et al.* Completeness of the circle of Willis and risk of ischemic stroke in patients without cerebrovascular disease. *Neuroradiology* 2015; 57(12)**:** 1247-51.

199. van Seeters T, Biessels GJ, van der Schaaf IC, Dankbaar JW, Horsch AD, Luitse MJ *et al.* Prediction of outcome in patients with suspected acute ischaemic stroke with CT perfusion and CT angiography: the Dutch acute Stroke Trial (DUST) study protocol. *BMC Neurol.* 2014; 14**:** 37.

200. van der Willik D, Pelzer N, Algra A, Terwindt GM, Wermer MJ. Assessment of Migraine History in Patients with a Transient Ischemic Attack or Stroke; Validation of a Migraine Screener for Stroke. *Eur. Neurol.* 2016; 77(1-2)**:** 16-22.

201. Headache Classification Subcommittee of the International Headache Society. The International Classification of Headache Disorders: 2nd edition. *Cephalalgia* 2004; 24 Suppl 1**:** 9-160.

202. Headache Classification Committee of the International Headache Society. The International Classification of Headache Disorders, 3rd edition (beta version). *Cephalalgia* 2013; 33(9)**:** 629-808.

203. van Seeters T, Biessels GJ, Kappelle LJ, van der Schaaf IC, Dankbaar JW, Horsch AD *et al.* The prognostic value of CT angiography and CT perfusion in acute ischemic stroke. *Cerebrovasc. Dis.* 2015; 40(5-6)**:** 258-269.

204. El-Barhoun EN, Gledhill SR, Pitman AG. Circle of Willis artery diameters on MR angiography: an Australian reference database. *J. Med. Imaging Radiat. Oncol.* 2009; 53(3)**:** 248-60.

205. Kapoor K, Singh B, Dewan LI. Variations in the configuration of the circle of Willis. *Anat Sci Int* 2008; 83(2)**:** 96-106.

206. Krabbe-Hartkamp MJ, van der Grond J, de Leeuw FE, de Groot JC, Algra A, Hillen B *et al.* Circle of Willis: morphologic variation on three-dimensional time-of-flight MR angiograms. *Radiology* 1998; 207(1)**:** 103-11.

207. Li Q, Li J, Lv F, Li K, Luo T, Xie P. A multidetector CT angiography study of variations in the circle of Willis in a Chinese population. *J. Clin. Neurosci.* 2011; 18(3)**:** 379-83.

208. Riggs HE, Rupp C. Variation in form of circle of Willis. The relation of the variations to collateral circulation: anatomic analysis. *Arch. Neurol.* 1963; 8**:** 8-14.

209. Alpers BJ, Berry RG, Paddison RM. Anatomical studies of the circle of Willis in normal brain. *AMA Arch. Neurol. Psychiatry* 1959; 81(4)**:** 409-18.

210. Cassot F, Vergeur V, Bossuet P, Hillen B, Zagzoule M, Marc-Vergnes JP. Effects of anterior communicating artery diameter on cerebral hemodynamics in internal carotid artery disease - A model study. *Circulation* 1995; 92(10)**:** 3122-31.

211. Waaijer A, van Leeuwen MS, van der Worp HB, Verhagen HJ, Mali WP, Velthuis BK. Anatomic variations in the circle of Willis in patients with symptomatic carotid artery stenosis assessed with multidetector row CT angiography. *Cerebrovasc. Dis.* 2007; 23(4)**:** 267-74.

212. Schomer DF, Marks MP, Steinberg GK, Johnstone IM, Boothroyd DB, Ross MR *et al.* The anatomy of the posterior communicating artery as a risk factor for ischemic cerebral infarction. *N. Engl. J. Med.* 1994; 330(22)**:** 1565-70.

213. Chuang YM, Lin CP, Wong HF, Chang YJ, Chang CH, Chang TY *et al.* Plasticity of circle of Willis: a longitudinal observation of flow patterns in the circle of Willis one week after stenting for severe internal carotid artery stenosis. *Cerebrovasc. Dis.* 2009; 27(6)**:** 572-8.

214. Rutgers DR, Klijn CJ, Kappelle LJ, van Huffelen AC, van der Grond J. A longitudinal study of collateral flow patterns in the circle of Willis and the ophthalmic artery in patients with a symptomatic internal carotid artery occlusion. *Stroke; a journal of cerebral circulation* 2000; 31(8)**:** 1913-20.

215. de Monye C, Dippel DW, Siepman TA, Dijkshoorn ML, Tanghe HL, van der Lugt A. Is a fetal origin of the posterior cerebral artery a risk factor for TIA or ischemic stroke? A study with 16-multidetector-row CT angiography. *J. Neurol.* 2008; 255(2)**:** 239-45.

216. Hoksbergen AW, Legemate DA, Csiba L, Csati G, Siro P, Fulesdi B. Absent collateral function of the circle of Willis as risk factor for ischemic stroke. *Cerebrovasc. Dis.* 2003; 16(3)**:** 191-8.

217. Mawet J, Kurth T, Ayata C. Migraine and stroke: in search of shared mechanisms. *Cephalalgia* 2015; 35(2)**:** 165-81.

218. van Raamt AF, Mali WP, van Laar PJ, van der Graaf Y. The fetal variant of the circle of Willis and its influence on the cerebral collateral circulation. *Cerebrovasc. Dis.* 2006; 22(4)**:** 217-24.

219. Borgdorff P, Tangelder GJ. Incomplete circle of Willis and migraine: role for shear-induced platelet aggregation? *Headache* 2014; 54(6)**:** 1054-6.

220. Russell MB, Olesen J. A nosographic analysis of the migraine aura in a general population. *Brain* 1996; 119 (Pt 2)**:** 355-61.

221. Bugnicourt JM, Garcia PY, Picard C, Godefroy O, Peltier J, Bonnaire B. Anatomical variations in the circle of Willis and migraine susceptibility: is there an association? A comment. *Headache* 2010; 50(2)**:** 323.

222. Marbacher S, Fandino J, Kitchen ND. Standard intracranial in vivo animal models of delayed cerebral vasospasm. *Br. J. Neurosurg.* 2010; 24(4)**:** 415-34.

223. Kooijman E, Nijboer CH, van Velthoven CT, Kavelaars A, Kesecioglu J, Heijnen CJ. The rodent endovascular puncture model of subarachnoid hemorrhage: mechanisms of brain damage and therapeutic strategies. *J. Neuroinflammation* 2014; 11**:** 2.

224. Stetler RA, Leak RK, Gan Y, Li P, Zhang F, Hu X *et al.* Preconditioning provides neuroprotection in models of CNS disease: paradigms and clinical significance. *Prog. Neurobiol.* 2014; 114**:** 58-83.

225. Oliff HS, Coyle P, Weber E. Rat strain and vendor differences in collateral anastomoses. *J. Cereb. Blood Flow Metab.* 1997; 17(5)**:** 571-6.

226. Lee RM. Morphology of cerebral arteries. *Pharmacol. Ther.* 1995; 66(1)**:** 149-73.

227. Busch E, Beaulieu C, de Crespigny A, Moseley ME. Diffusion MR imaging during acute subarachnoid hemorrhage in rats. *Stroke* 1998; 29(10)**:** 2155-61.

228. Ostergaard L, Dreier JP, Hadjikhani N, Jespersen SN, Dirnagl U, Dalkara T. Neurovascular coupling during cortical spreading depolarization and -depression. *Stroke* 2015; 46(5)**:** 1392-401.

229. Koide M, Wellman GC. Activation of TRPV4 channels does not mediate inversion of neurovascular coupling after SAH. *Acta Neurochir. Suppl.* 2015; 120**:** 111-6.

230. Kelly ME, Battye RA, McIntyre DC. Cortical spreading depression reversibly disrupts convulsive motor seizure expression in amygdala-kindled rats. *Neuroscience* 1999; 91(1)**:** 305-13.

231. Albe-Fessard D, Sanderson P, Condes-Lara M, Delandsheer E, Giuffrida R, Cesaro P. [Leao's spreading depression in the study of the relationship of central structures]. *An. Acad. Bras. Cienc.* 1984; 56(4)**:** 371-83.

232. Streit DS, Ferreira Filho CR, Martins-Ferreira H. Spreading depression in isolated spinal cord. *J. Neurophysiol.* 1995; 74(2)**:** 888-90.

233. Hinzman JM, DiNapoli VA, Mahoney EJ, Gerhardt GA, Hartings JA. Spreading depolarizations mediate excitotoxicity in the development of acute cortical lesions. *Exp. Neurol.* 2015; 267**:** 243-53.

234. Desland FA, Afzal A, Warraich Z, Mocco J. Manual versus Automated Rodent Behavioral Assessment: Comparing Efficacy and Ease of Bederson and Garcia Neurological Deficit Scores to an Open Field Video-Tracking System. *J Cent Nerv Syst Dis* 2014; 6**:** 7-14.

235. Garcia JH, Wagner S, Liu KF, Hu XJ. Neurological deficit and extent of neuronal necrosis attributable to middle cerebral artery occlusion in rats. Statistical validation. *Stroke* 1995; 26(4)**:** 627-34; discussion 635.

236. Bederson JB, Pitts LH, Tsuji M, Nishimura MC, Davis RL, Bartkowski H. Rat middle cerebral artery occlusion: evaluation of the model and development of a neurologic examination. *Stroke* 1986; 17(3)**:** 472-6.

237. Sherchan P, Lekic T, Suzuki H, Hasegawa Y, Rolland W, Duris K *et al.* Minocycline improves functional outcomes, memory deficits, and histopathology after endovascular perforation-induced subarachnoid hemorrhage in rats. *J. Neurotrauma* 2011; 28(12)**:** 2503-12.

238. Busch E, Hoehn-Berlage M, Eis M, Gyngell ML, Hossmann KA. Simultaneous recording of EEG, DC potential and diffusion-weighted NMR imaging during potassium induced cortical spreading depression in rats. *NMR Biomed.* 1995; 8(2)**:** 59-64.

239. Pan WJ, Thompson G, Magnuson M, Majeed W, Jaeger D, Keilholz S. Simultaneous FMRI and electrophysiology in the rodent brain. *J Vis Exp* 2010; (42).

240. Drenckhahn C, Winkler MK, Major S, Scheel M, Kang EJ, Pinczolits A *et al.* Correlates of spreading depolarization in human scalp electroencephalography. *Brain* 2012; 135(Pt 3)**:** 853-68.

241. Gollwitzer S, Groemer T, Rampp S, Hagge M, Olmes D, Huttner HB *et al.* Early prediction of delayed cerebral ischemia in subarachnoid hemorrhage based on quantitative EEG: A prospective study in adults. *Clin. Neurophysiol.* 2015; 126(8)**:** 1514-23.

242. Hall SD, Barnes GR, Hillebrand A, Furlong PL, Singh KD, Holliday IE. Spatio-temporal imaging of cortical desynchronization in migraine visual aura: a magnetoencephalography case study. *Headache* 2004; 44(3)**:** 204-8.

243. Lam JM, Hsiang JN, Poon WS. Monitoring of autoregulation using laser Doppler flowmetry in patients with head injury. *J. Neurosurg.* 1997; 86(3)**:** 438-45.

244. Bosche B, Graf R, Ernestus RI, Dohmen C, Reithmeier T, Brinker G *et al.* Recurrent spreading depolarizations after subarachnoid hemorrhage decreases oxygen availability in human cerebral cortex. *Ann. Neurol.* 2010; 67(5)**:** 607-17.

245. Feuerstein D, Manning A, Hashemi P, Bhatia R, Fabricius M, Tolias C *et al.* Dynamic metabolic response to multiple spreading depolarizations in patients with acute brain injury: an online microdialysis study. *J. Cereb. Blood Flow Metab.* 2010; 30(7)**:** 1343-55.

246. Lee WS, Lee JK, Lee SA, Kang JK, Ko TS. Complications and results of subdural grid electrode implantation in epilepsy surgery. *Surg. Neurol.* 2000; 54(5)**:** 346-51.

247. Ferro JM, Pinto F. Poststroke epilepsy: epidemiology, pathophysiology and management. *Drugs Aging* 2004; 21(10)**:** 639-53.

248. Houwink PE. [Farmacotherapeutisch Kompas 1997]. *Ned. Tijdschr. Geneeskd.* 1997; 141(16)**:** 796.

249. Taylor CP, Gee NS, Su TZ, Kocsis JD, Welty DF, Brown JP *et al.* A summary of mechanistic hypotheses of gabapentin pharmacology. *Epilepsy Res.* 1998; 29(3)**:** 233-49.

250. Futagi Y, Otani K, Imai K. Reduction in internal carotid arterial blood flow velocity in children during antiepileptic drug therapy with clinical dosages. *Epilepsia* 1994; 35(4)**:** 827-31.

251. Oliver DW, Dormehl IC. Cerebral blood flow effects of sodium valproate in drug combinations in the baboon model. *Arzneimittelforschung* 1998; 48(11)**:** 1058-63.

252. Bell EC, Willson MC, Wilman AH, Dave S, Silverstone PH. Differential effects of chronic lithium and valproate on brain activation in healthy volunteers. *Hum Psychopharmacol* 2005; 20(6)**:** 415-24.

253. Faye L, Gomord V. Success stories in molecular farming-a brief overview. *Plant Biotechnol J* 2010; 8(5)**:** 525-8.

254. Bradley DP, Smith MI, Netsiri C, Smith JM, Bockhorst KH, Hall LD *et al.* Diffusion-weighted MRI used to detect in vivo modulation of cortical spreading depression: comparison of sumatriptan and tonabersat. *Exp. Neurol.* 2001; 172(2)**:** 342-53.

255. Goadsby PJ, Ferrari MD, Csanyi A, Olesen J, Mills JG, Tonabersat TONSG. Randomized, double-blind, placebo-controlled, proof-of-concept study of the cortical spreading depression inhibiting agent tonabersat in migraine prophylaxis. *Cephalalgia* 2009; 29(7)**:** 742-50.

256. Sarrouilhe D, Dejean C, Mesnil M. Involvement of gap junction channels in the pathophysiology of migraine with aura. *Front. Physiol.* 2014; 5**:** 78.

257. Smith MI, Read SJ, Chan WN, Thompson M, Hunter AJ, Upton N *et al.* Repetitive cortical spreading depression in a gyrencephalic feline brain: inhibition by the novel benzoylamino-benzopyran SB-220453. *Cephalalgia* 2000; 20(6)**:** 546-53.

258. Dreier JP, Reiffurth C. The stroke-migraine depolarization continuum. *Neuron* 2015; 86(4)**:** 902-22.

259. Chen SP, Ay I, de Morais AL, Qin T, Zheng Y, Sadeghian H *et al.* Vagus nerve stimulation inhibits cortical spreading depression. *Pain* 2016; 157(4)**:** 797-805.

Summary

This thesis is about the role of spreading depolarization (SD) in subarachnoid hemorrhage (SAH). A SAH is a type of stroke usually caused by rupture of an aneurysm that is most often located at the intracranial arterial roundabout called the circle of Willis, or one of its branches. Patients who survive the first days after the SAH are prone to develop detrimental complications, such as delayed cerebral ischemia (DCI). One possible mechanism associated with the development of DCI after a SAH is metabolic tissue exhaustion due to SD. SDs are self-propagating waves (at 2-6 mm/minute) of mass neuronal and glial cell depolarization in brain tissue. They have been associated with the visual disturbances in migraine patients, i.e. aura, where SD is followed by cerebral hyperperfusion to restore the electrolyte balance, without accompanying tissue damage. However, in pathological states, such as after a SAH, a paradoxical hemodynamic response of hypoperfusion can occur, which can contribute to (worsening of) cerebral tissue damage.

In the experiments described in this thesis, we used a multidisciplinary, translational approach, combining data obtained in rats and humans, to investigate the associations between SD and DCI after SAH.

In **chapters 2** and **3** we used a rat model of subarachnoid hemorrhage (SAH). At day one post-SAH, we measured brain tissue damage with MRI, followed by artificial induction of spreading depolarization (SD) versus sham induction. At day three post-SAH, we repeated MRI to measure lesion growth. In **chapter 2**, we describe that the lesion growth was more than eight times larger in the SD group than in the no-SD group. Neuronal damage in the lesions was confirmed by histology. In **chapter 3**, both experimental groups of rats from **chapter 2**, which were treated with saline (placebo), were compared to two additional groups of rats that were treated with SD inhibitor valproate for four weeks prior to SAH. We found a significant interaction effect on lesion growth between treatment and placebo of 161mm^3 (p=0.04). **Chapters 2** and **3** combined suggest a direct association between SD and lesion growth after experimental SAH, which can be counteracted by valproate.

MRI techniques for recording SD are based on either hemodynamic (blood perfusion) changes or tissue water diffusion changes (such as caused by cell swelling). Hemodynamic changes may be measured with gradient-echo MRI techniques. In **chapter 4**, we explored the application of MRI techniques to monitor SD induced in rats. First, we compared a balanced-steady-state-free-precession (b-SSFP) technique to gradient-echo MRI, and showed significantly larger relative signal intensity changes, narrower peak widths and greater spatial specificity associated with SD. Second, we applied diffusion-weighted multi-spin-echo (DT2) scans, which allowed for simultaneous recording of hemodynamic and diffusion changes. Both b-SSFP and DT2 scanning improved the monitoring of SD by providing more sensitive image-based detection and additional information on the interaction between perfusion and diffusion responses, respectively.

For translating the findings of **chapters 2, 3** and **4** to the clinical setting, we performed clinical observational studies in **chapters 5** and **6.** For **chapter 5**, we collected data on home

medication, occurrence of delayed cerebral ischemia (DCI) and clinical outcome assessed by the modified Rankin Score three months after SAH from four cohorts of SAH patients. Based on a comprehensive literature review, the home medication was classified for SD modulation properties: i.e. likely, possible or weak evidence for being SD facilitating or inhibiting. We found a trend towards less DCI in patients using SD-inhibiting drugs (adjusted hazard ratio 0.66; 95% confidence interval 0.42-1.06), but this did not result in a better clinical outcome (adjusted relative risk 1.13; 95% confidence interval 0.90-1.41). This suggests a possible protective effect of SD-inhibition on DCI but an unclear possible detrimental effect on other factors that affect clinical outcome.

In **chapter 6** we tested, in a cohort with a different kind of stroke, namely ischemic stroke, the hypothesis that anatomic variations in the arterial circle of Willis are more common in patients with migraine. A high rate of incomplete circles amongst migraine patients was found in some, but not all previous population-based studies, which may contribute to the increased ischemic stroke risk in migraine patients, for example by reduced collateral flow. In our cohort, we found no statistically significant differences in the percentage of incomplete circles of Willis between migraine (87%) and non-migraine patients (85%; adjusted odds ratio 1.47; 95% confidence interval 0.63-3.44). Based on this finding, we conclude that it is unlikely that circle of Willis variants play an important pathophysiological role in the relation between migraine and stroke.

Chapter 7 provides a general discussion of the findings from **chapter 2-6**.

Samenvatting

Dit proefschrift gaat over de rol van spreading depolarizations (SD) bij subarachnoïdale bloedingen (SAB). Een SAB wordt meestal veroorzaakt door een scheur in een verwijding in een slagader (aneurysma). Meestal betreft dit een slagader die onderdeel uitmaakt van de cirkel van Willis, een soort rotonde van slagaders aan de onderzijde van de hersenen. Als patiënten de eerste dagen na een bloeding overleven lopen ze risico op secundaire complicaties, zoals hersenschade door late ischemie ofwel delayed cerebral ischemia (DCI). Metabole uitputting van het hersenweefsel door SD's is een mechanisme dat mogelijk een rol speelt bij het ontstaan van DCI na een SAB. SD's zijn massale ontladingen van zenuwcellen en gliacellen, die zich als golven voortplanten over de hersenschors met een snelheid van 2-6 mm/minuut. Ze zijn ook het mechanisme achter visuele stoornissen, zogenaamde aura's, die vaak voorkomen bij migrainepatiënten. Bij patiënten met migraine wordt een SD golf gevolgd door verhoogde doorbloeding van het hersenweefsel om de elektrolytbalans te herstellen, zodat er geen permanente weefselschade optreedt in de hersenen. Als de hersenen in een pathologische toestand verkeren, zoals na een SAB of een herseninfarct, kan na een SD juist een paradoxale verminderde doorbloeding optreden wat kan bijdragen aan weefselschade in de hersenen.

In de experimenten beschreven in dit proefschrift gebruiken we een multidisciplinaire, translationele aanpak, waarbij we studies in zowel ratten als mensen hebben gedaan om de samenhang tussen SD's en DCI na een SAB nader te onderzoeken.

In **hoofdstuk 2** en **3** gebruikten we een experimenteel model waarin we bij ratten een SAB opwekten. Een dag na de SAB maten we hersenschade met MRI, waarna bij de een helft van de ratten kunstmatig SD's werden opgewekt en bij de andere helft niet. Op dag drie na de SAB herhaalden we de MRI om laesiegroei te meten. In **hoofdstuk 2** beschrijven we dat de laesiegroei acht keer hoger was in de SD groep. De weefselschade op de MRI werd onder de microscoop (histologisch) bevestigd. In **hoofdstuk 3** vergeleken we beide groepen ratten uit **hoofdstuk 2** die gedurende 4 weken waren voorbehandeld met fysiologisch zout (placebo) met twee andere groepen ratten die 4 weken waren voorbehandeld met SD-remmer valproaat. Er werd een statistisch significant interactie-effect gevonden van 161mm^3 (p=0.04) van de behandeling met valproaat op laesiegroei. **Hoofdstukken 2** en **3** suggereren een directe associatie tussen SD en laesiegroei na experimentele SAB en geven een eerste aanwijzing dat de deze laesiegroei kan worden tegengegaan door valproaat.

MRI technieken voor het vastleggen van SD's zijn gebaseerd op hemodynamische (doorbloedings-) veranderingen en water diffusie veranderingen (zoals zwelling van cellen). De gebruikelijke techniek om hemodynamische veranderingen vast te leggen is gradiënt-echo MRI. In **hoofdstuk 4**, hebben we SD's opgewekt in ratten tijdens MRI om nieuwe MRI technieken voor het detecteren van SD's te verkennen. Ten eerste hebben we balanced-steady-state-free-precession (b-SSFP) vergeleken met gradiënt-echo en aangetoond dat b-SSFP significant grotere veranderingen van de relatieve intensiteit, smallere piekbreedtes en hogere spatiële specificiteit heeft bij het vastleggen van SD's. Ten tweede hebben we diffusie gewogen multi-spin-echo (DT2) scans gemaakt, waarmee zowel hemodynamische als diffusie veranderingen

tegelijkertijd vastgelegd kunnen worden. B-SSFP bleek aanvullende informatie te geven over SD's in vergelijking met gradiënt-echo MRI door gevoeliger registratie. DT2 scans idem door meer begrip van de interactie tussen perfusie- en diffusieprocessen.

Om de bevindingen van **hoofdstuk 2, 3** en **4** naar de kliniek te vertalen, hebben we in **hoofdstuk 5 en 6** klinische observatie studies gedaan. Voor **hoofdstuk 5** hebben we van vier cohorten SAB patiënten gegevens verzameld over thuismedicatie. We onderzochten hoe vaak DCI bij deze SAB patiënten voorkwam en hoe hun klinische uitkomst drie maanden na de bloeding was (met behulp van de modified Rankin Score). Op basis van een uitgebreid literatuuroverzicht werd de thuismedicatie ingedeeld naar invloed op SD's: 1) remmende invloed, 2) neutrale/geen invloed of 3) faciliterende invloed. In dit onderzoek vonden we een trend richting minder DCI bij patiënten die SD-remmende medicatie gebruikten (adjusted hazard ratio 0.66; 95% betrouwbaarheidsinterval 0.42-1.06). Patiënten bleken echter niet een betere klinische uitkomst te hebben. Dit suggereert dat SD-remmende medicatie DCI mogelijk kan verminderen maar ook dat er behalve DCI andere belangrijke factoren zijn die uiteindelijk de klinische uitkomst van een patiënt bepalen.

In **hoofdstuk 6**, hebben we in een cohort met een ander type beroerte, namelijk een herseninfarct, de hypothese getest dat anatomische variaties in de arteriële cirkel van Willis vaker voorkomen bij migrainepatiënten. Eerder werd een verhoogd percentage incomplete cirkels onder migrainepatiënten gevonden in sommige, maar niet in alle, populatiestudies. Een hoger percentage incomplete cirkels zou dan een van de oorzaken kunnen zijn van de verhoogde kans op herseninfarcten in de achterste hersen gebieden bij patiënten met migraine, bijvoorbeeld door minder goede collaterale bloedvoorziening of doorbloedingsproblemen met hierdoor een verhoogde gevoeligheid voor SD's. In deze studie vonden we geen statistisch significante verschillen in varianten van de cirkel van Willis tussen herseninfarct patiënten met (87%) en zonder (85%) migraine (adjusted odds ratio 1.47; 95% betrouwbaarheidsinterval 0.63-3.44). Daarom concluderen we dat het onwaarschijnlijk is dat variatie in de cirkel van Willis een belangrijke factor is bij het ontstaan van herseninfarcten bij migrainepatiënten.

Hoofdstuk 7 bevat een algemene discussie van de bevindingen in **hoofdstuk 2-6.**

Acknowledgements

Completing this thesis was a ten year journey. The limited space of these acknowledgements isn't enough to thank all the people who helped me navigate through it and illustrates the journey.

This voyage started when Marieke Wermer had just started working in Leiden and got a PhD student, because there was some funding-without-a-plan. After extensively exploring unsuitable topics such as endothelial progenitor cells, we finally settled for relating stroke to a theme that was already big in Leiden: migraine. Michel Ferrari was kind enough to adopt us and the role of spreading depolarizations in stroke turned out to be a fascinating topic. But the hypotheses we generated required animal research. And if you say animal stroke research in the Netherlands, you say Rick Dijkhuizen, who runs a lab that's both very professional and a joy to work in. While all three of my thesis advisors taught me a lot in their own way, one person deserves special mention: Arn van den Maagdenberg who advised us a lot.

Umesh, what a great chemistry we had, both professionally and socially. I hope to see you many times in the future. I can't mention all the colleagues I've met along this journey, but I'd like to thank Gerard van Vliet, Ann Stowe and Annette van der Toorn for the enjoyable collaboration. Inge Mulder and Wouter Mol, we complemented each other, which made it a strong collaboration.

The reflection skills I learnt in occupational health care were a great compass while completing this thesis. If only I had learnt them at the start! Special thanks to Bedrijfsartsen5, Team Europoort, Ger Kaldenborg and Jos van Rooyen.

My friends keep me afloat; Acoutes (Bram, Hessel, Joost, Paul, Roger), Round Table 154, Jottum sailing team, Barbara, Barkhad, Coen, Dewi, Jeroen, Lien, Marko, Micha, Paula, Rianne, Robin, Ruth, Thomas, Ton, Thorvald, Wendy, Feuten and all those I can't mention here. Tim, the journey of a PhD thesis ends for me too now, but I hope to embark on many more trips with you.

Family is my buoy. Thanks to my parents and parents in law for looking after the kids. Rosa, a boat stands firmer with two anchors. Mirjam, we both enjoy sailing. The waters are sometimes rough and I'm glad to share my life boat with you. Fenna, Maarten: land ho!

List of publications

Het blijft kwakzalverij (3). Hamming AM. Medisch Contact. 2006 Sep; 61(36) 1422-1422

Spreading depolarization modulating drugs and delayed cerebral ischemia in patients with aneurysmal subarachnoid hemorrhage. Mulder IA, Hamming AM, Gathier CS, van den Bergh WM, Dankbaar, JW, Hoff, RG, Ferrari, MD, Rinkel, GJE, Algra, A, Wermer, MJH. Cerebrovasc Dis 2014;37, Supplement: 1: B2117, 539-539

The Dutch String-of-Pearls Stroke Study: protocol of a large prospective multicenter genetic cohort study. Nederkoorn PJ, van Dijk EJ, Koudstaal PJ, Luijckx GJ, van Oostenbrugge RJ, Visser MC, Wermer MJ, Ruigrok YM, Algra A, Kappelle LJ; Dutch String-of-Pearls Stroke Study-Group. Int J Stroke. 2015 Jan;10(1):120-122.

Measurement of Distinctive Features of Cortical Spreading Depolarizations with Different MRI Contrasts. Umesh Rudrapatna S, Hamming AM, Wermer MJH, van der Toorn A, Dijkhuizen RM. NMR Biomed 2015 May; 28(5):591-600.

Spreading depolarization-modulating drugs and delayed cerebral ischemia in patients with subarachnoid haemorrhage. Mulder IA, Hamming AM, Gathier CS, van den Bergh WM, vandertop WP, Verbaan D, Ferrari MD, Rinkel GJE, Algra A, Wermer MJH. Cephalalgia 2015 May; vol. 35, 6_suppl, 178-178

Spreading depolarizations increase delayed brain injury in a rat model of subarachnoid hemorrhage. Hamming, AM, Wermer MJH, Rudrapatna U, Lanier C, van Os HJ, van den Bergh W, Ferrari MD, van der Toorn A, van den Maagdenberg, AMJM, Stowe AM. Dijkhuizen RM. Int j Stroke 2015 May; 10, Supplement 2, 194-194

Migrainde and anatomical variations in the ricle of Willis in patients with ischemic stroke. Hamming AM, van Walderveen MAA, Mulder IA, van der Schaaf IC, Kapelle LJ, Velthuis BK, Ferrari MD, Visser MC, Schonewille W, Algra A. and Wermer MJH. European Stroke Journal 2016 May; vol. 1, 1_suppl, 3-612, 190-191

Valproate reduces brain injury by spreading depolarizations in a rat model of subarachnoid haemorrhage. Hamming AM, van der Toorn A, Rudrapatna SU, Ma L, van Os H, Ferrari MD, van den Maagdenberg A, Stowe A, Dijkhuizen R, Wermer MJH. European Stroke Journal 2016 May; vol. 1, 1_suppl, 3-612, 395-396

Spreading depolarization-modulating drugs and delayed cerebral ischemia in patients with subarachnoid haemorrhage. Hamming AM, Mulder IA, Gathier CS, van den Bergh WM, Dankbaar JW, Hoff RG, vandertop WP, Verbaan D, Ferrari MD, Rinkel GJE, Algra A, Wermer MJH. J Neurol Sci 2016 Jul 15; 366:224-228.

Valproate reduces brain injury by spreading depolarizations in a rat model of subarachnoid haemorrhage. Hamming AM, van der Toorn A, Rudrapatna SU, Ma L, van Os H, Ferrari MD, van den Maagdenberg A, Stowe A, Dijkhuizen R, Wermer MJH. J Cereb Blood Flow Metab 2016 Jun; 36, Supplement 1, 350-351

Spreading depolarizations increase delayed brain injury in a rat model of subarachnoid haemorrhage. Hamming AM, Wermer MJH, Umesh Rudrapatna S, Lanier C, van Os HJ, van den Bergh WM, Ferrari MD, van der Toorn A, van den Maagdenberg AM, Stowe AM, Dijkhuizen RM. J Cereb Blood Flow Metab 2016 Jul; 36(7):1224-1231.

Landelijk Opleidingsplan Bedrijfsarts. Coffeng P, Smits P, Hoekstra H, Bastiaanssen M, Jurgens E, Thunnissen MJ, Sijderius R, Vissers P, de Jong P, Hamming AM, Guijt M, Yntema C. Nederlandse Vereniging voor Arbeids- en Bedrijfsgeneeskunde (NVAB), 2016 Nov.

Valproate reduces brain injury by spreading depolarizations in a rat model of subarachnoid haemorrhage. Hamming AM, van der Toorn A, Rudrapatna US, Ma L, van Os HJ, Ferrari MD, van den Maagdenberg AM, van Zwet E, Poinsatte K, Stowe AM, Dijkhuizen RM, Wermer MJH. Stroke 2017 Feb; 48(2):452-458.

Wat een bedrijfsarts voor je kan betekenen. Hamming AM. Werk en veiligheid. 2017 Mrt. Published online (https://www.werkenveiligheid.nl/preventie/de-praktijk/wat-een-bedrijfsarts-voor-je-kan-betekenen)

Bedrijfsarts zoekt contact met preventiemedewerker. Hamming AM. Werk en veiligheid. 2017 Nov. Published online (http://www.werkenveiligheid.nl/preventie/rollen-en-verantwoordelijkheden/bedrijfsarts-zoekt-contact-met-preventiemedewerker)

Ontdek net als Arend het vak van bedrijfsarts. Hamming AM, Hoedemakers K, Arbo Unie. YouTube 2018 Aug (youtu.be/J7NFohLGIGc)

Circle of Willis variations in migraine patients with ischemic stroke. Hamming AM, van Walderveen MAA, Mulder IA, van der Schaaf AC, Kapelle LJ, Velthuis BK, Ferrari MD, Terwindt GM, Visser MC, Schonewille W, Algra A, Wermer MJH, On behalf of the Dutch acute Stroke Trial (DUST) investigators. Brain Behav 2019 Mar 9(3):e01223.

Een arbeidsarts voor zzp’ers zij aan zij met de huisarts. Hamming A, thanks to De Bruin TAPM, Van Rhenen W. Medisch Contact 75(41), Oktober 8 2020: 18-19.

Cognitieve beperkingen. Handvatten om persoonlijk functioneren in kaart te brengen. Hamming AM, Brand T. Tijdschrift voor Bedrijfs- en Verzekeringsgeneeskunde 2020; 28(10): 43-46.

Curriculum Vitae

Arend (Maarten) Hamming was born August 20, 1979 in Amsterdam. After graduating from secondary school at the Hervormd Lyceum Zuid with an extra subject and all eights or higher, he studied psychology and medicine at Maastricht University. During a side job in home care, he became aware of the impact of health on daily life. During another side job as statistics tutor, he developed an interest for scientific research and for education. After that he worked as neurology resident at the Amphia hospital in Breda (ANIOS) and the Leiden University Medical Center (AIOS). There he was involved in the implementation of a biobank and electronic health record and he performed the research of this thesis. He attended several conferences and courses, such as laboratory animal science (Artikel 9) and the Invivo NMR course.

In 2015 he switched to occupational medicine. The hospital approach, focussed on diagnoses and organs were too limited for him. Sending patients back to the general practitioner with a note saying "there is no neurological explanation for the symptoms" was not in line with his desire to help people get healthier, which often requires a broader perspective on prevention, the causes of symptoms and a positive health approach to the consequenses of disease. In 2020 he finished his four-year training as an occupational health physician, a job which he enjoys greatly. He likes to advise individuals about health and prevention and finds partnership in discussing these themes with companies. He has a guest appointment at the Polikliniek Mens en Arbeid of Amsterdam University Medical Center. He also has a passion for teaching new colleagues the ins and outs of occupational health care.

He is married to Mirjam and has two children: Fenna and Maarten. In his spare time he likes sea/match sailing, vegetarian cooking, running and ballroom and latin dancing.